AN ANN BASED MODEL FOR DIRECTLY COUPLED PHOTO-VOLTAIC WATER PUMPING SYSTEM

A DISSERTATION

Submitted in partial fulfillment of the requirements for the award of the degree of

MASTER OF TECHNOLOGY

in

ELECTRICAL ENGINEERING

(With Specialization in Power System Engineering)

By

SOPPALI VIJAYA PRASAD

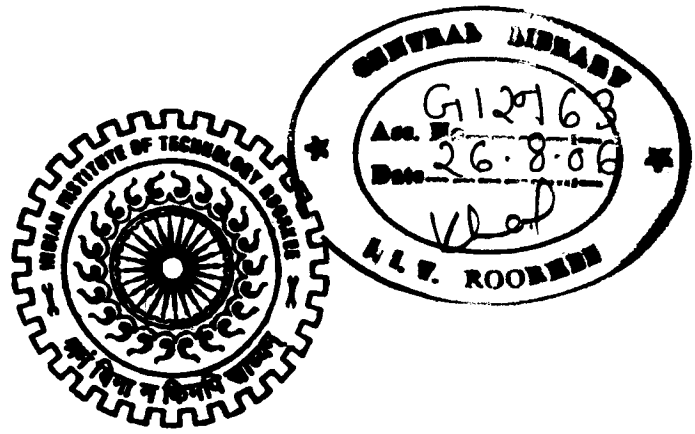

DEPARTMENT OF ELECTRICAL ENGINEERING
INDIAN INSTITUTE OF TECHNOLOGY ROORKEE
ROORKEE-247 667 (INDIA)

JUNE, 2006

Id. NO. MT-362 / 2006-57/SVP-EF

CANDIDATE'S DECLARATION

I hereby declare that the work presented in this Dissertation report entitled, "**An ANN Based Model for Directly Coupled Photo-voltaic Water Pumping System**" submitted in partial fulfillment of the requirements for the award of the degree of **Master of technology** in **Electrical Engineering** with specialization in **Power System Engineering**, in the **Department of Electrical Engineering, Indian Institute of Technology Roorkee, Roorkee**, is an authentic record of my own work under the guidance of **Dr. E.Fernandez**, Assistant Professor, Department of Electrical Engineering, Indian Institute of Technology Roorkee, Roorkee.

The matter embodied in this report has not been submitted by me for the award of any other degree or diploma.

Date: 30/06/2006
Place: Roorkee

S. Vijaya Prasad
Soppali Vijaya Prasad
(Reg. No. 044015)

CERTIFICATE

This is to certify that the above statements made by the student are correct to the best of my knowledge.

E. Fernandez

Dr.E.Fernandez
Assistant Professor
Department of Electrical Engineering
Indian Institute of Technology Roorkee
Roorkee.

ACKNOWLEDGEMENTS

I take this opportunity to express my sincere gratitude to **Dr.E.Fernandez,** Assistant Professor, Electrical Engineering Department IIT Roorkee for encouraging me to undertake this dissertation work as well as providing me all the necessary guidance and inspirational support throughout this work, without which this work would not have been in its present shape.

I am indebted to my friends especially Mr. Ganga Venkat Kumar who took interest in discussing the problem and encouraging me.

Special sincere heartfelt gratitude to my mother and family members, whose sincere prayer, best wishes, concern, support, unflinching encouragement and thoughtfulness has been a constant source of strength and upliftment to me during the entire work.

Also, I cordially thank Mr. Kapoor, Lab Assistant, PSS Lab for providing very good environment to work and availing computer facilities.

I thank all the members of Power System group for their help and encouragement at the hour of need.

Last, but not the least, I thank to Almighty God whose Divine Light provided me guidance, inspiration and strength to complete this work.

(Soppali Vijaya Prasad)

ABSTRACT

This work on Photovoltaic pumping systems is composed of two broad sections. The first section presents an application of an Artificial neural network (ANN) for the identification of optimal operating point of a PV supplied separately excited dc motor driving two different load torques. An ANN model is developed to control a directly coupled photovoltaic water pumping system. A gradient descent algorithm is used to train the ANN controller for the identification of maximum power point of the Solar Cell Array (SCA) and gross mechanical energy operation of the combined system. A non-adaptive off-line trained controller using ANN is developed for obtaining the MP (maximum power) and GME (gross mechanical energy) of the PV supplied motor-pump system. The model and algorithm is developed based on matching of the SCA to the motor load through a buck-boost power converter. Performance analysis is evaluated for the simulated results in MATLAB.

The second section of this work consists of modeling a directly coupled photovoltaic pumping system using ANN to predict the pump flow rate for a given pumping system for different head values. A method for modelling the output of solar photovoltaic water pumping was adopted for training the neural network. This method relies on the data that can be quickly measured. Performance evaluation was done in terms of predicted output values of pump flow rate and percentage error in prediction. It also demonstrates the error of back propagation technique for the neural network.

LIST OF FIGURES

LIST OF TABLES

CHAPTER 1

PHOTOVOLTAIC TECHNOLOGY OVERVIEW

1.1 Introduction

As conventional energy sources are depleting fast with a gradual rise in cost, considerable attention is being paid to other alternative sources. Solar energy which is free and abundant in most parts of the world has proven to be an economical source of energy in many applications. On a clear day the sun's radiation on the earth can be 1000 watts per square meter depending on the location. The photovoltaic process is completely solid state and self contained.

1.2 History of Photovoltaic technology

Solar Photovoltaic cells also called "Photovoltaic" cells or "PV" is a solid-state semiconductor device with no moving parts that convert sunlight into direct-current electricity. Although based on science that began with Alexander Edmond Becquerel's discovery of light-induced voltage in electrolytic cells over 150 years ago, which is known as **Photovoltaic effect**, significant development began following invention of the silicon solar cell in 1954 by Chappin at the Bell Laboratories in Murray Hills, New Jersey. This first solar cell had a 4% conversion Efficiency. The conversion efficiency is soon improved to 6% and then to 11%. Scientists such as Smith, Adams, Day, Fritts, Hertz, Hollwack, Planck, Einstein and Antoine Becqueral advanced Photovoltaic science.

The cross-sectional view of a solar cell connected to external load is shown below.

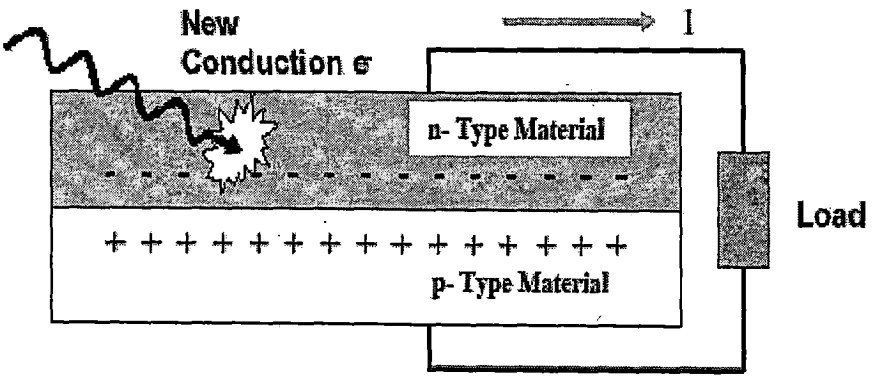

Fig. 1. Solar cell connected to an external load.

1.3 Advantages of Photovoltaic Technology

1. They are non-polluting with no detectable emissions or odors.
2. They can be stand-alone systems that reliably operate unattended for long periods.
3. They require no connection to an existing power source or fuel supply.
4. They may be combined with other power sources to increase system reliability.
5. They can withstand severe weather conditions including snow and ice.
6. They consume no fossil fuels - their fuel is abundant and free.
7. They can be installed and upgraded as modular building blocks - as power demand increases; more photovoltaic modules may be added.

1. 4 Disadvantages of Photovoltaic technology

The disadvantages of PV technology are given below

1. It operates at lower efficiencies than other sources of power.

2. The capital cost of purchasing and installation are high.

3. A solar cell only produces energy when there is sufficient sunlight.

4. Technical barriers to widespread use and dissemination.

1.5 PV or Solar Generator

The photovoltaic system with a large capacity power requires photovoltaic modules. The voltage output of the solar-generator depends on the photovoltaic modules in series. The integrated assembly of the photovoltaic modules together with support structure (foundation, tracking, box junction, cable and other components) is defined as the photovoltaic array or PV generator.

1.5.1 Modules in Series

In an ideal case when n number of identical photovoltaic modules is connected in series, then the total voltage of the PV generator is given below.

$$V_{SG} = \sum_{i=1}^{n} V_n = V_1 + V_2 + V_3 + \cdots + V_n \quad (I>0) \ldots\ldots\ldots\ldots (1)$$

The result of the ideal characteristic of n identical modules in series model is shown in the Figure below at constant temperature.

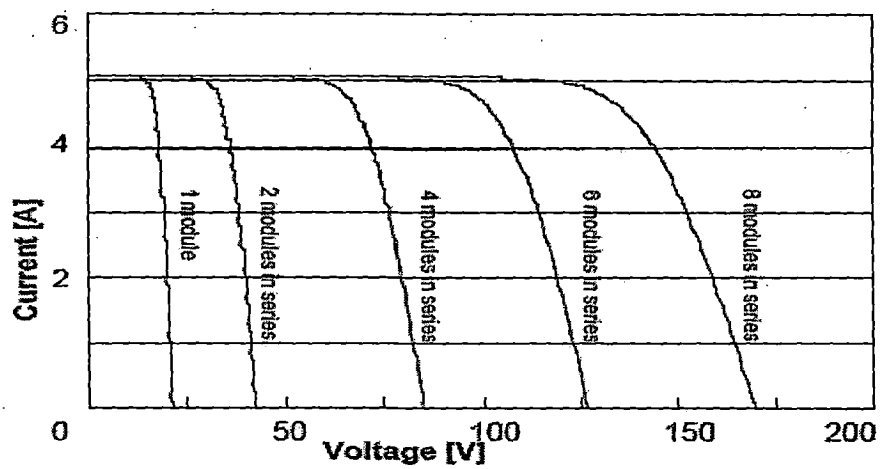

Fig. 2. I-V characteristics of series of PV modules.

1.5.2 Modules in parallel

The numbers (n) of the identical modules are joined in parallel. The resulting voltage V_{SG} is the same for each module and the resulting current I_{SG} is the sum of the respective currents I_1 until I_n of the module:

$$I_{SG} = \sum_{i=1}^{n} I_n = I_1 + I_2 + I_3 + \cdots + I_n \quad \ldots\ldots\ldots\ldots\ldots\ldots\ldots (2)$$

$$V_{SG} = V_1 = V_2 = V_3 = V_n \quad \ldots\ldots\ldots\ldots\ldots\ldots\ldots\ldots\ldots\ldots\ldots\ldots (3)$$

Where V_{SG} is total voltage of solar generator.

I_{SG} is the total current of solar generator.

The current and voltage output of the solar-generator in the photovoltaic array is given by the following equations:

$$V_{OUT} = \sum_{i=0}^{n} V_n = V_1 + V_2 + V_3 + \cdots + V_n \quad \ldots\ldots\ldots\ldots\ldots\ldots (4)$$

Where V_n is the voltage of n^{th} solar generator.

$$I_{OUT} = \sum_{i=0}^{m} I_m = I_1 + I_2 + I_3 + \cdots + I_m \quad \ldots\ldots\ldots\ldots\ldots\ldots\ldots\ldots (5)$$

Where I_m is the current of m^{th} solar generator.

The power of the solar-generator (Pout) is written in the Equation below:

$$P_{OUT} = \sum_{i=0}^{n} V_n \sum_{i=0}^{m} I_m = (V_1 + V_2 + V_3 + \cdots + V_n)(I_1 + I_2 + \cdots + I_m) \ldots (6)$$

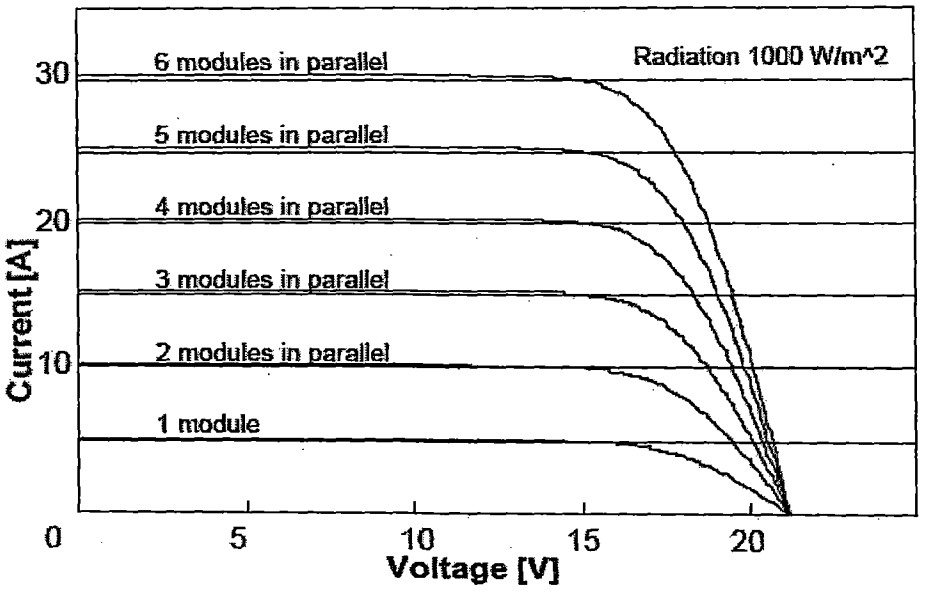

Fig. 3. I-V characteristics of modules connected in parallel.

1.6 I-V Characteristic of a PV cell

The ideal I-V characteristic equation is given below

$$I = I_l - I_0(e^{\frac{qV}{kT}} - 1) \quad \text{..... (7)}$$

Where I_l is the component of cell current due to photons (in A).

q = Charge of electron = $1.6 * 10^{-19}$ Coulomb

k = Boltzmann'sconstant = $1.38 * 10^{-23}$ j/K

T is the cell temperature in K.

Fig. 4. shown below depicts the I-V characteristics of a typical solar cell for different solar intensities at a constant temperature of 25 C. As solar radiation or insolation intensity increases the maximum power level from a cell also increases. The voltage output is relatively constant at various radiations, but the current output is proportionally varying with the radiation.

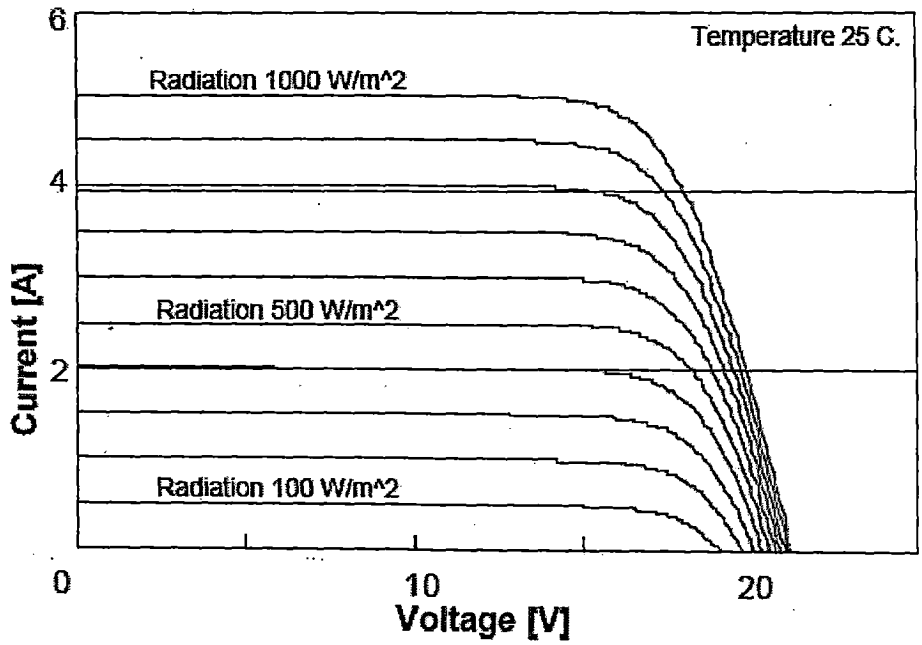

Fig. 4. Influence of solar insolation at constant temperature (T=25°C).

1.7 Temperature Characteristic

The PV cell I-V curve is also temperature sensitive. The open circuit voltage is directly proportional to the absolute temperature of the cell. The saturation current is highly temperature dependent. The open circuit voltage of a silicon PV cell decreases by 2.3 mV for each degree Celsius increase in temperature. The temperature dependence of the PV cell is shown in fig. 5.

An operating point of a solar cell will vary by varying insolation, cell temperature, and load values. For a given insolation and operating temperature, the output power depends on the value of a load resistance. As the load increases (or the resistance decreases), the operating point moves along the curve (I-V) towards the right. So only one load value gives

the PV generator its maximum power. When the temperature varies, the maximum power points are generated in such a manner that the output current stays approximately constant.

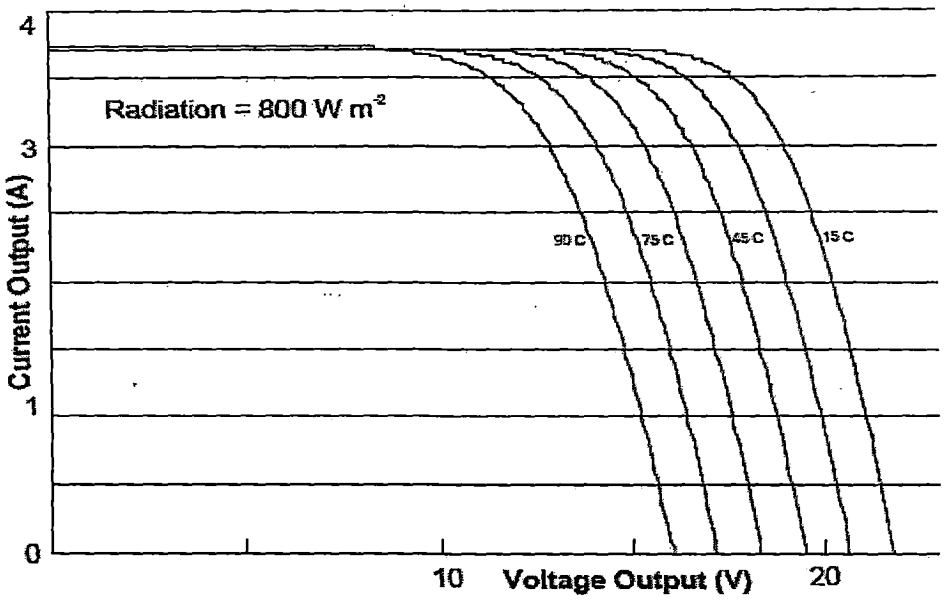

Fig. 5. Influence of temperature at constant solar radiation (G=800W/m^2).

1.8 Configurations of PV systems

1.8.1 Grid connected or grid-tied PV systems

Generally, two types of Grid-connected Photovoltaic Systems are employed

1. Grid-Connected PV systems without Battery storage.
2. Grid-Connected PV systems with Battery storage.

1.8.1.1 Grid Connected PV systems without Battery storage

PV systems without batteries are simple and reliable, requiring little maintenance. Grid-connected or utility-interactive PV systems are designed to operate in parallel and interconnected with the electric utility

grid as shown in fig. 6. The primary component in grid-connected PV systems is the inverter, or power-conditioning unit (PCU). The PCU converts the DC power produced by the PV array into AC power consistent with the voltage and power quality requirements of the utility grid.

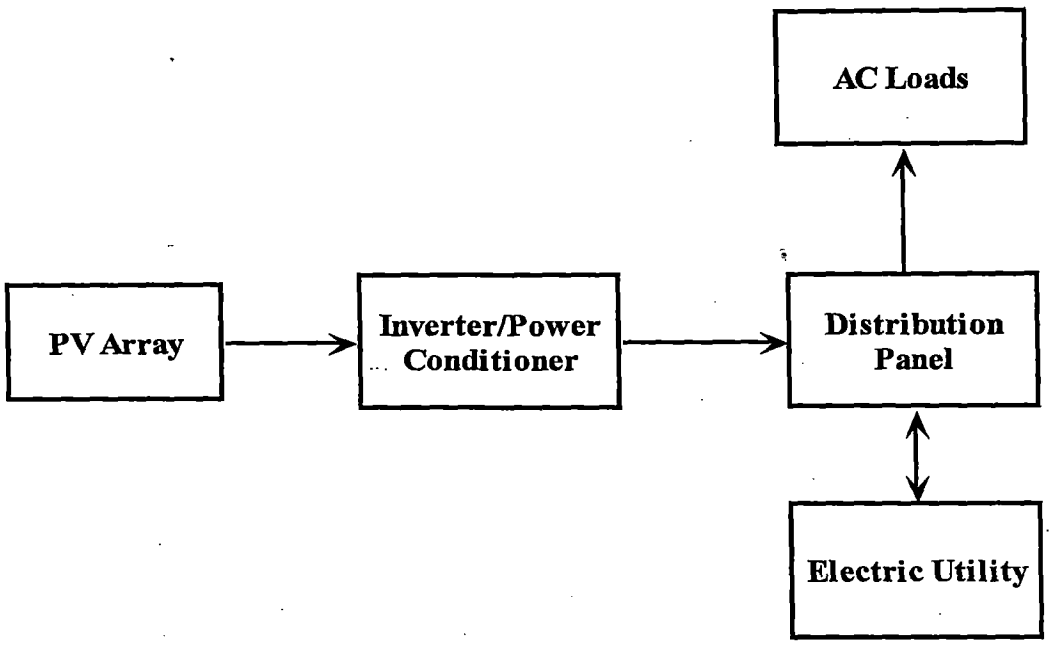

Fig. 6. Block diagram of Grid-Connected systems without batteries.

A bi-directional interface is made between the PV system AC output circuits and the electric utility network at an onsite distribution panel or service entrance. This allows the AC power produced by the PV system to either supply on-site electrical loads, or to back feed the grid when the PV system output is greater than the on-site load demand. At night and during other periods when the electrical loads are greater than the PV system output, the balance of power required by the loads is received from the electric utility. When the utility grid is down, these systems automatically shut down and disconnect from the grid. This safety feature is required in all grid-connected PV systems, and ensures that the PV system will not

continue to operate and feed back onto the utility grid when the grid is down for service or repair. A typical interconnection of a grid-connected PV power plant including two dc-ac inverters and transformers is shown in fig. 7. The capacitor in parallel with the PV array operates to limit the change of the PV voltage, Vpv, supplied to the dc-ac inverters. The inverters comprise of two 6-switch 3-phase bridge converters. Switching signals for the inverters are generated by a neural network controller for MPPT of the PV array. The objective of the transformer setup is to reduce harmonics involved in the inverter output ac voltage.

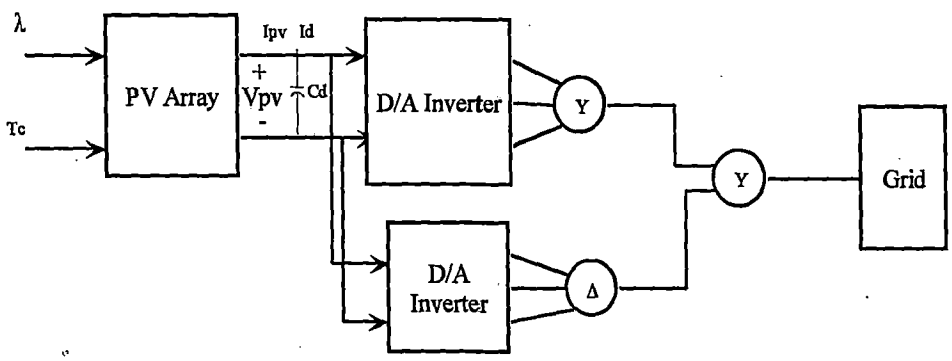

Fig. 7. Diagram of the Grid-connected PV system.

1.8.1.2 Grid Connected PV systems with Battery storage

This type of system is extremely popular for homeowners and small businesses where backup power is required for critical loads such as refrigeration, lighting. It is shown in fig.8. Under normal circumstances, the system operates in a grid-connected mode, supplementing the on-site loads or sending excess power back onto the grid while keeping the battery fully charged. In the event the grid becomes de-energized, control circuitry in the inverter opens the connection with the utility through a

bus transfer mechanism, and operates the inverter from the battery to supply power to the dedicated critical loads only. In this configuration, the critical loads must be supplied from a dedicated sub panel.

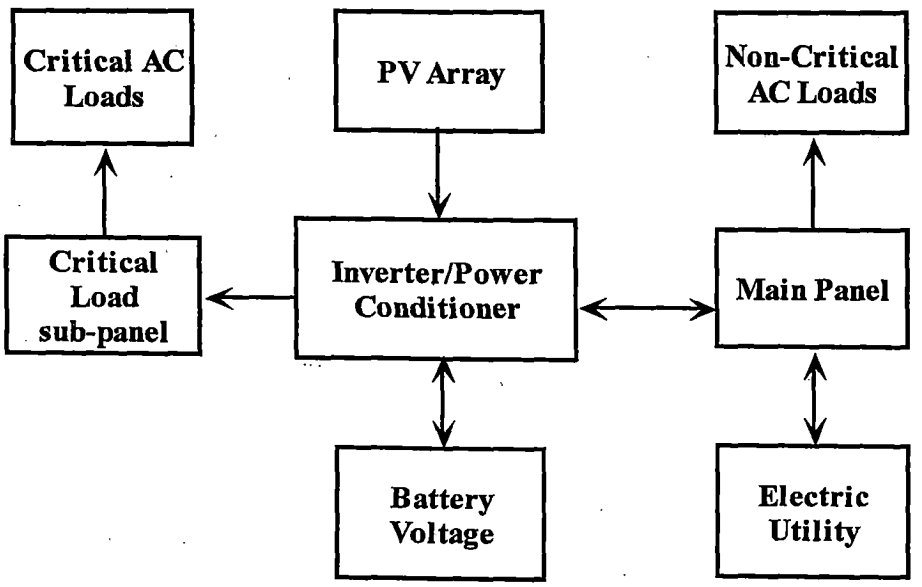

Fig. 8. Synoptic of Grid-Connected systems with battery storage.

From an operational point of view, a photovoltaic array experiences large variations of its output power under intermittent weather conditions. Fig. 9. Illustrates two samples of PV power variations in one day.

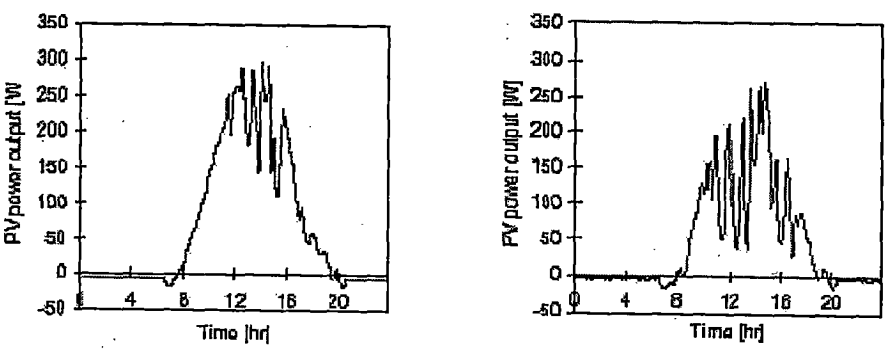

Fig. 9. Samples of PV power output variations.

1.8.2 PV Hybrid System

Integration of the PV power plant with other power sources such as diesel backup, fuel cell backup or battery backup is called a PV hybrid system. The diesel backup for PV power is able to make a continuous 24-hour power supply be possible. However, it has a few severe drawbacks. Its electrical efficiency decreases significantly at a low level of power output, and the diesel power generation is environmentally not viable as well. Both the battery backup and the fuel cell backup are the most likely technologies to provide backup power for the PV power system in the near future. A typical PV hybrid system is shown below.

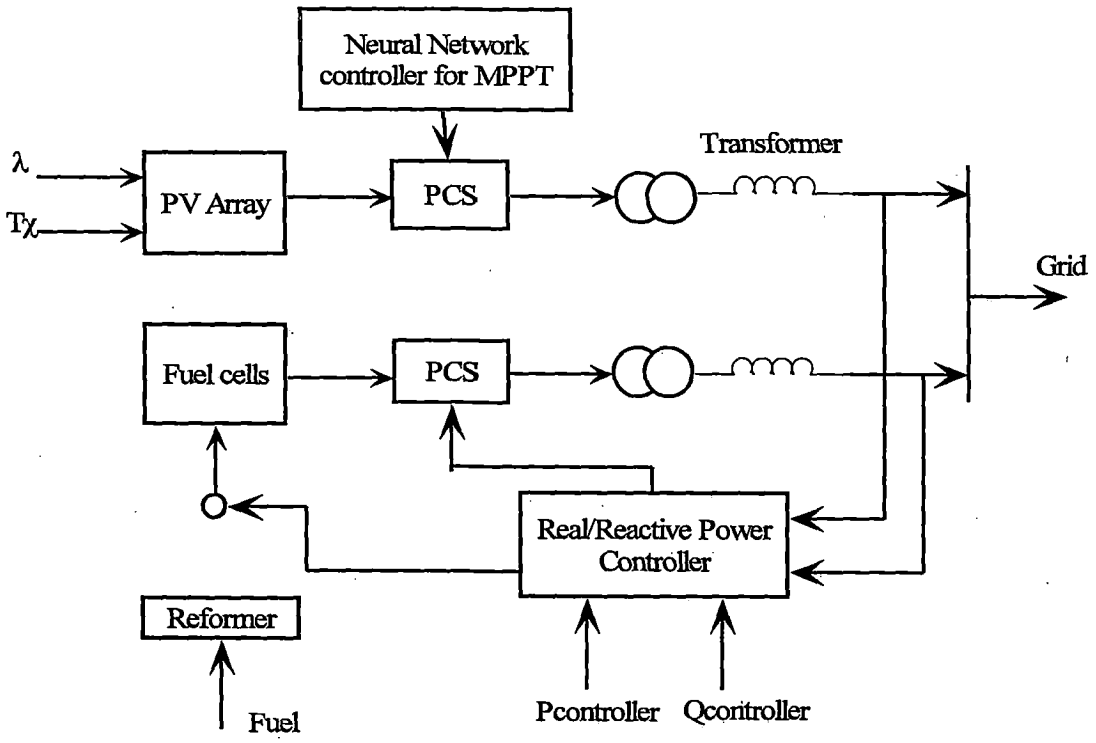

Fig. 10. Diagram of the Grid-connected PV-fuel system

1.9 Literature Review

The literature review of this work covers many related papers published by many authors. Many conference papers have been reviewed in order to get first hand information. The first section of the literature review covers aspects of Photovoltaic pumping systems in good detail.

J. A. Roger [1] has studied theoretically direct coupling between photovoltaic solar panels and various d.c. motors (series shunt and separate excitation) is as a function of the load. Operating curves are given in some specific cases (centrifugal pumps and fans).

Y.Roger Hsiao and Bruce Blevins [2] Direct coupling between a photovoltaic (PV) solar panel and a water pumping system driven by a permanent magnet dc motor is analyzed theoretically. Hourly insolation data obtained from typical meteorological year SOLMET data are used in the simulation.

W.Z.Fam and M.K.Balachander [3] analysed the dynamic performance of a D.C. shunt motor directly connected to a photovoltaic array. The motor is represented by the dynamic equations of its mechanical and electrical equivalents. The results are also compared with those obtained from experiments on a 1h.p, D.C. shunt motor connected to a 4kW photovoltaic array.

P. K. Koner, J. C. Joshi and A. K. Mukerjee [4] analyzed theoretically direct coupling between a photovoltaic (PV) generator and a monoblock DC

series motor connected with ventilator load torque centrifugal pump as a function of the no flow motor-pump speed and the water head of the pump.

M.Akbabi and M.A.Alattawi [5] developed a new model of solar cell generators and the implications on the optimal operation of the combined system. The subsequent modeled equations are used to find the optimal operating point of directly coupled stand-alone systems.

M.M.Saied and Hanafy [6] designed optimal parameters for a PV array coupled to a DC motor via DC-DC transformer for maximum power point operation. A buck-boost regulator tracks the optimal point of the photovoltaic array and matches the characteristic of the load with the output V-I characteristic of the array.

Appelabaum and sarma [7] analyzed and studied the operation of PMDC motors powered by a common source of solar cells. PMDC motor is best suited to match with the photovoltaic array for optimal operation at different insolations. The system operates at higher efficiency.

S.M.Alghuwainem [8, 9] analyzed the steady-state of dc motors supplied from photovoltaic generators with a step-up converter. The performance of dc motors is analysed by modelling of system components and then by operating the system at maximum power points irrespective of change in solar insolation.

Appelbaum [10] studied the starting and steady-state characteristics of dc motors powered by solar cell generators and compared their performance for different motors.

M.M.Saied [11] developed a new model for matching of dc motors to photovoltaic generators for maximum daily gross mechanical energy. The gross mechanical energy of the combined system may be at an operating point which is higher than the maximum power operating point of solar cell array.

G.Kou and W.A.Beckman [12] proposed a new method for estimating the long-term performance of directly coupled PV pumping systems. This method uses only information available from the PV module and pump-motor manufacturers. Weather data is generated from monthly averages of horizontal radiation and ambient temperatures using well-known weather data statistics.

A. Bennouna and Y. Ijdiyaou [13] presented a model for the simulation of photovoltaic D.C. solar pumping plants .The model also includes simple meteorological data simulations. The computations are based on an energy balance at the pump input and take into account the effect of meteorological data on the array efficiency and the effect of the configuration instantaneous state on the subsystems efficiency.

M.Moechtar, M.Julwono and Eddy kantosa [14] tested and studied the performance evaluation of ac and dc direct coupled photovoltaic water

pumping systems. Comparison of the performance data of different systems had been done. These pumping systems were installed at Sumba Island.

A. Hadj Arab, F. Chenlo, K.Mukadam [15] analyzed the performance of different photovoltaic water pumping systems. The Typical Meteorological Year "TMY" data from four distinct Algerian climatic sites was used to study the performance of three different PV array configurations and several pumping heads applied to two centrifugal pumps. The best couple generator configuration and pump for a given installation site and a daily load was determined.

Sui Weerasooriya, M. A. El-Sharkawi [16] introduced an artificial neural network based high performance speed control system for a dc motor. The rotor speed of the dc motor can be made to follow an arbitrarily selected trajectory. The purpose is to achieve accurate trajectory control of the speed, especially when motor and load parameters are unknown. The unknown nonlinear dynamics of the motor and the load are captured by an artificial neural network.

Chen Kumlun, Zha Zhengming, Yuan Liqiang [17] proposed a simple method of tracking the maximum power points and forcing the system to operate close to the maximum power points. A MCU (micro control unit) is employed to implement the proposed controller. Experimental results were compared with actual theoretical algorithm.

Ahmed Hussein, Kotaro Hirasawa [18] discussed a new robust control method and its application to a photovoltaic (PV) supplied, separately excited DC motor loaded with a constant torque. The robust controller is designed against the load torque changes by using the first and second ordered derivatives of the universal learning networks (ULNs).

M.Akbaba, I.Qamber, A.Kamal [19] addressed the matching of separately excited dc motors to photovoltaic generators (PVG) for maximum power output. In this paper a procedure is developed to express the field current of the motor directly in terms of maximum power point current and voltage of the PVG. It is shown that by adjusting the field current, the motor is forced to follow the maximum power trajectory of the PVG.

Mohanlal Kolhe, J. C. Joshi, and D. P. Kothari [20] analyzed the performance of a PV-powered dc permanent-magnet (PM) motor coupled with a centrifugal pump at different solar intensities and corresponding cell temperatures. The results obtained by experiments are compared with the calculated values, and it is observed that this system has a good match between the PV array and the electromechanical system characteristics.

B. Reshef, H. Suehrcke [21] discussed the results of the experiment based on field measurements and compared with the computer modelling of the various system components and evaluated the efficiency of individual components and the combined system.

Wagdy anis and M. A. Nourz [22] considered the design of a switched mode PV pumping system and discussed the effect of different parameters influencing the system design.

O. C. Vilela and N. Fraidenraich [23] studied the relationship between water pumping capacity, reservoir size and water demand, for a given water deficit. Curves of equal water deficit (iso-deficit lines) are obtained for various combinations of PV pumping capacity and reservoir size.

E.H. Amer, M.A. Younes [24] developed a simple algorithm for estimating the long term performance of a photovoltaic water pumping system without battery storage. The method uses the standard solar utilizability correlation equation to calculate the flow rate of the system, knowing an insolation threshold value.

Tomonobu Senj, Mummadi Veerachary, Katsumi Uezato[25] studied an application the effectiveness of interleaved dual boost converter for PV supplied separately excited DC motor is studied through simulation.

A. Hadj Arab, F. Chenlo et al. [26] presented a method for estimating the loss-of-load probability (LLP) of a photovoltaic water pumping system. The procedure can be used to draw LLP maps with normalised parameters using long term observed or generated sequences of meteorological data.

A. Hadj Arab, F. Chenlo et al. [27] presented two mathematical motor-pump models for photovoltaic (PV) applications. These models allow

determining the operating point with the PV array and the flow rate of the pumped water. The modelled motor-pump characteristics are current–voltage and flow–voltage.

A.Saadi and A.Moussi [28] developed a neural network model for photovoltaic pumping system for estimation of pumped water quantity. Experimental results are compared with neural model for the system and the results are said to be satisfactory.

W.Lawrance, B.Wichert et al. [29] described an efficient system for pumping water using a brushless dc motor driven by a PV array. Development of a system model from the individual component models allows overall system performance to be predicted effectively.

1.91 Outline of the Thesis Report

This thesis work is primarily concerned with the control of a photovoltaic pump using artificial neural network. An ANN model is developed for controlling a photovoltaic pump supplied by permanent magnet dc motor and series motor. A second ANN model is developed for directly coupled photovoltaic water pumping system. This thesis work is organized into several chapters which are given below.

Chapter 1: This chapter provides with the basic introduction to photovoltaic technology. The basic configurations of photovoltaic systems are briefly outlined with emphasis on stand-alone systems. The central theme of the work, i.e. photovoltaic pumping systems is given a brief

introduction along with their background. Literature review of photovoltaic technology in general and photovoltaic pumping systems in particular are given in good detail.

Chapter 2: This chapter gives brief introduction to photovoltaic pumping systems, their advantages and disadvantages. The basic components or elements which constitute a photovoltaic pumping system were described. Different configurations of PVPS (photovoltaic pumping system) were presented with their block diagrams.

Chapter 3: This chapter defines the statement of problem. The mathematical model of the whole pumping system is developed by detailed modeling of individual components that make up the system. Steady-state analysis of centrifugal pump supplied by PV coupled dc permanent magnet motor and series motor was analysed and performance comparison is made for both cases of operation.

Chapter 4: This chapter develops a neural network model for optimal operation and identification of operating point of PV pumping system. ANN architecture, training parameters, training algorithms and functions were described in detail. Training of the proposed neural network was done with the results obtained from previous chapter (chapter 3).

Chapter 5: This chapter presents the results of training for all the three conditions mentioned in chapter 4. Comparative analysis has been done to determine which architecture model is better and results were concluded.

Chapter 6: This chapter introduces with the statement of problem which is a neural network model for a directly coupled photovoltaic pumping system. A model of a specified photovoltaic pumping system has been reported based on the measured values of pump parameters. These data and the corresponding best-fit equations are used to train an ANN model. Results of training for all training conditions are analyzed in terms of ANN prediction and percentage error.

Chapter 7: This chapter gives conclusions to this work. Further scope of applications and use of photovoltaic pumping systems was outlined in brief.

CHAPTER 2

PHOTOVOLTAIC PUMPING SYSTEMS

2.1 Introduction

The simplest and least expensive method to convert solar energy into mechanical energy is to supply a motor from a photovoltaic generator. The use of Photovoltaics as the power source for pumping water is one of the most promising areas in photovoltaic applications. The use of photovoltaic power for water pumping is appropriate, as there is a natural relationship between the availability of solar power and the water requirement. The water requirement increases during hot weather periods when the solar radiation intensity is high and the output of the solar array is at its maximum. They are commonly used for water pumping in rural villages all over the world where no grid electricity exists.

2.2 Advantages of Photovoltaic water pump

The following are the advantages of Photovoltaic pump

1. Photovoltaic water pumping systems are particularly suitable for water supply in remote areas where no electricity supply is available.

2. Low maintenance, ease of installation, reliability and the matching between the powers generated and the water usage needs. In addition, water tanks can be used instead of batteries in photovoltaic pumping systems.

2.3 Disadvantages of Photovoltaic water pumping systems

Factors that have inhibited the widespread implementation of PV pumping systems are given below.

1. High initial capital cost.
2. Lack of awareness.
3. Lack of technical installation expertise.
4. History of failures and.
5. Lack of sufficient knowledge to predict accurately system daily output.

Different types and sizes of PVP systems are available commercially, in various stages of product development, which meet the range of existing pumping needs. The significant design variations of these systems depend mainly on:

- The choice of the solar cell material.
- The type of electric motor.
- The type of pump and the method of source/load matching.

2.4 Elements of a PV water pumping system

(1) **Photovoltaic array** – To provide electricity supply for the motor-pump. This supply could be direct current (DC), usually at 110 volts, or alternating current (AC) which is produced by inverting the DC power to AC power.

(2) **Motor-Pump set.**

(3) **Battery storage** if used – To provide electricity storage and allow pumping in cloudy conditions or at night.

(4) **Storage tank** – normally elevated, making water available at night or when it is cloudy.

(5) **Maximum power point tracker (MPPT)** which forces the PV array to generate its Maximum power.

The volume of pumped water is dependent on five major factors:

(1) The radiation level which is a measure of the sun's available energy.

(2) The photovoltaic array area.

(3) The conversion efficiency of the photovoltaic array.

(4) The ambient temperature.

(5) The pump-motor –hydraulic system characteristics.

2.5 Photovoltaic Pumping system Configurations

(1) The first is the directly coupled system without MPPT where a PV array is directly coupled to a DC motor and a pump.

(2) The second system is the battery buffered PV pumping system where a battery is connected across the array to feed the DC motor driving a pump.

(3) The third system uses maximum power point tracker (MPPT) or array tracking to improve the efficiency of system.

The typical range of sizes for photovoltaic-powered pumps is a few hundred watts to a few kilowatts.

2.5.1 Directly coupled without MPPT

A direct coupled system, where the PV array is directly coupled to a DC motor-pump system, is shown below. Such a system is simple and reliable, but the system does not operate continuously at its optimum point due to the continuous variation of solar radiation.

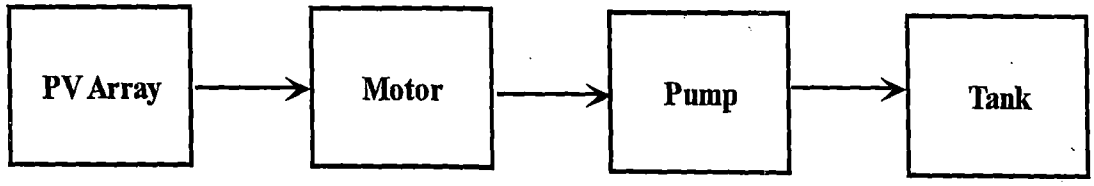

Fig. 11. Directly coupled PV pumping system without MPPT.

2.5.2 Battery buffered systems

Battery buffered systems with a storage battery is shown in fig 12. In this system, a battery is connected across the PV array and the DC motor is operating at almost constant voltage, and as a result, the DC motor is operated close to its optimum operating point.

Advantages

This system has two advantages over the directly coupled one:

- Water may be pumped day and night, thus the water discharge is larger.
- The DC motor is operating at its optimum operating point, and consequently, the system efficiency is enhanced.

Disadvantage

A major disadvantage of such a system is the extra system cost and unreliability due to the battery.

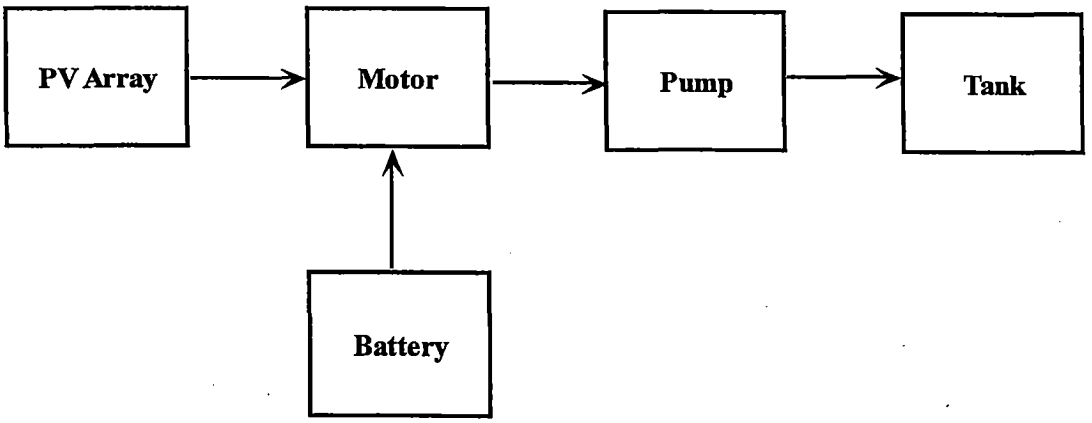

Fig. 12. PV pumping system with battery storage.

The photovoltaic modules are often mounted on a tracking device that maximizes energy production by tracking the sun from east to west each day as shown in fig. 13. The tracker consumes little or no power and may increase water production as much as 20 to 40 percent during summer months.

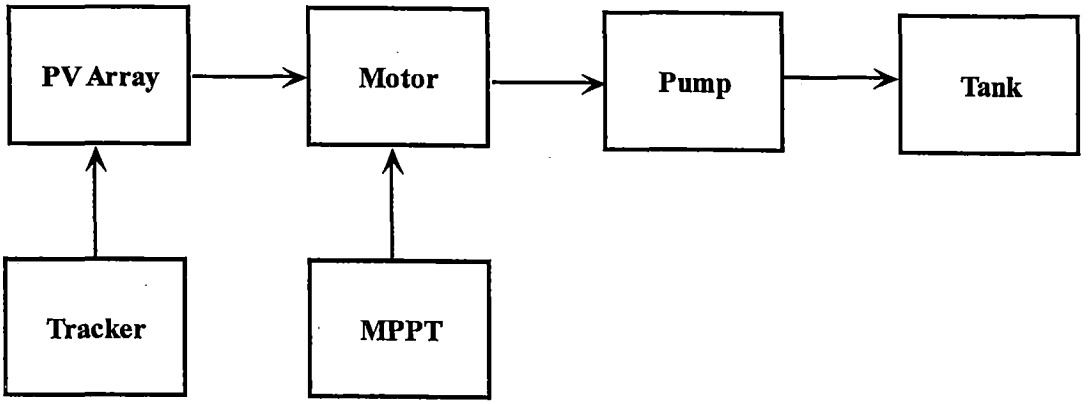

Fig. 13. PV pumping scheme with sun tracker and MPPT.

2.6 Types of Photovoltaic pumping systems

Photovoltaic pumping systems can also be classified broadly into two categories. They are

1. DC Pumping systems
2. AC Pumping systems

2.6.1 DC pumping systems

In DC pumping system the Photovoltaic pump (either centrifugal pump or volumetric pump) is driven by a DC motor. The DC motor used may be any of the following

1. Separately Excited motor.
2. Series motor.
3. Shunt motor.
4. Brushed and brushless Permanent magnet motors.
5. Variable switch reluctance motor.

2.6.1.1 Advantages of DC motor coupled Pumping system

The following are disadvantages of DC motor Pumping system

1. They are simple to operate.
2. Inexpensive.

2.6.1.2 Disadvantages

1. DC motors are not suitable for high-power (above 7 kW) applications.
2. Utilization efficiency of the whole pumping system is poor.

2.6.1.3 Advantages of Permanent magnet Brushless DC motor

The following are the advantages of PMBDC motor

1. Electronically-commuted brushless DC motors require less maintenance than standard DC motors.

2. They have high efficiency, high reliability and minimum maintenance requirements.

2.6.1.4 Disadvantages

1. Complexity of the system.
2. Cost is higher.
3. It is not suitable for village level operation and maintenance.

2.6.2 AC Pumping systems

In an AC pumping system the photovoltaic pump is driven by AC motor. The AC motor can be any of the following

1. Induction motor or Asynchronous motors
2. Synchronous motor

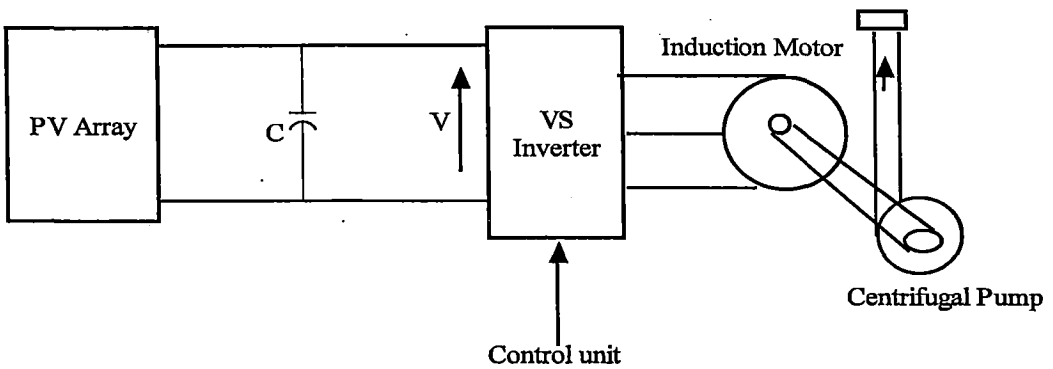

Fig. 14. PV pumping system driven by inverter controlled induction machine.

2.6.2.1 Advantages of AC Pumping systems

The advantages of AC pumping systems are given below

1. PV water pumping system driven by an induction motor is reliable.
2. Maintenance-free operation.
3. Induction motors provide more possibilities of efficiency improvements.

4. diversity of control strategies and

5. The disadvantage of additional inverter cost is offset as system size increases.

2.7 Selection of motor

The choice of the motor is dependent on numerous factors which are given below

1. Size requirements.
2. Efficiency.
3. Price.
4. Reliability and availability.

2.8 Hydraulic system and Model of Pump-motor combination

A pump is a machine for converting input kinetic power (mechanical power) into fluid output power (hydraulic power). The output power is represented by the delivery of the pump in terms of flow rate and head. Depending on the application and the type of water source supply (deep well or surface water), different pumps are used in PV-pumping systems. For the selection of a solar pump, the following factors are taken in to consideration:

1. Meet the required performances such as:
    a. Capacity
    b. Head
    c. Suction
2. Provide satisfactory working, such as:

a. Efficient

b. Easy to maintain

Many different varieties of pumps are suitable for operation in conjunction with PV powered pumping systems. Pumps can be generally divided into two categories which are given below

1. Centrifugal (rotodynamic) pumps and
2. Volumetric (positive displacement) pumps

These two different pumps have completely different characteristics. Centrifugal pumps are simple, low cost and are available for a wide range of flow rates and heads. Pumps are generally described by their total head (H) as a function of the pump flow rate (Q). The hydraulic load of a PV pumping system varies with the time and pump flow rate. So, in order to analyze the performance of a PV pumping system, we have to consider the behavior of the well during the system operation.

The head versus flow rate profile usually characterizes the different types of pumps. The typical head, as shown in Fig. 15. below, consists of a static component and a dynamic component. The static head is defined as the height or vertical distance from the water surface to the point of free discharge or the height required to pump the water (i.e. static head = A + B).

When the well is pumped, the water level drops, and the water being pumped through the pipe causes frictional losses. So, the total

dynamic head is the sum of the static head, the drawdown distance and the distance equivalent to the friction losses in the pipe (i.e. total dynamic head = A + B + C + friction losses).

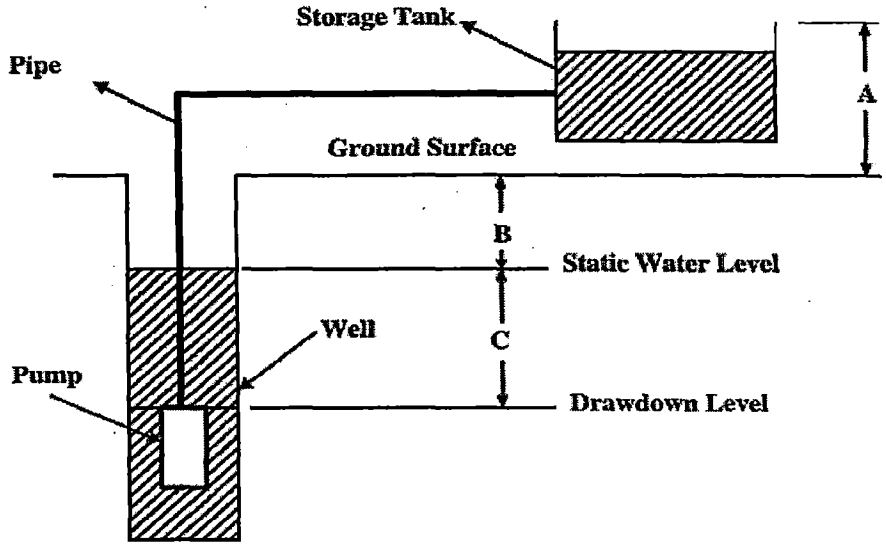

Fig. 15. Static and total dynamic head.

Eckstein developed a detailed theoretical analysis to determine the characteristics of the motor and pump. The model is briefly presented below. In this model, the performance of the pump can be predicted by using the affinity laws, which relates the pump speed (n) to flow rate (Q), head (H) and power (P) as

$$Q = F(n) \text{ or } Q = Q_{ref}(n/n_{ref}) \quad \ldots\ldots (8)$$

$$H = F(n^2) \text{ or } H = H_{ref}(n/n_{ref})^2 \quad \ldots\ldots (9)$$

$$P = F(n^3) \text{ or } P = P_{ref}(n/n_{ref})^3 \quad \ldots\ldots (10)$$

Where n_{ref}, Q_{ref}, H_{ref} and P_{ref} are the corresponding values at reference conditions. These equations imply that for a given set of speed, flow rate and power, the corresponding values at a different speed can be

determined for constant efficiency. This model can be implemented to simulate the performance of both the pump and the motor.

$$\eta = a + bQ + cQ^2 + dQ^3 \quad \text{..... (11)}$$

Where a, b, c and d are the coefficients at reference conditions.

For a small PV pumping system, the total head can be assumed to be the static head and is assumed to be constant in the following analysis. The manufacturer normally provides the head-flow-current-voltage data for the pump-motor combination, not the pump and motor individually. Instead of using individual motor and pump models, the characteristics of a pump-motor combination are represented by two functions. One is the current-voltage-head function represented in the form shown below:

$$V = F_1(I, H) \quad \text{..... (12)}$$

$$V = a_0 + a_1 I + a_2 I^2 + a_3 H + a_3 H^2 \quad \text{... ... ... (13)}$$

The coefficients of the function (a_0, a_1, a_2, a_3) are constants. Where the form of the function is a polynomial in both I and H and can easily be obtained from linear regression using data supplied by the manufacturer.

At any solar radiation, ambient temperature and head, the I-V-H function is used to find the I-V characteristics of the PV pumping system. Equations for the I-V relationship of the PV array, and Equation for the I-V relationship of the motor-pump for a given head, are solved simultaneously to find the system operating point. The second function (motor-pump characteristic) relates the pump flow (Q) to voltage (V) and head (H) and can be expressed as

$$Q = F_2(V, H) \quad \text{..... (14)}$$

$$Q = b_0 + b_1 I + b_2 H \quad \text{..... (15)}$$

The coefficients of the function (b_0, b_1 and b_2) are constants. The coefficients of the above equations can be found from the data sheet provided by the manufacturer of the solar pump.

The mechanical part modeling of an electric motor is given by

$$T_e = J_m p w_m + B_m w_m + T_l \quad \text{..... (16)}$$

Where B_m = Viscous friction co-efficient

J_m = Total inertia of the motor shaft

T_l = Load torque in N/m.

In this case of centrifugal pump T_l is given by

$$T_l = T_p = A_p w_m^2 \quad \text{..... (17)}$$

$$\text{Where } A_p = \frac{P_n}{w_m^3} \quad \text{..... (18)}$$

The centrifugal pump is also described by an H (Q) characteristic equation given by

$$H = C_1 w_m^2 - C_2 w_m Q - C_3 \quad \text{..... (19)}$$

The pump performance is predicted by specifying a load curve given by

$$H = H_g + \Delta H \quad \text{..... (20)}$$

Where H_g = Geometrical head which is the difference between the free level of the water to the pump and the highest point of canalization

ΔH = Pressure losses in the canalization which is given by

$$\Delta H = \left(\frac{\lambda l}{d} + \xi\right) \frac{8Q^2}{\pi^2 d^4 g} \quad \text{..... (21)}$$

Where λ = Co-efficient of regular pressure losses in the canalization

l = Length of canalization

d = Diameter of canalization

ξ = Co-efficient of pressure losses in elbows and canals

2.9 Efficiency of the system

The performances of the PVP system can be explained in term of its efficiency. The efficiency is categorized into photovoltaic efficiency η_{pv}, $efficiency$ of sub-system η_{sub} and total efficiency or system efficiency η_{sys}. The photovoltaic efficiency η_{pv} is the comparison between energy output of the solar generator and irradiation. The PV efficiency depends on the quality and kind of the crystal (cell). The mono-crystal has efficiency higher than the poly-crystal. The PV efficiency is written by the following equation:

$$\eta_{pv} = \frac{V_{SG} I_{SG}}{G * A_{pv}} * 100\% \quad \text{..... (22)}$$

Where A_{pv} is total area of the solar generator [m^2]; V_{SG} voltage output [V] and I_{SG} current output [A] of the solar generator. The PV efficiency is also dependent on the impedance load.

The subsystem efficiency η_{sub} is the ratio between the hydraulic power and the power of the solar generator. The value of η_{sub} reflects the efficiencies: dc-dc converter, motor and pump. The subsystem efficiency is:

$$\eta_{sub} = \frac{Q * H}{0.367 * V_{SG} * I_{SG}} * 100\% \quad \text{..... (23)}$$

Where Q = pump flow rate (lit/sec), H = Head of the pump (in m)

The total efficiency η_{sys} is the comparison between the energy output and the energy input to the system. The total efficiency is an integration of several efficiencies: PV efficiency and subsystem efficiency and can be written as:

$$\eta_{sys} = \eta_{pv} * \eta_{sub} = \frac{Q * H}{0.367 * G * A_{pv}} * 100\% \quad \text{..... (24)}$$

CHAPTER 3

STEADY-STATE PERFORMANCE ANALYSIS

3.1 Introduction

The steady-state performance of PM (Permanent magnet DC) and series motors coupled to centrifugal pump supplied from Photovoltaic source through intermediate buck-boost converter is analyzed. The effect of duty ratio selection based on maximum power operation (MP) of PV source and maximum daily gross mechanical power (GME) is analysed on the solar cell array operating point, motor armature voltage, armature current and motor effciency variation. Analysis has been carried out by formulating the mathematical models for individual components such as photovoltaic source (SCA), DC motors, power converter (DC-DC converter), Centrifugal Pump load and volumetric pump.

Starting torque variation, Torque magnification factors expressions are derived and their variations are plotted for the above two cases. Steady-state performance characteristics are tabulated and graphically shown for both cases of operation. The performance of PM DC motor is compared with the series motor operating under identical conditions. The tabulated (Calculated) values are used for training the Artificial Neural network (ANN) for modeling the control of Centrifugal pump. Data from manufacturer's data sheet is used for training the neural network in case of controlling volumetric pump.

3.2 Mathematical model of the system for steady-state analysis

The system consists of solar cell array (SCA), DC-DC converter (Intermediate converter) and DC motor coupled to centrifugal pump as shown in Fig. 16. The DC-DC converter is a buck-boost converter with variable duty ratios, which regulates the motor voltage and current such that SCA operates at maximum power point (MP), or gross mechanical energy (GME) output point. The DC motor may be either PM DC motor or series motor coupled to centrifugal pump load. Mathematical models are developed in the following sections for individual components and combined together for the performance studies.

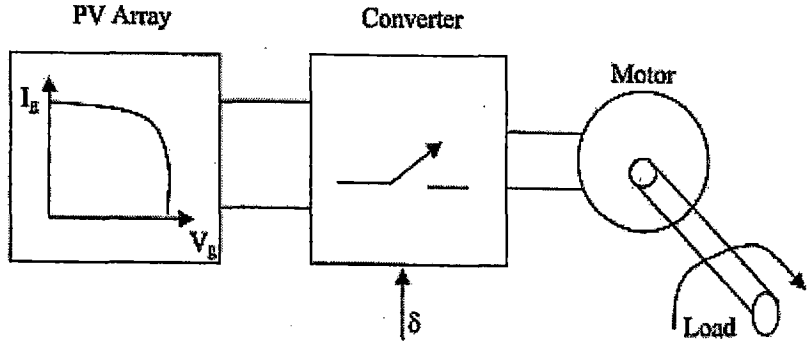

Fig. 16. Schematic diagram of pumping system

3.2.1 PV Generator Model

The PV array that converts the solar insolation into electrical energy consists of several solar cells connected in series and parallel fashion in order to form a PV source capable of delivering desired voltages, currents. The solar insolation dependent V-I characteristic of the PV array with Ns cells in series and Np cells in parallel is given by the following equation

$$V_g = I_g R_s \left(\frac{N_s}{N_p}\right) + \left(\frac{N_s}{\Lambda}\right) \ln \left\{1.0 + \left(\frac{N_s I_{ph} - I_g}{N_p I_0}\right)\right\} \quad \text{.....(25)}$$

$$V_g = I_g R_{sg} + \frac{1}{\Lambda_g} \ln \left\{1.0 + \left(\frac{I_{phg} - I_g}{I_{0g}}\right)\right\} \quad \text{.....(26)}$$

Where $\wedge = (q/AKT)$, $\wedge_g = \frac{\wedge}{N_s}$

q = Electric charge, A = Completion factor =1.0

K = Boltzmanns constant, T = Absolute Temperature

R_{sg} = Series resistance

I_{sg} = Insolation dependant photo-current

I_{og} = Cell reverse saturation current

The PV generator considered in this work consists of 18 parallel paths and each path contains 324 cells in series. After substituting the cell constants the V-I characteristic of the PV generator becomes

$$V_g = -0.9I_g + 23.697 \ln\{1.0 + \left(123.456\left(13.45K_i - I_g\right)\right)\} \quad \text{..... (27)}$$

Where K_i is the percentage of insolation.

3.2.2 Power Converter Model

The intermediate DC-DC converter is a buck-boost converter with a variable duty ratio. This converter produces a chopped output DC voltage regulating the motor voltage and current and continuously matches the output characteristics of the PV generator to the input characteristic of the motor so that maximum power (MP) is extracted from the SCA or the gross mechanical energy (GME) per day of the system is maximum. Assuming the DC-DC converter is ideal, the output voltage and current of the converter] for a duty ratio of δ is related to the solar cell voltage V_g by the following equation

$$V_{av} = V_g Y \quad \text{..... (28)}$$

$$I_{av} = \left(\frac{I_g}{Y}\right) \quad \text{..... (29)}$$

$$\delta = \left(\frac{t_{on}}{T_p}\right) \quad \text{..... (30)}$$

$$Y = \left(\frac{\delta}{1-\delta}\right) \quad \text{..... (31)}$$

Where Y = Chopping ratio of the buck-boost converter

δ = Duty-ratio of the converter

T_p = Time-period of buck-boost converter

3.2.3 Model of the DC Motor

When the DC motor is supplied from PV generator through intermediate power modulator/converter, the motor voltage and torque equations under steady state are

$$V_{av} = E_b + R_a I_{av} \text{ ... ...} \quad (32)$$

$$T_e = K_t I_{av} \Phi \text{.....} \quad (33)$$

$$E_b = K_b w_m \Phi \text{.....} \quad (34)$$

For PM DC motor flux is constant hence the above equations becomes

$$V_{av} = E_b + R_{ap} I_{av} \text{ ... ...} \quad (35)$$

$$T_e = C_e I_{av} \text{.....} \quad (36)$$

$$E_b = C_e w_m \text{ ... ...} \quad (37)$$

For series motor assuming linear magnetic conditions Eqs. (32)- (34) becomes

$$V_{av} = E_b + R_{af} I_{av} \text{ .....} \quad (38)$$

$$T_e = M_{af} I_{av}^2 \text{ .....} \quad (39)$$

$$E_b = M_{af} I_{av} w_m \text{ .....} \quad (40)$$

Here $R_{af} = R_a + R_f$

3.2.4 Model for the Pump loads

Pumps may be volumetric or centrifugal types having different head vs. flow characteristics. These pump-loads will develop speed dependent torques. In these studies a centrifugal pump and a volumetric pump is considered whose speed-torque characteristic including friction torque given by the following equations

The speed-torque characteristic of centrifugal pump is given by the following equation:

$$T_l = A_1 + B_1 w + C_1 w^{1.8} \quad \text{..... (41)}$$

The speed-torque characteristics of volumetric pump loads including friction torque is given by equation 42.

$$T_l = A_1 + B_1 w + C_1 w^{1.8} \quad \text{..... (42)}$$

3.3 Performance analysis in steady-state operation

3.3.1 Maximum power operation of SCA

For maximum utilization of SCA, a power converter is introduced in between SCA and motor. The duty ratio of the converter is changed accordingly to match the load to SCA. Assuming power converter is ideal, all of the array power is delivered to the motor. When SCA operating at maximum power point, the power absorbed by the motor is equal to the power delivered by the SCA, i.e.

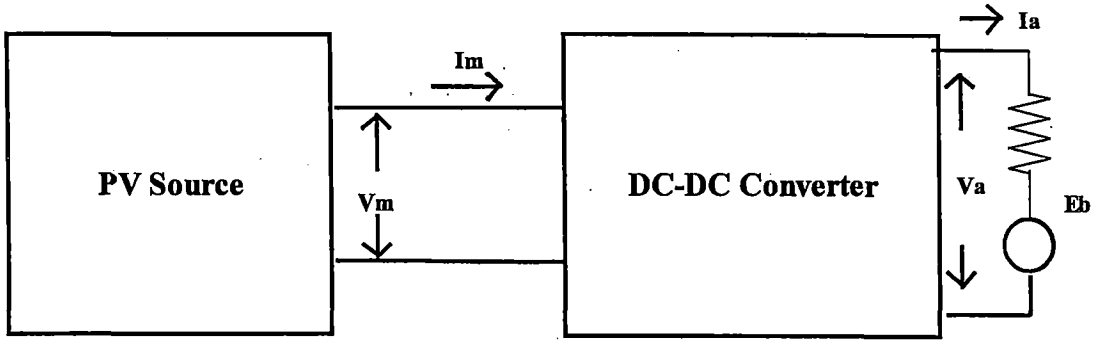

Fig. 17. Equivalent circuit of the combined system.

$$P_m = V_m I_m \quad \text{..... (43)}$$

$$P_m = V_{av} I_{av} \quad \text{..... (44)}$$

Where V_m, I_m is PV array voltage, current, respectively, at maximum power point; V_{av}, I_{av} is the motor armature voltage, current respectively at maximum power point of SCA. The motor armature voltage and currents are expressed in terms of SCA voltage and current at maximum power point as

$$V_{av} = \delta_{mp} V_m \quad \text{..... (45)}$$

$$I_{av} = \frac{I_{mp}}{\delta_{mp}} \quad \text{..... (46)}$$

Transforming the motor equivalent circuit to SCA side then the motor armature voltage equation becomes

$$V_m = \left(\frac{E_b}{\delta_{mp}}\right) + I_{mp} \frac{R_a}{\delta_{mp}^2} \quad \text{..... (47)}$$

Simplifying the above equation

$$V_m \delta_{mp}^2 - E_b \delta_{mp} - I_m R_a = 0 \quad \text{..... (48)}$$

For the above quadratic equation two solutions exist. Since the duty ratio can never be negative, the expression which gives positive duty ratio is

$$\delta_{mp} = \frac{E_b}{2V_m} + \left(\left(\frac{E_b}{2V_m}\right)^2 + \left(\frac{I_m R_a}{V_m}\right)\right)^{\frac{1}{2}} \quad \text{..... (49)}$$

For a given SCA maximum power the motor armature current is obtained from the following equations:

$$P_m = E_b I_{av} + I_{av}^2 R_a \quad \text{..... (50)}$$

$$R_a I_{av}^2 + E_b I_{av} - P_m = 0 \quad \text{..... (51)}$$

$$I_{av} = -\frac{E_b}{2V_m} + \left(\left(\frac{E_b}{2V_m}\right)^2 + \left(\frac{P_m}{R_a}\right)\right)^{\frac{1}{2}} \quad \text{..... (52)}$$

Where E_b is given by Eq. (37) for PM motor and Eq. (40) for series motor. The duty ratio of the converter depends (Eq. (49)) on the motor back emf, which in turn depends on motor load. When the DC motor coupled to the centrifugal pump-load Eq. (41), for a given SCA maximum power (P_m, V_m, I_m) the back emf is obtained by solving Eqs. (36), (41) and (52) for

PM DC motor; (39), (41) and (52) for series motor. Once back emf is calculated corresponding toP_m, the duty ratio of the converter, motor voltage and current are obtained. Efficiency of the motor is calculated from the following equation:

$$\eta = \left(\frac{\text{Motor input}-\text{losses}}{\text{Motor input}}\right) * 100 \quad \ldots\ldots (53)$$

3.3.2 Maximum Gross Mechanical Energy output from SCA

For a given value of flux coefficient of the machine it is not possible to make the SCA and motor to operate at maximum power points (P_m, V_m, I_m) at all solar insolations. This is because of the motor V-I characteristic dependent on motor flux coefficient and copper losses in the machines. In such cases the system is made to operate at a point (P_m^*,V_m^*, I_m^*) of gross mechanical energy output per day for a given insolation curve. At these operating points the machine under consideration, the optimal parameters (Saied, 1988) make the combined system operate at maximum gross mechanical energy output. At a given solar insolation the voltage and current (V_m, I_m) corresponding to MP operation are determined. With these (V_m, I_m) the voltage and currents (V_m^*, I_m^*) corresponding to GME operation are computed using the following equations.

$$V_m^* = \frac{V_m(2R_a+89.8\, I_m^{0.127})}{(R_a+89.8\, I_m^{0.127})} \quad \ldots\ldots (54)$$

$$I_m^* = \frac{89.8\, I_m^{0.873})}{(R_a+89.8\, I_m^{0.127})} \quad \ldots\ldots (55)$$

$$P_m^* = V_m^* * I_m^* \quad \ldots\ldots (56)$$

$$I_{av}^* = -\frac{E_b^*}{2V_m} + \left(\left(\frac{E_b^*}{2V_m}\right)^2 + \left(\frac{P_m^*}{R_a}\right)\right)^{\frac{1}{2}} \quad \ldots\ldots (57)$$

Where back emf (E_b^*) is calculated using Eqn. (37), Eqn. (41), and Eqn. (57) in case of centrifugal pump load; Eqn. (37), Eqn. (42), and Eqn. (57) in case of volumetric pump load at different solar insolations. Knowing (E_b^*) the duty ratio of the buck-boost converter for GME operation is obtained from the following equation.

$$\delta_{mg}^* = \frac{E_b^*}{2V_m} + \left(\left(\frac{E_b^*}{2V_m}\right)^2 + \left(\frac{I_m^* R_a}{V_m}\right)\right)^{\frac{1}{2}} \quad \text{..... (58)}$$

3.3.3 The torque magnification factor

Matching the solar cell array to the motor by means of maximum power point tracker (MPPT) the motor starting torque can be increased as compared to without MPPT. The torque magnification factor for PM DC motor is

$$m_T = \left(\frac{I_m}{I_{sc}}\right)\sqrt{\frac{V_m}{I_m R_a}} \quad \text{..... (59)}$$

For series motor it is

$$m_T = \left(\frac{I_m}{I_{sc}}\right)^2\sqrt{\frac{V_m}{I_m R_{af}}} \quad \text{..... (60)}$$

The increase in the starting torque magnification factor for gross mechanical energy operation as compared to maximum power operation of SCA is obtained. The torque magnification factor for gross mechanical power operation for PM DC motor is

$$m_T^* = \left(\frac{I_m^*}{I_{sc}}\right)\sqrt{\frac{V_m^*}{I_m^* R_a}} \quad \text{..... (61)}$$

At gross mechanical energy output

$$V_m^* = k_v V_m \quad \text{..... (62)}$$

$$I_m^* = k_I I_m \quad \text{..... (63)}$$

From Eqs. (62)- (63)

$$m_T^* = \left(\sqrt{K_v} K_I\right) m_T \quad \text{..... (64)}$$

The torque magnification factor at gross mechanical energy operation for series motor is

$$m_{TS}^{*} = \left(\frac{I_m^{*}}{I_{sc}}\right)^2 \sqrt{\frac{V_m^{*}}{I_m^{*} R_{af}}} \quad \text{..... (65)}$$

From Eqs. (41), (42) and (44)

$$m_{TS}^{*} = (K_v K_I) m_{TS} \quad \text{..... (66)}$$

3.3.4 Variation of motor starting torque with solar insolation

Defining solar radiation starting torque factor 't(s)' by the ratio of the motor starting torque at an arbitrary solar insolation '*s*' to the starting torque at a reference solar insolation 'S_r' as

$$t(s) = \frac{T_{st(s)}}{T_{st(s_r)}} \quad \text{..... (67)}$$

These torque factors for PM and series motors [9] for maximum power operation are

$$t_{PM}(s) = \sqrt{\frac{s}{s_r}} \quad \text{..... (68)}$$

$$t_s(s) = \frac{s}{s_r} \quad \text{..... (69)}$$

Assuming the array power proportional to the solar insolation, the above torque factors for the PM and a series motor at gross mechanical power operation becomes $t_{PM}^{*}(s) = \left(\sqrt{K}\right) t_{PM}(s)$ ..... (70)

$$t_s^{*}(s) = (K) t_s(s) \quad \text{..... (71)}$$

$$\text{Where } K = \left(\frac{K_I K_V}{K_{Ir} K_{Vr}}\right) \quad \text{..... (72)}$$

3.4 Results of the Analysis

A 120 V, 9.2 A, 1500 rpm PM and DC series motors are considered for simulation studies. The parameters of the machines and load and PV generator are given in Appendix A, in Table 14 and Table 15. Based on the mathematical models developed in the preceding Section the converter chopping ratio's are calculated at different solar insolations (1 p.u. =100% solar insolation=1000 W/m^2).

Figs. (18-23) represents the steady-state simulation results obtained for the above two cases. From the Fig. 19B and 19D it is observed that the armature voltages for both the motors are higher for GME operation than MP operation satisfying the relation ($V_m^* > V_m$). For a given solar insolation (Fig. 21) the chopping ratio of the converter is smaller for maximum power operation of SCA than the gross mechanical energy output operation, since ($V_m^* > V_m$) under such conditions the motor armature current decreases ($I_m^* > I_m$) which in turn decreases the copper losses as shown in Fig. 20B and 20D resulting in reduced thermal loading on the machines. We have A, B, C and D designated as below.

A- PM motor maximum power operation.

B- PM motor gross mechanical energy operation.

C- Series motor maximum power (MP) operation.

D- Series motor gross mechanical energy (GME) operation.

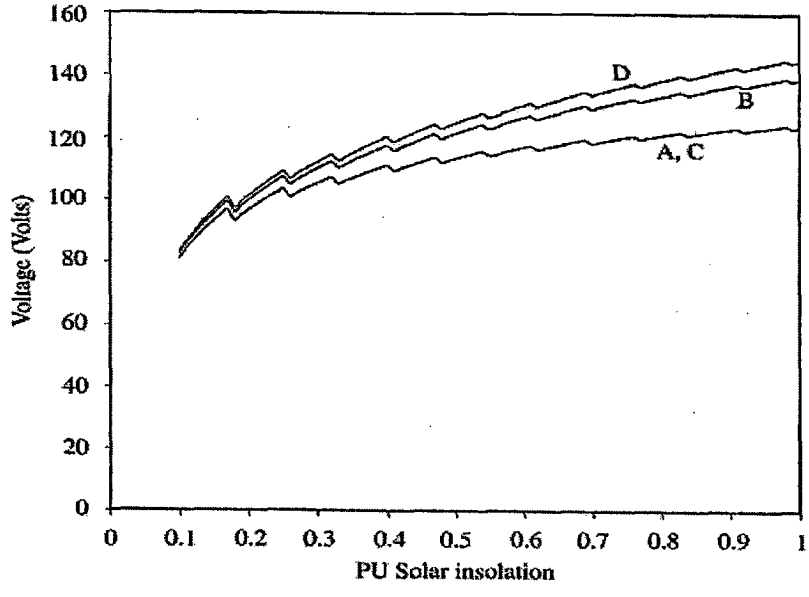

Fig. 18. PV array voltage variation for MP, GME operations.

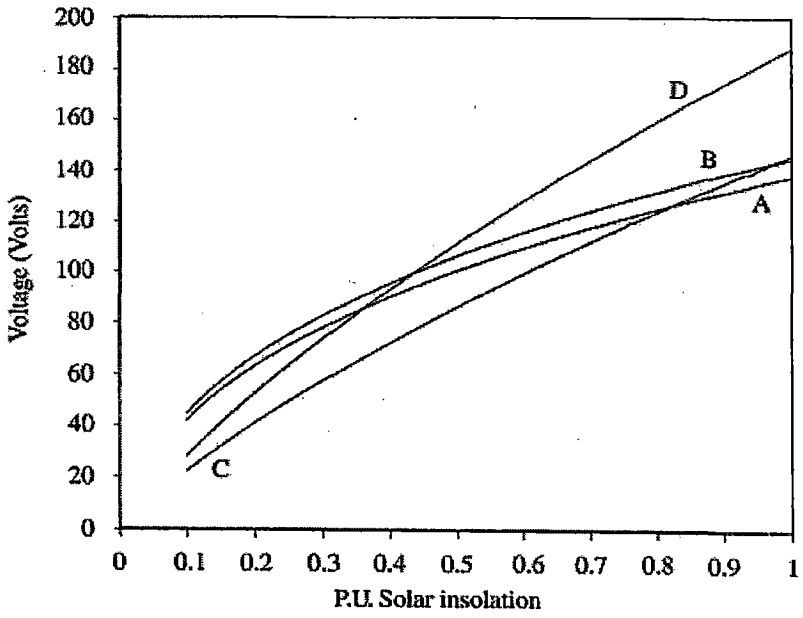

Fig. 19. PM and series motor armature voltage variation.

For both the machines on account of reduced losses, the GME operation results in efficiency improvement which is depicted in Fig.21. But, the efficiency of the series motor is slightly lesser value than the PM motor for the obvious reasons of additional losses in the series field and increases with solar insolation. Further, the series motor efficiency reduction is more at lower solar insolations for both GME and MP operations. In case of PM DC motor efficiency is higher at lower solar insolations because of $V_{PM} > V_{SE}, I_{PM} < I_{SE}$ and falls slightly with increase in insolation.

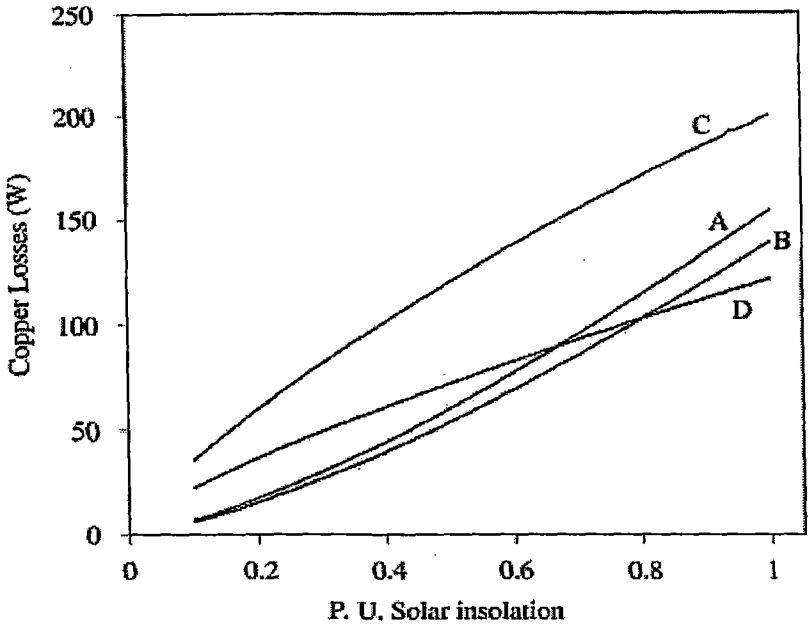

Fig. 20. PM and series motor armature copper losses.

From Fig. 23 when the system is operating at maximum daily gross mechanical energy output the starting torque magnification factors increases for the PM motor, decreases for the series motor with solar insolation. Fig. 23H indicates that, at GME operation the starting torque variation with solar insolation as compared to MP operation is more in case of series motor. However, the variation of motor starting torque with solar insolation is very much influenced by the gross mechanical power operation for the series motor than the PM DC motor. From the simulation studies it is found that the PM DC motor with optimal value of '*Ce*' gives higher motor efficiencies at gross mechanical energy operation as compared to series motor.

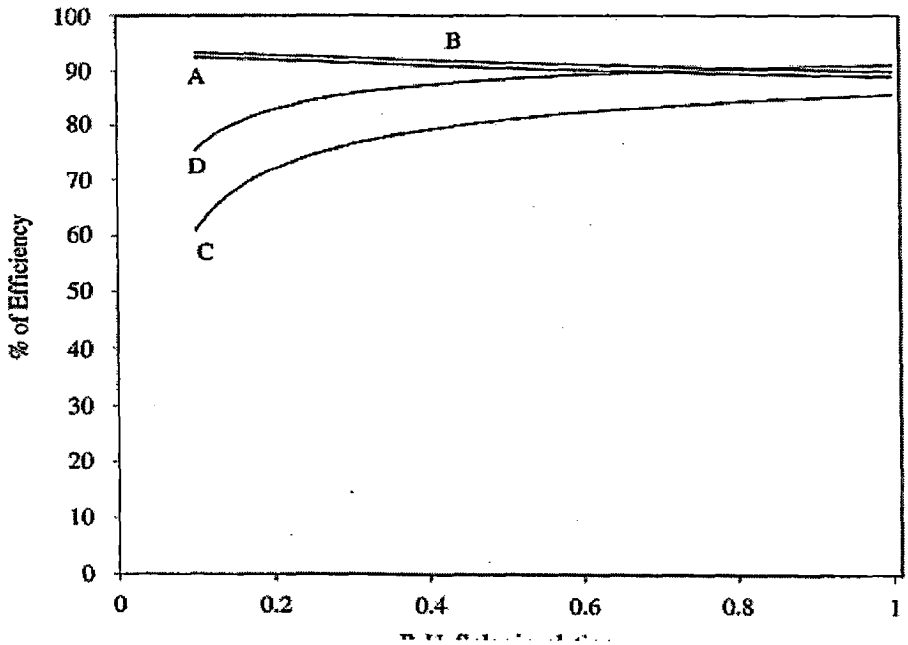

Fig. 21. Variation of PM and series motor efficiency.

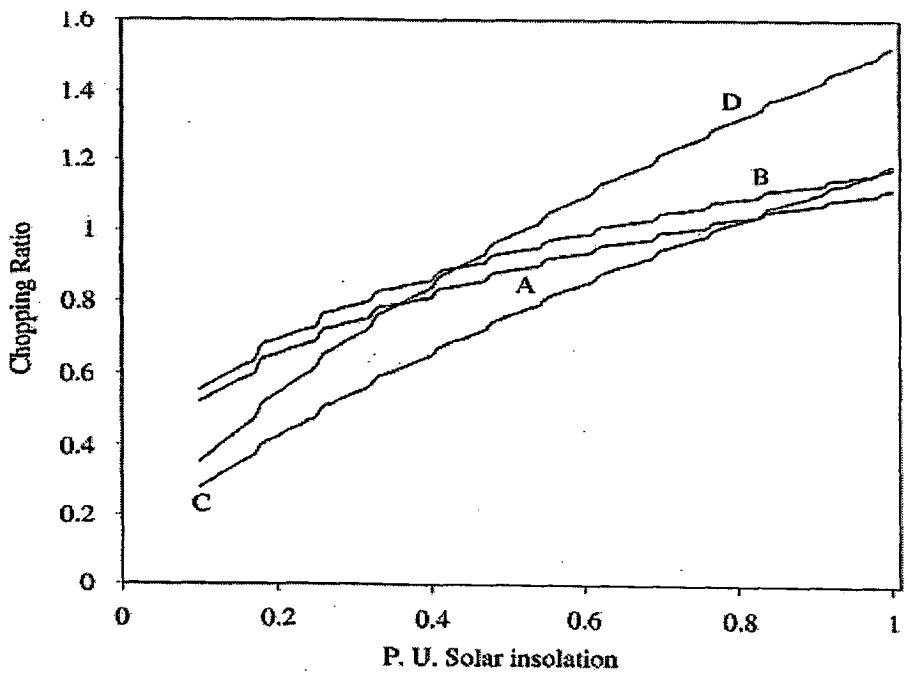

Fig. 22. Power converter chopping ratio variation for MP, GME operations.

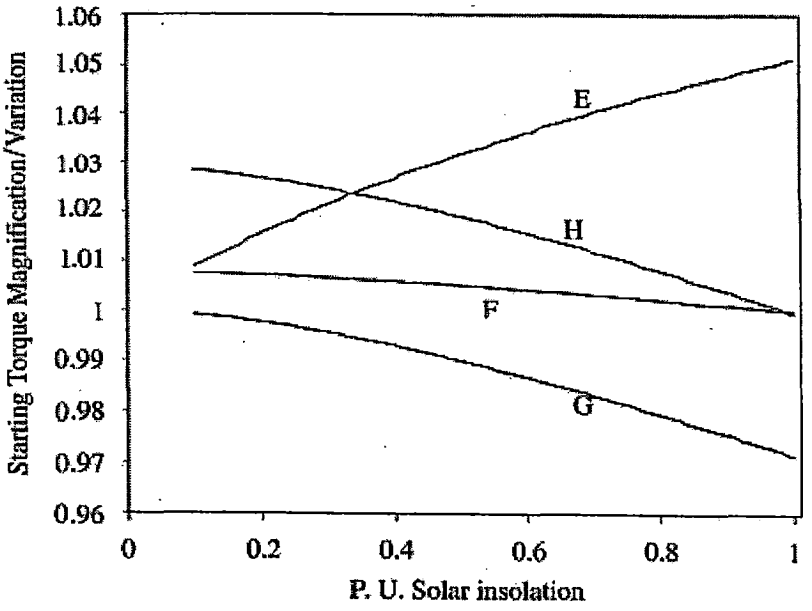

Fig. 23. PM and series motor starting torque magnification.

In the above figure E, F, G and H are given below.

E- Starting Torque ratio with GME operation to MP operation of PM motor

F- Starting Torque ratio with GME operation to MP operation of series motor

G- Starting Torque variation ratio with GME operation to MP operation of PM motor

H- Starting Torque variation ratio with GME operation to MP operation of series motor

CHAPTER 4

ANN MODEL FOR CONTROLLING PHOTOVOLTAIC PUMP

4.1 Introduction

The present work brings out the identification of optimal point (corresponding to MP or GME operation) of the PV supplied separately excited dc motor and series motor fed from intermediate power converter driving centrifugal pump or volumetric pump loads. The converter-chopping ratio is selected adaptively using ANN to get maximum power from SCA or GME output from the combined system. This off-line training approach avoids adjustment of optimal operating point through trial and error procedure and does not require high-resolution sensors.

4.2 Statement of Problem

The problem is to design an off-line non-adaptive controller by using Artificial Neural Network for obtaining the MP or GME operation of the PV supplied dc motor system. These MP or GME operations can be achieved at different solar insolations by controlling the power converter duty ratio, which is adjusted by the ANN controller. The SCA operating point is shifted to its maximum power point by using a voltage control type inverter, which is identified by the ANN.

4.3 Functional Block Diagram of the system

Based on the mathematical models developed in the preceding Sections the converter chopping ratios are computed for the following two cases of operation

1. Maximum power operation of SCA at different solar insolations.
2. Gross mechanical energy output operation at different solar insolations for two load torques mentioned above.

The basic functional diagram of the combined system is depicted below where the intermediate DC-DC converter's Chopping ratio is adaptively controlled by a neural network controller.

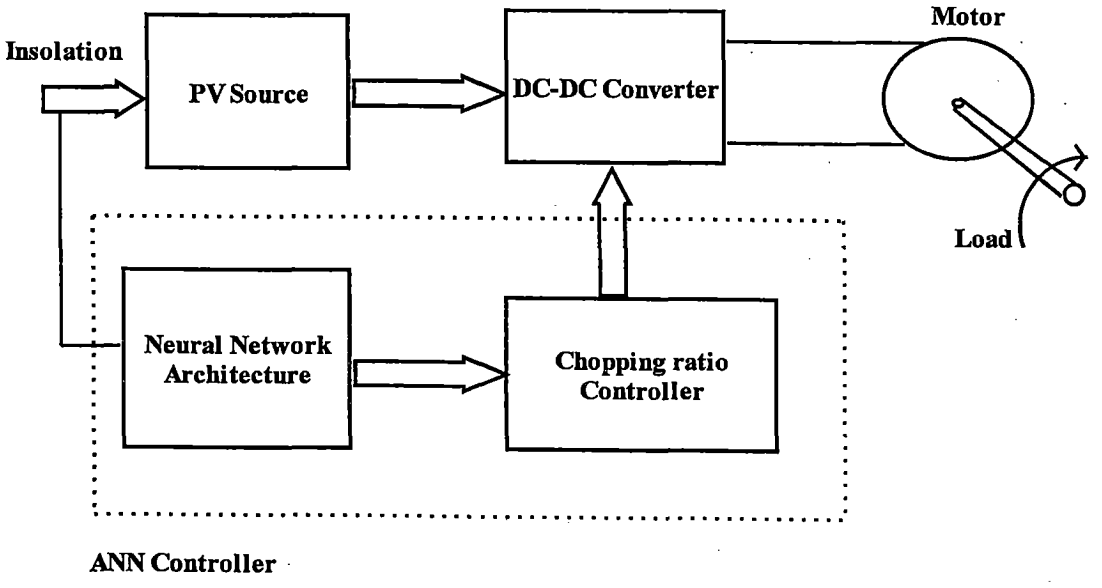

Fig. 24. Functional Block Diagram of Combined system.

4.4 Block diagram for ANN training

The ANN training block diagram for MP or GME operation is shown in Fig. 24. Using the mathematical models developed in preceding Sections the reference patterns for MP and GME operation are computed. Block-1 represents these reference patterns. The ANN training is performed by initially assigning random values to the weight terms. Gradient descent algorithm is used in the training, as it improve the performance of the ANN by reducing the total error by changing the weights along its gradient. The learning rate is close to the computed values. The training process was terminated as and when the mean square error E is less than the specified value.

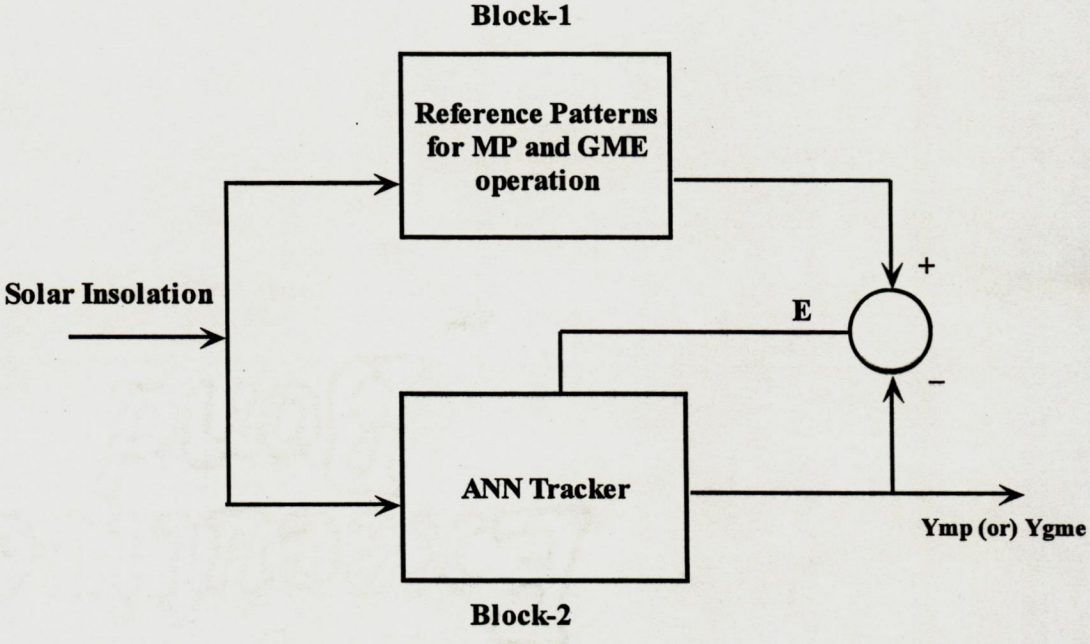

Fig. 25 Block diagram for ANN training

4.5 ANN Architecture

The ANN model/Architecture for the combined system is shown below in fig. 26. The architecture consists of three neural layers with each layer having different no. of neurons. Input layer consists of single input which is percentage of solar insolation (Kins). The hidden layer consists of varied number of neurons for different conditions and for each case the results were analysed on the complexity of the system as a whole. The output layer consists of a single neuron. The output from the neural network is chopping ratio (Y). The model is same for both centrifugal pump and volumetric pump. The chopping ratios are predicted for each pump load for both maximum power operation and gross mechanical energy operation. The values of input pattern (Kins) for training neural network is calculated from the method mentioned above and subsequently chopping ratios (output values of the neural network).

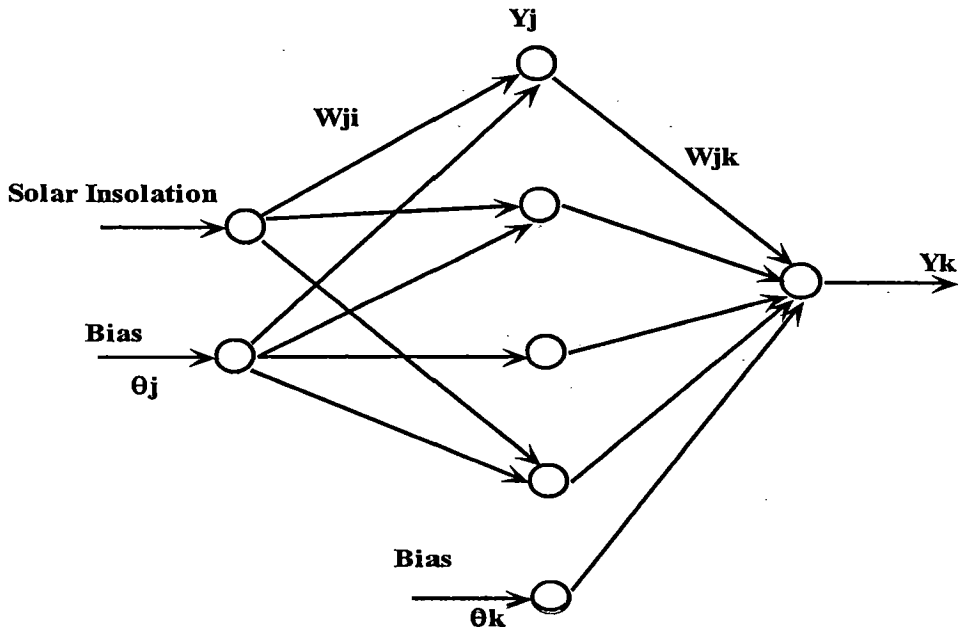

Fig. 26. Schematic diagram of an artificial neural network.

4.6 ANN Training

The work has been performed in **MATLAB7.0.** The training was performed using TRAINGDM (gradient descent algorithm) .The following procedure/steps has been followed for training the network.

Step 1: Construct the network and initialize the synaptic weights with random values.

Step 2: Apply an input vector to the network and calculate the corresponding output values.

Step 3: Compare the actual outputs with the desired outputs and determine a measure of the error.

Step 4: Determine the amount by which each weight is to be changed and make corrections to each weight.

Step 5: Repeat step 2 to step 4 with all the training vectors until the error for the vectors in the computed and predicted values of chopping the training set is reduced to an acceptable value.

4.7 MATLAB/SIMULINK model for the neural network

MATLAB/SIMULINK model of the developed architecture of neural network is depicted below using MATLAB 7.0 command **gensim (net,-1).** This command generates a SIMULINK block for neural network simulation.

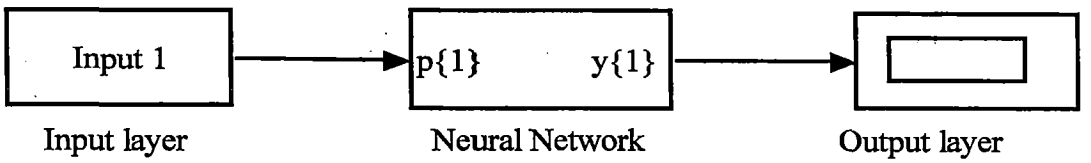

Fig. 27. Block model for input layer1.

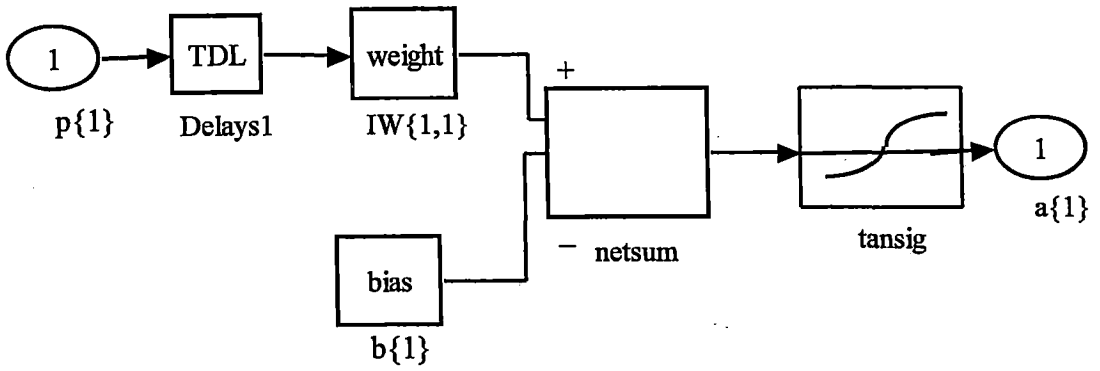

Fig. 28. Block model for input layer 1.

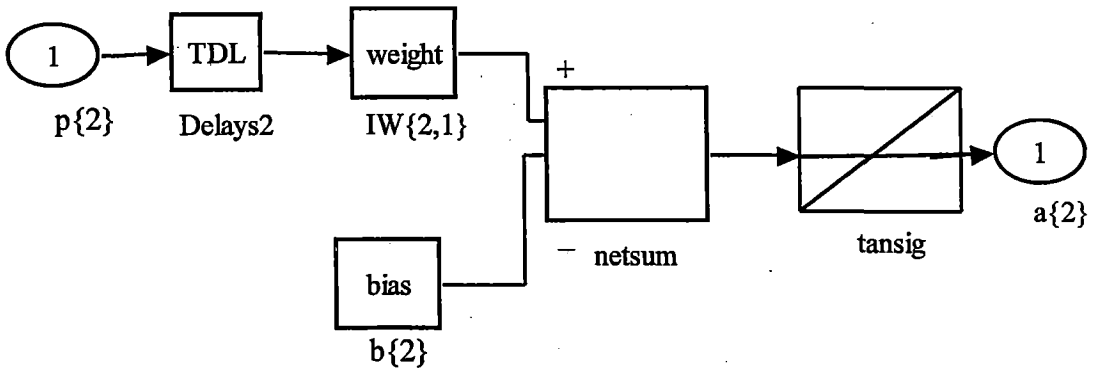

Fig. 29. Block diagram for layer 2.

4.7.1 Feed-forward neural network architecture

The created feed-forward multi-layer perceptron model neural network has been trained with Back-propagation algorithm. The architecture of a multilayer network is not completely constrained by the problem to be solved. The number of inputs to the network is constrained by the problem, and the number of neurons in the output layer is constrained by the number of outputs required by the problem. However, the number of layers between network inputs and the output layer and the sizes of the

layers depend on the type of application. The neural network consists of three layers with different transfer or activation functions. The application of a particular type of transfer function depends on the range and values of the training inputs and their corresponding outputs. The learning or training employed is supervised biased learning with bias values of each layer randomly generated by the computer. The network is trained with initial random weights generated by the computer.

4.7.2 Training function (TRAINGDM)

The performance function or error criteria (goal) for the algorithm have been Mean square error (MSE). The training algorithm used is TRAINGDM (Gradient Descent method). Gradient descent algorithm is used, as it improves the performance of ANN by reducing the total error by changing weights along its gradient. An adaptive learning rate will keep the learning step size as large as possible. An adaptive learning rate requires some changes in the training procedure used by 'traingdm'. First, the initial network output and error are calculated. At each epoch new weights and biases are calculated using the current learning rate. New outputs and errors are then calculated learning stable. The learning rate is made responsive to the complexity of the local error. As with momentum, if the new error exceeds the old error by more than a predefined ratio max_perf_inc (typically 1.04), the new weights and biases are discarded. In addition, the learning rate is decreased (typically by multiplying by lr_dec = 0.7). Otherwise, the new weights are kept. If the new error is less than the old error, the learning rate is increased (typically by multiplying by lr_inc = 1.05). This procedure increases the learning rate, but only to the extent that the network can learn without large error increases. Thus, a

near-optimal learning rate is obtained for the local terrain. When a larger learning rate could result in stable learning, the learning rate is increased. TRAINGDM is a network training function that updates weight and bias values according to gradient descent with momentum.

4.7.3 Limitations and cautions of TRAINGDM

The gradient descent algorithm is generally very slow because it requires small learning rates for stable learning. The momentum variation is usually faster than simple gradient descent, since it allows higher learning rates while maintaining stability, but it is too slow for many practical applications. These two methods would be used only when incremental training is desired. You can use Levenberg-Marquardt training for small and medium size networks, if you have enough memory available. If memory is a problem, then there are a variety of other fast algorithms available.

4.7.4 Transfer or Activation functions

The selection of activation function plays an important role in designing neural network. In the present model (network) a bipolar sigmoid function f [u (t)] = tanh [g.u (t)] for the hidden layer and linear function f [u (t)] = g.u for the output layer were considered. The transfer functions used in the proposed neural network are TANSIG and PURELIN. The training input vectors which are % of solar insolation are values which range between 0 and 1.So, the transfer function used in the input layer is TANSIG. The transfer function used in the output layer is PURELIN. The output of network can take any value as it is with pure linear transfer function. The output of neural network which is chopping ratio can take any value as

calculated in the preceding section. Neurons of this type are used as linear approximators in various applications like linear filters.

4.7.4.1 TANSIG activation function

Multi-layer feed-forward and other neural network architectures use tan-sigmoid transfer function tansig. The input-output characteristic of tan-sigmoid transfer function is shown below.

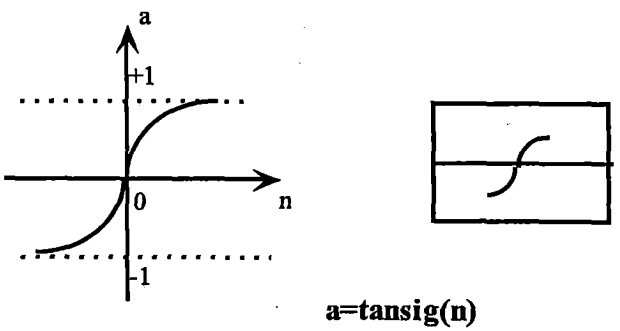

Fig. 30. Input-Output characteristic of tan-sigmoid function

4.7.4.2 PURELIN activation function

The input-output characteristic of pure-linear activation function is shown in the following graph and the corresponding to it.

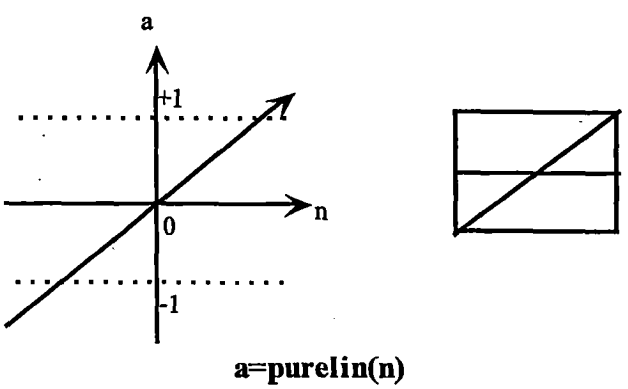

Fig. 31. Input-Output characteristic of pureline activation function

CHAPTER 5

SIMULATION RESULTS

5.1 Introduction

This chapter presents the results of ANN training for all the three training conditions mentioned in chapter 4. Training performance for each training condition and for each mode of operation i.e., MP operation and GME operation is analyzed in terms of ANN prediction of output chopper values and percentage error.

5.2 Training of Neural network for MP operation of SCA

A 120V, 9.2A, 1500 rpm PV supplied PM dc separately excited motor driving both centrifugal pump load and volumetric pump load was modeled using mathematical models of individual components and controlled by a neural network. The architecture of the network has been discussed in the previous section. Training has been performed on various architectures using traingdm training function algorithm and back-propagation algorithm. The no. of input layer (neurons) and no. of output neurons are 1. This is constant for various cases of operation and for different training conditions.

The no. of epochs/iterations, error criteria and performance functions are judiciously varied and prediction or estimation results are calculated for both the pump types. Analysis has been done for the following two cases and their subsequent sub-cases.

5.2.1 Cases of Operation

Case 1: PM DC motor driving centrifugal pump.

Case 2: PM DC motor driving volumetric pump.

Case 3: Series motor driving centrifugal pump.

For each of case 1 and case 2 and case 3, two further cases are analysed and results are reported. They are given below

Case a: Maximum power point (MP) operation

Case b: Gross mechanical energy (GME) operation

5.2.1.1 Case 1a: PMDC motor driving centrifugal pump for MP operation

The training data for **case 1a** is given in the table below and the results are obtained for MP operation.

Table 1. Training data for MP operation of PMDC motor driving centrifugal pump.

% of solar insolation	Chopping ratio with MP operation for centrifugal pump (Ymp)
0.10	0.5196
0.20	0.6526
0.30	0.7410
0.40	0.8105
0.50	0.8846
0.60	0.9342
0.70	0.9919
0.80	1.0324
0.90	1.0704
1.0	1.1186

5.2.1.1.1 Results of Case 1a

The results of training and testing for **case 1a** has been carried out for three conditions. They are given below.

1. Network with 1 hidden layer with 3 neurons in hidden layer with 10000 epochs.
2. Network with 1 hidden layer with 5 neurons in hidden layer with 10000 epochs.
3. Network with 2 hidden layers with 3 neurons in each hidden layer with 10000 epochs.

The error or performance criteria is set to 1e-7 with Mean square error as its performance function (MSE).The graph below shows Training patterns (inputs) versus Target chopping ratio values.

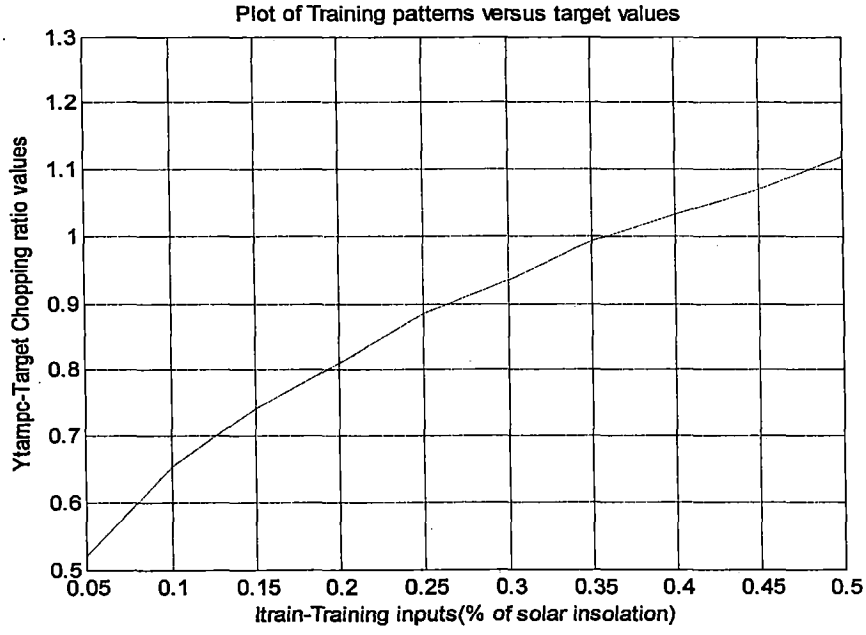

Fig. 32. Plot of Training inputs with target chopping ratio(PMDC-mpc).

5.2.1.1.1.1 Training condition 1

The training condition 1 consists of the following training parameters which are shown in table below.

Table 2. Training parameters for Training condition 1.

No. of Hidden layers	1
No. of neurons in hidden layer	3
No. of epochs	10000
Performance function (MSE) error	1e-7
Training function (Algorithm)	TRAINGDM
Learning rate (lr)	0.55
Momentum constant (mc)	0.8

The plot of computed values versus ANN predicted values of chopper duty ratio are shown in Fig. below.

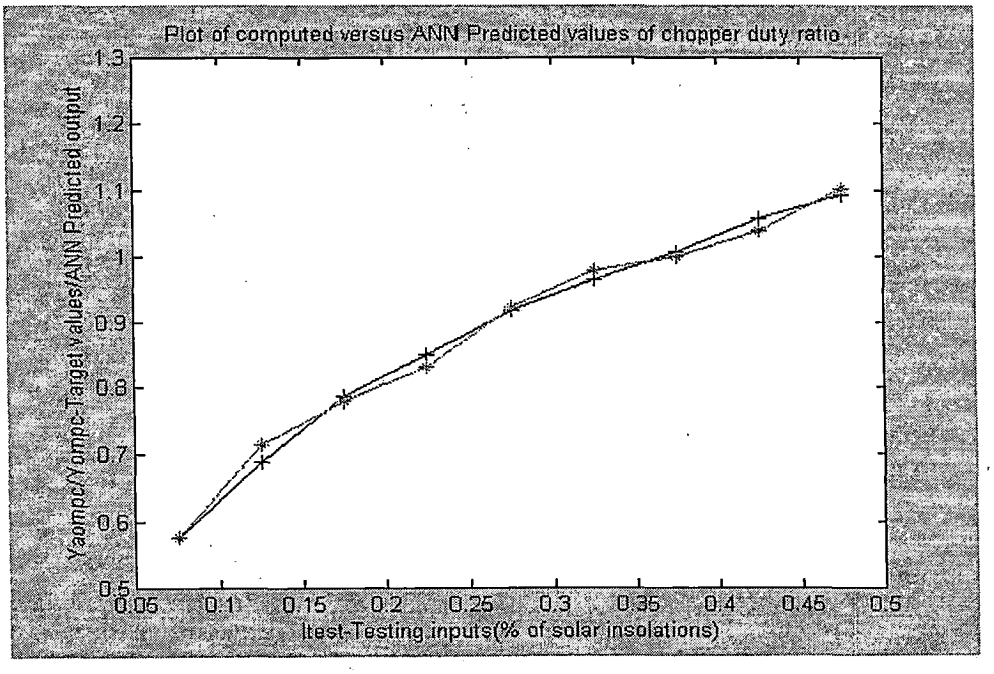

Fig. 33. Plot of calculated versus ANN predicted chopping ratios (tc1).

The plot of percentage error with testing inputs is shown below.

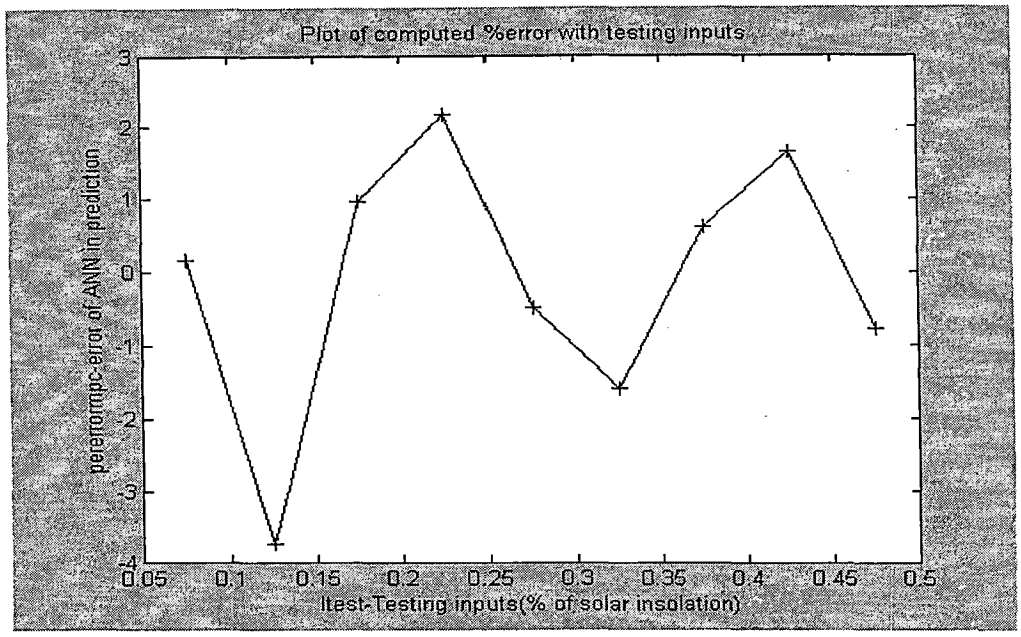

Fig. 34. Plot of percentage error versus testing inputs (tc1).

5.2.1.1.1.2 Training condition 2

The training condition 2 consists of the following training parameters which are shown in table below.

Table 3. Training parameters for Training condition 2

No. of Hidden layers	1
No. of neurons in hidden layer	5
No. of epochs	10000
Performance function (MSE) error	1e-7
Training function (Algorithm)	TRAINGDM
Learning rate (lr)	0.55
Momentum constant (mc)	0.8

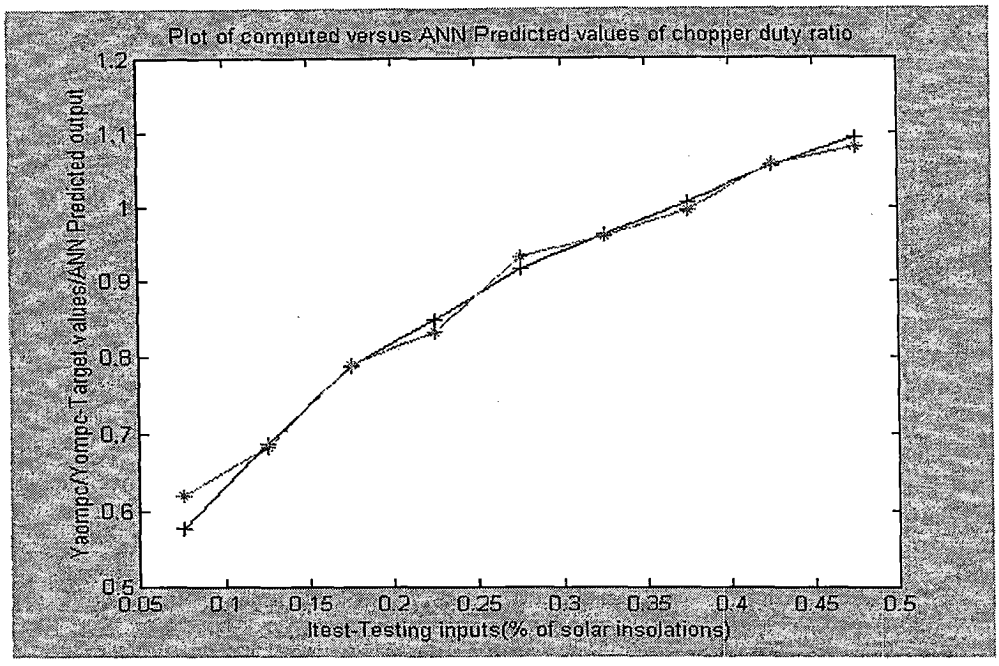

Fig. 35. Plot of calculated versus ANN predicted chopping ratio (tc2).

The plot of percentage error with testing inputs is shown below.

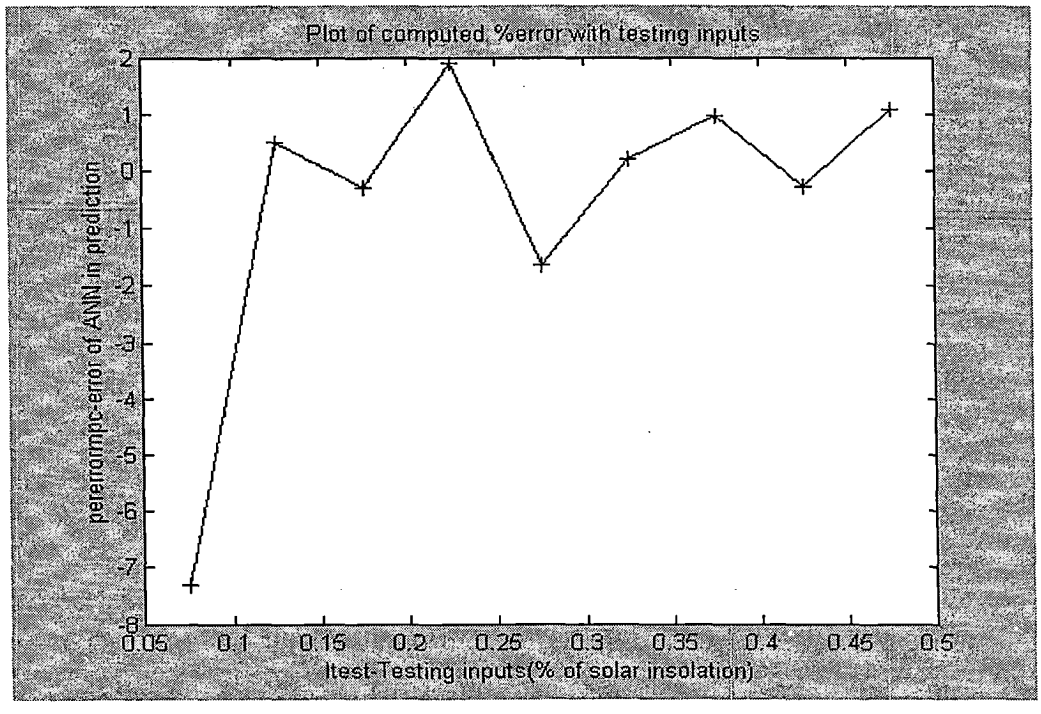

Fig. 36. Plot of percentage error versus testing inputs (tc2)

5.2.1.1.1.3 Training condition 3

The training condition 3 consists of the following training parameters which are shown in table below.

Table 4. Training parameters for Training condition 3.

No. of Hidden layers	2
No. of neurons in each hidden layer	3
No. of epochs	10000
Performance function (MSE) error	1e-7
Training function (Algorithm)	TRAINGDM
Learning rate (lr)	0.55
Momentum constant (mc)	0.8

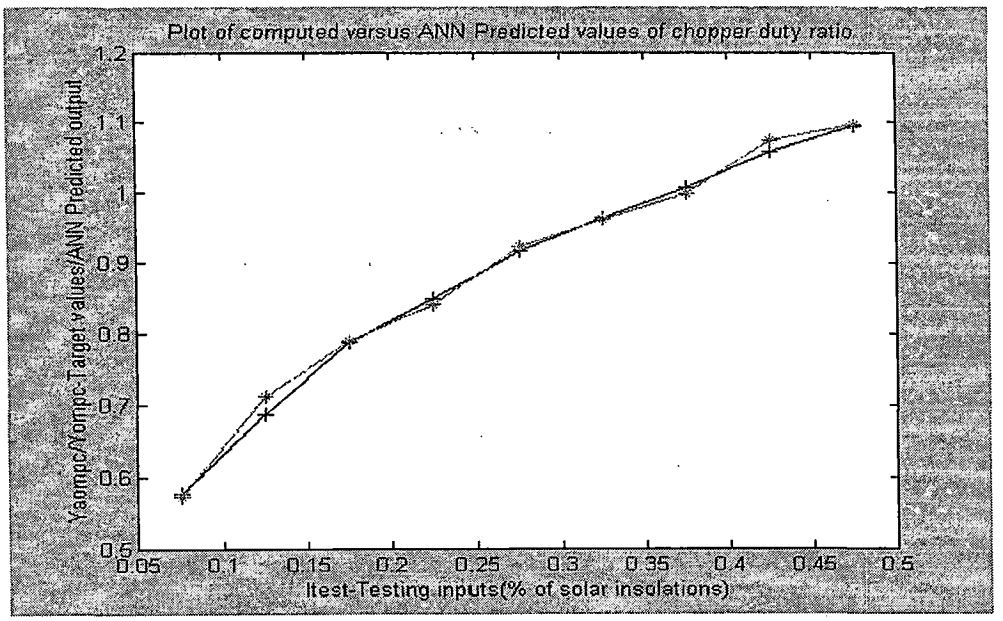

Fig. 37. Plot of calculated versus ANN predicted chopping ratio (tc3)

The plot of percentage error with testing inputs is shown below.

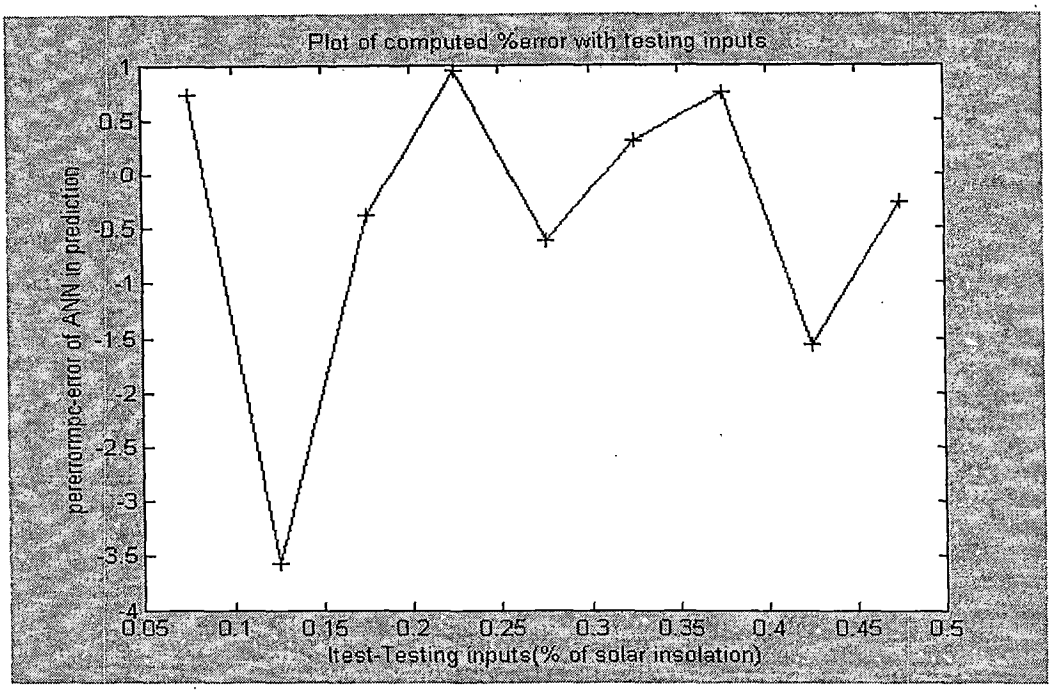

Fig. 38. Plot of percentage error versus testing inputs (tc3).

5.2.1.2 Case 1b: PMDC motor driving centrifugal pump for GME operation.

The training data for the network is shown in the below Table

Table 5. Training data for GME operation of PMDC motor driving centrifugal pump

% of solar insolation	Chopping ratio with GME operation for centrifugal pump (Ygmec)
0.10	0.5530
0.20	0.6814
0.30	0.7866
0.40	0.8582
0.50	0.9359
0.60	0.9876
0.70	1.0476
0.80	1.0889
0.90	1.1287
1.0	1.1784

5.2.1.2.1 Results of Case 1B.

The results of training and testing for **Case 1B** has been carried out for three conditions.

5.2.1.2.1.1 Training condition 1

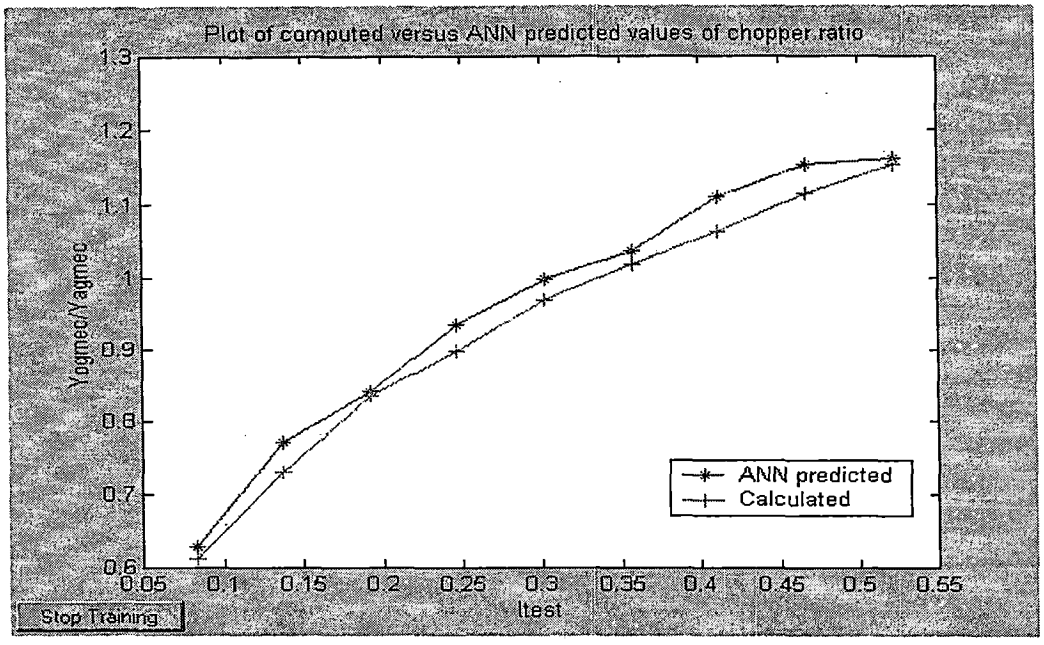

Fig. 39. Plot of calculated versus ANN predicted chopping ratio (tc1b)

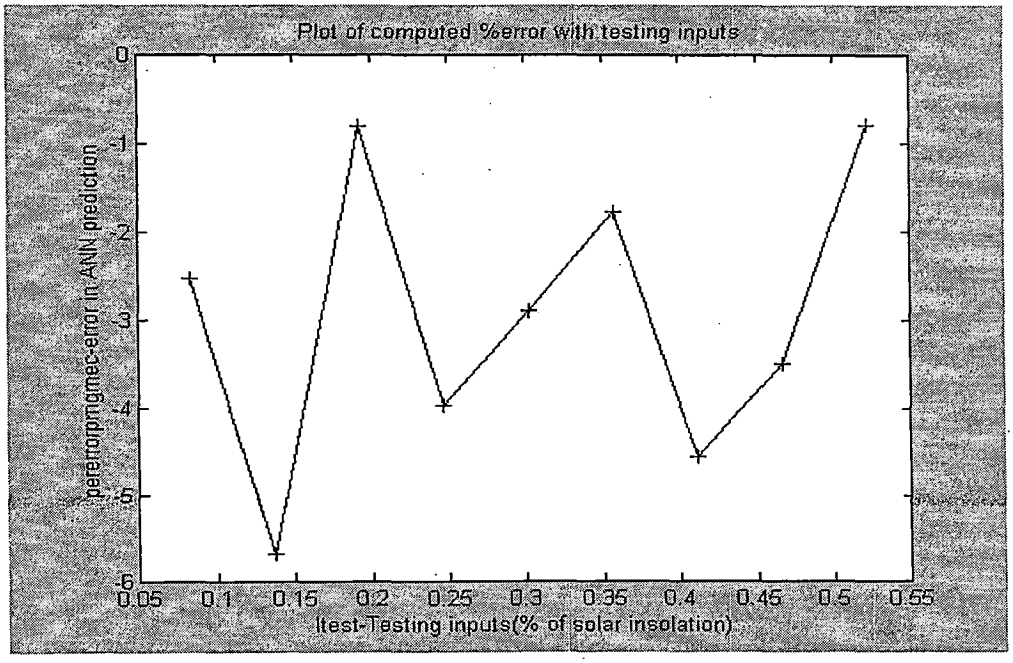

Fig. 40. Plot of percentage error versus testing inputs (tc1b).

5.2.1.2.1.2 Training condition 2

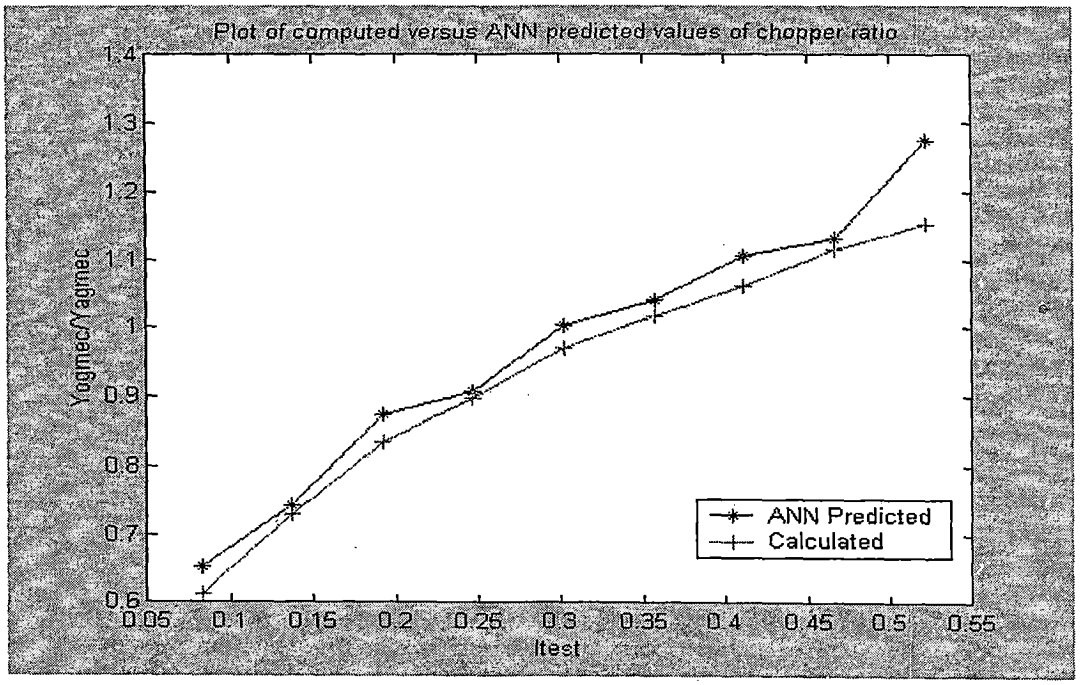

Fig. 41. Plot of calculated versus ANN predicted chopping ratio (tc2b)

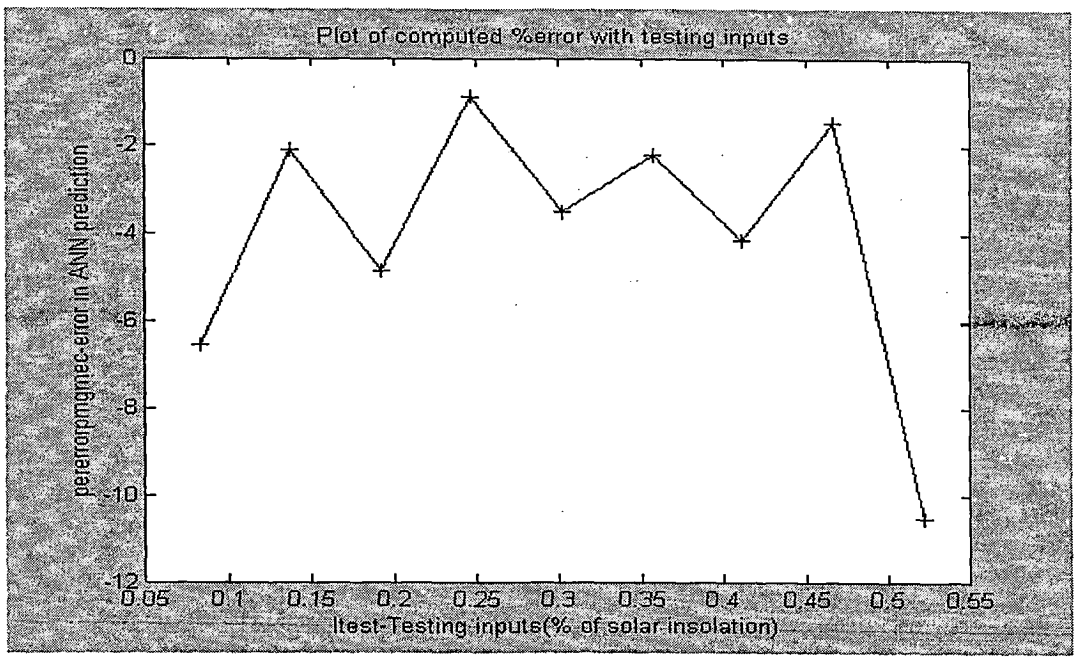

Fig. 42. Plot of percentage error versus testing inputs (tc2b).

5.2.1.2.1.3 Training condition 3

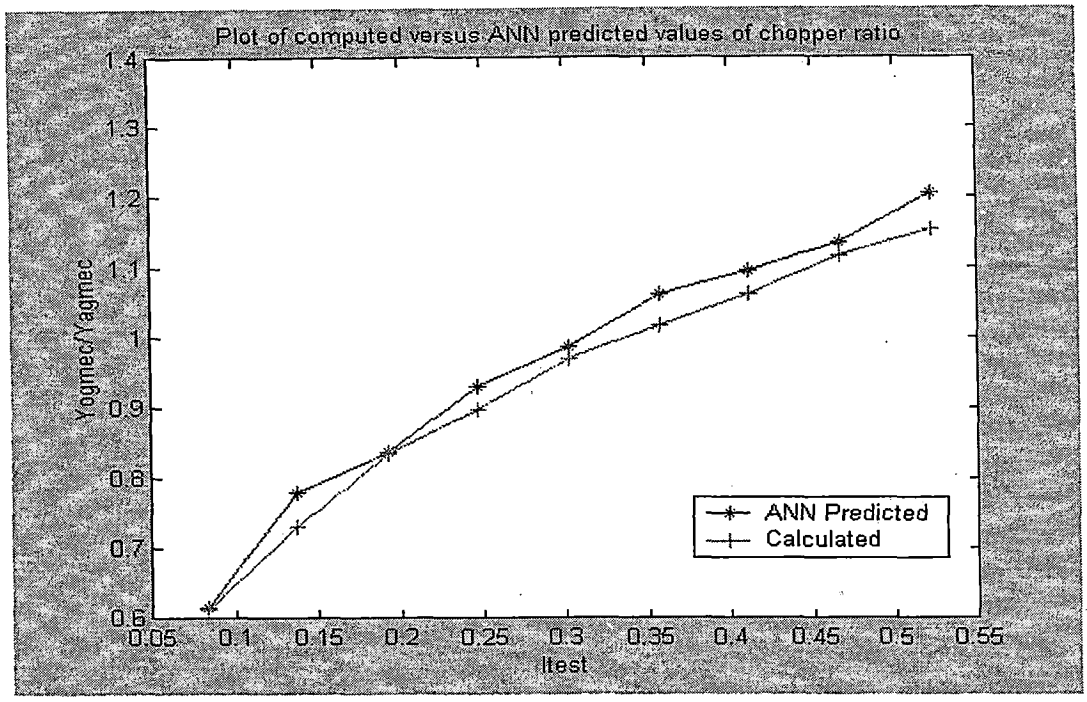

Fig. 43. Plot of calculated versus ANN predicted chopping ratio (tc3b).

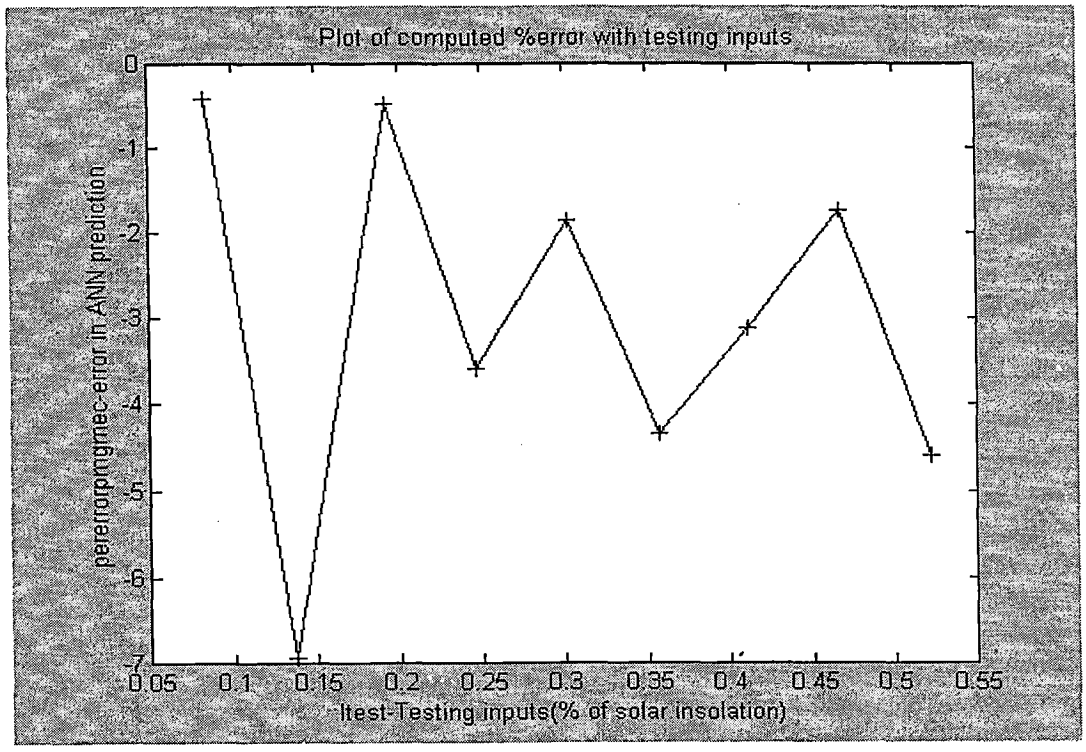

Fig. 44. Plot of percentage error versus testing inputs (tc3b).

Training of Neural network for MP operation of SCA

5.2.1.3 Case 2a: PMDC motor driving volumetric pump

The training data for the network is shown in the table below

Table 6. Training data for MP operation of PMDC motor driving volumetric pump

% of solar insolation	Chopping ratio with MP operation for Volumetric pump (Ympv)
0.10	0.1634
0.20	0.3201
0.30	0.4711
0.40	0.6167
0.50	0.7708
0.60	0.9061
0.70	1.0501
0.80	1.1766
0.90	1.2991
1.0	1.4305

5.2.1.3.1 Results of case 2a

The results of training and testing for **case 2a** has been carried out for three conditions. The error or performance criterion is set to 1e-7 with Mean square error as its performance function (MSE). For each training condition corresponding training performance in terms of output plots and percentage error in prediction is plotted below.

5.2.1.3.1.1 Training condition 1

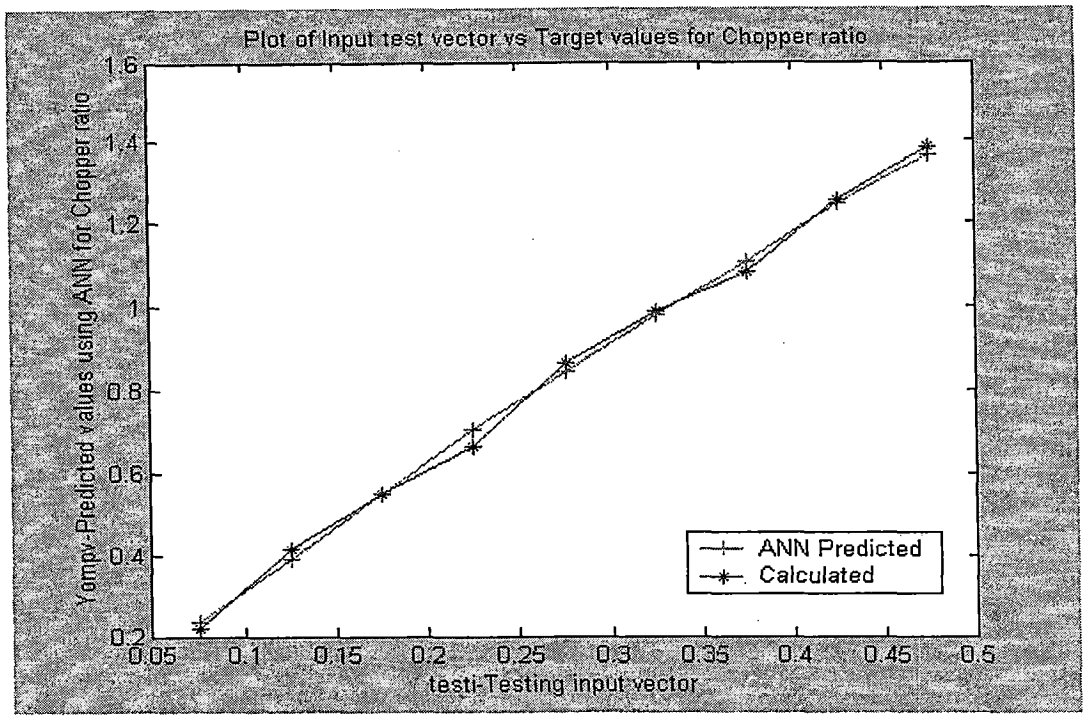

Fig. 45. Plot of calculated versus ANN predicted chopping ratio (tc1c).

5.2.1.3.1.2 Training condition 2

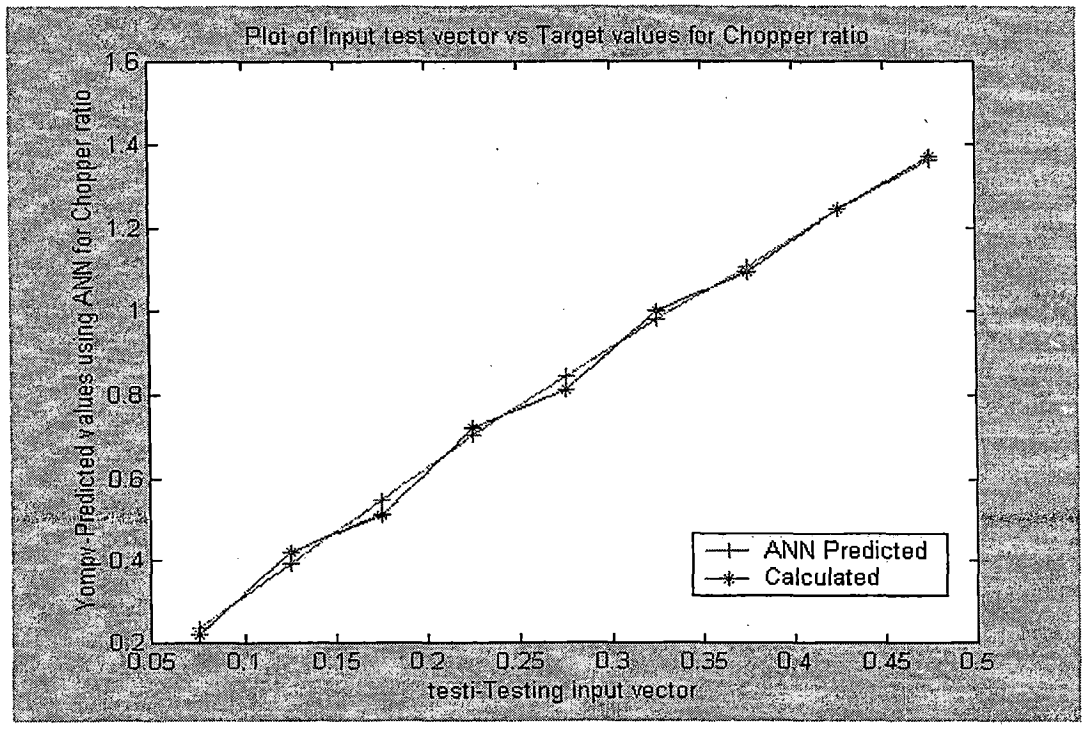

Fig. 46. Plot of calculated versus ANN predicted chopping ratio (tc2c).

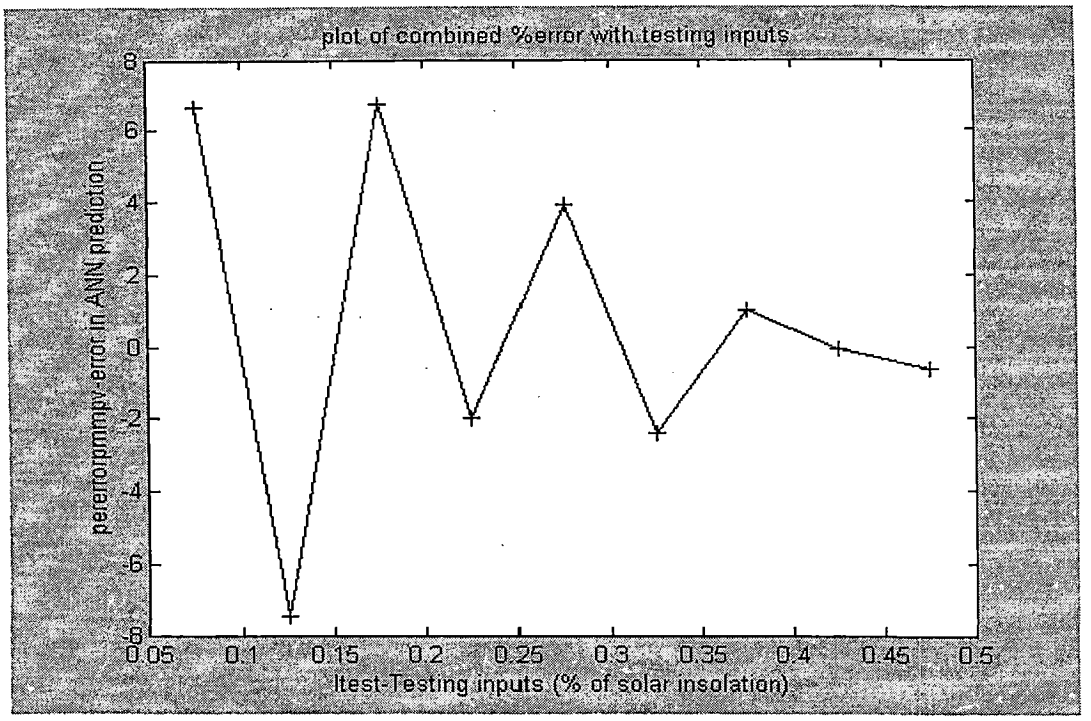

Fig. 47. Plot of percentage error versus testing inputs (tc2c)

5.2.1.3.1.3 Training condition 3

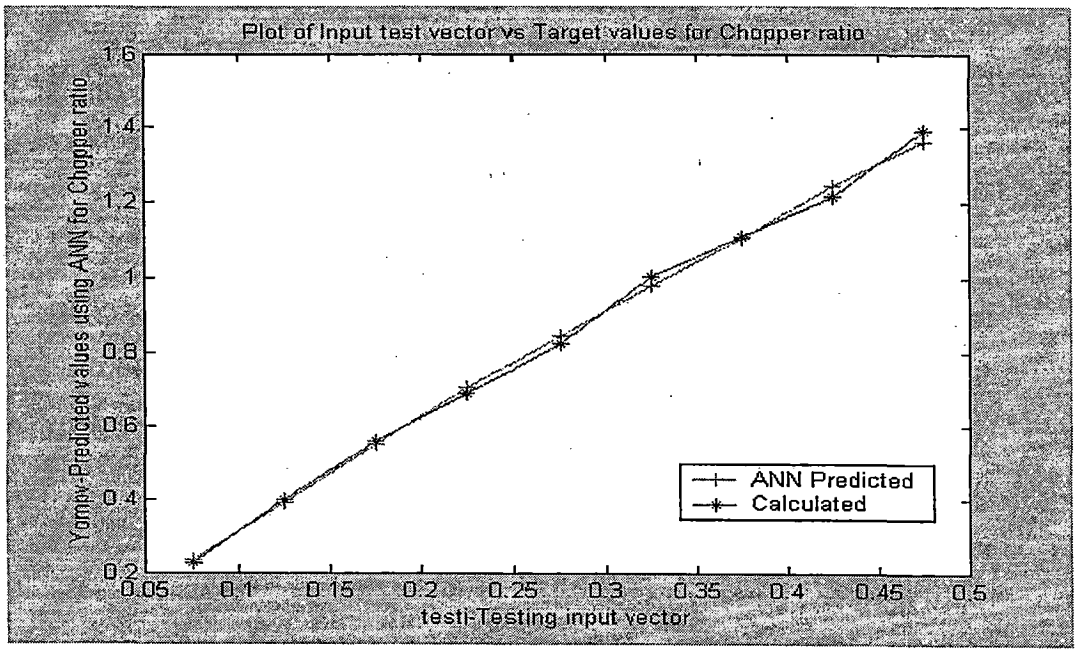

Fig. 48. Plot of calculated versus ANN predicted chopping ratio (tc3c).

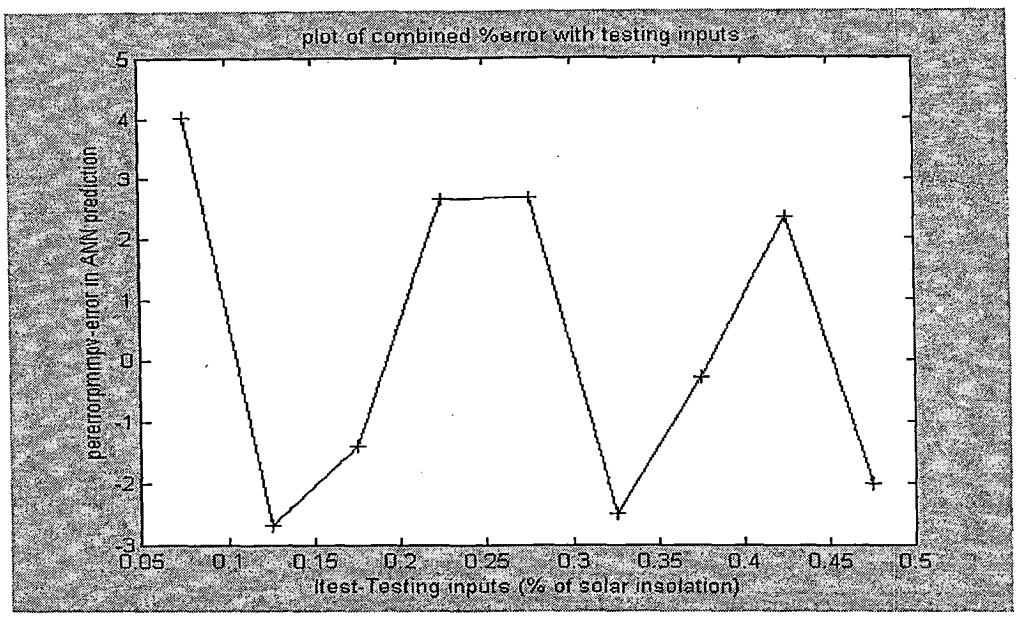

Fig. 49. Plot of percentage error versus testing inputs (tc3c)

Training of Neural network for GME operation

5.2.1.4 Case 2b: PMDC motor driving volumetric pump for GME operation

The training data for the network is shown below

Table 7.Training data for GME operation of PMDC motor driving volumetric pump

% of solar insolation	Chopping ratio with GME operation for Volumetric pump (Ygmev)
0.10	0.1741
0.20	0.3413
0.30	0.5028
0.40	0.6589
0.50	0.8247
0.60	0.9710
0.70	1.1271
0.80	1.2648
0.90	1.3990
1.0	1.5434

5.2.1.4.1 Results of Case 2b

The results of training and testing for **Case 2b** has been carried out for four conditions.

5.2.1.4.1.1 Training condition 1

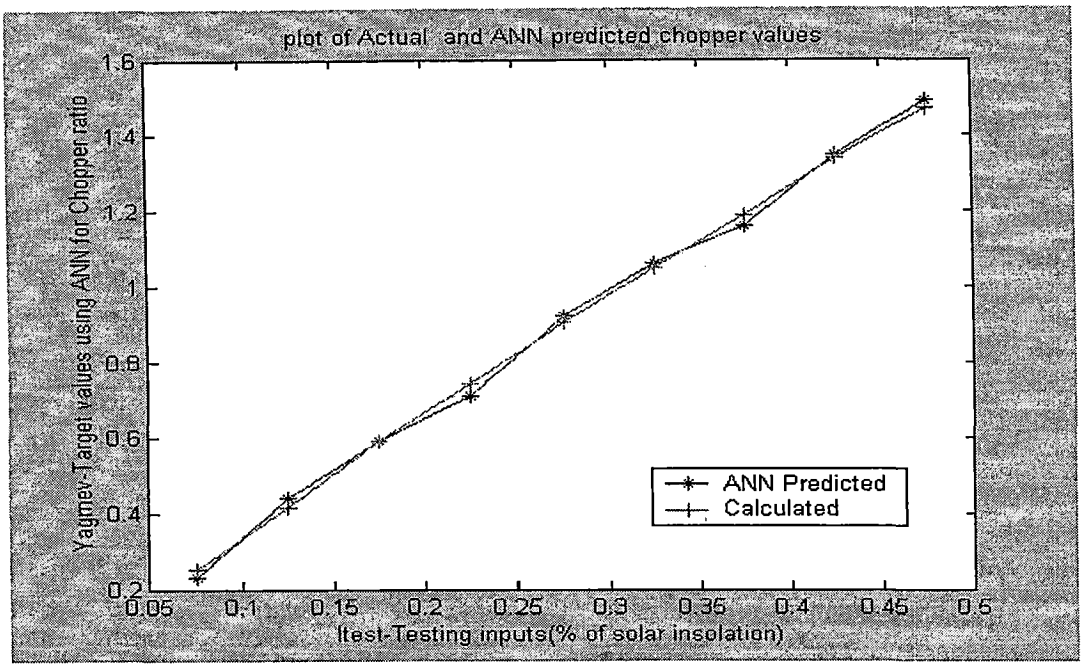

Fig. 50. Plot of calculated versus ANN predicted chopping ratio (tc1d)

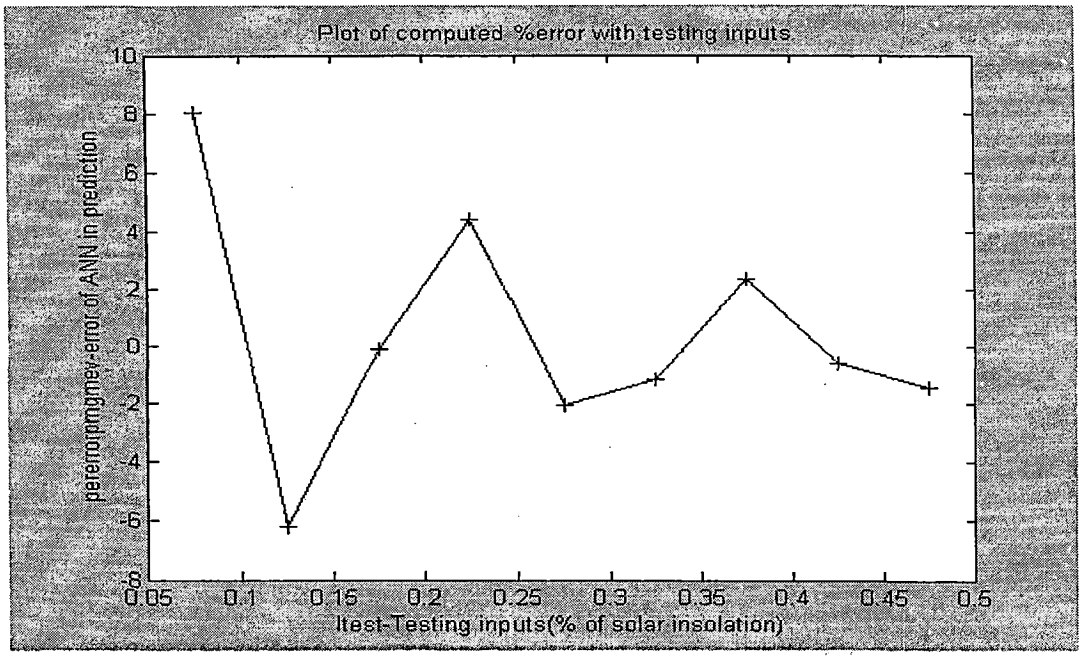

Fig 51. Plot of percentage error versus testing inputs (tc1d)

5.2.1.4.1.2 Training condition 2

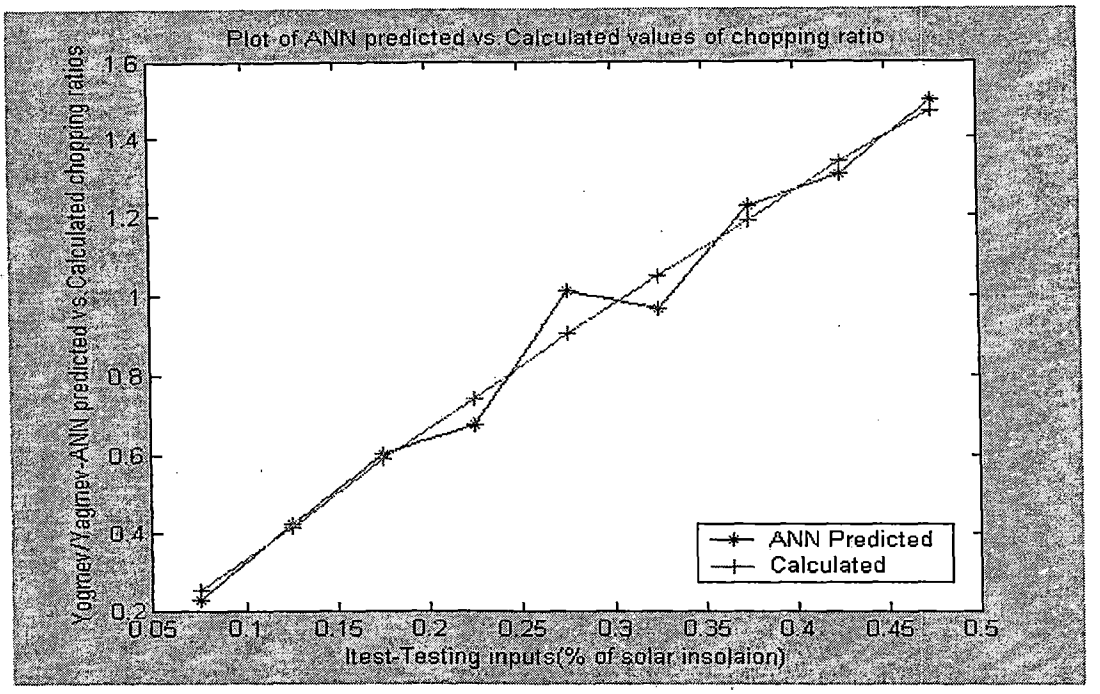

Fig. 52. Plot of calculated versus ANN predicted chopping ratio (tc2d).

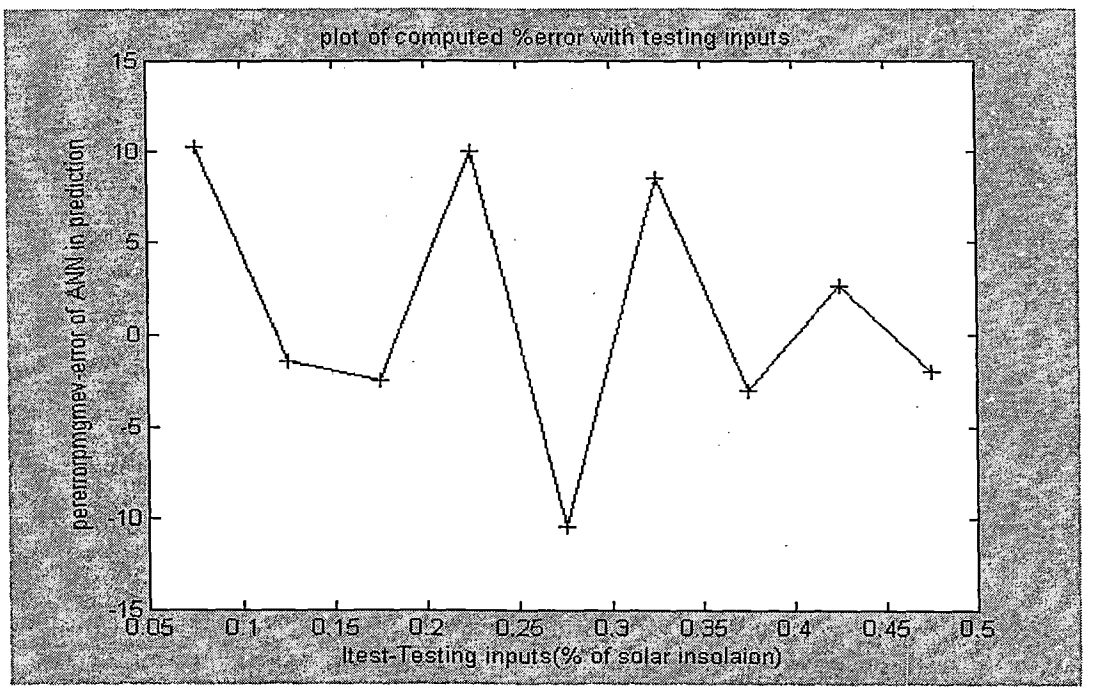

Fig. 53. Plot of percentage error versus testing inputs (tc2d)

5.2.1.4.1.3 Training condition 3

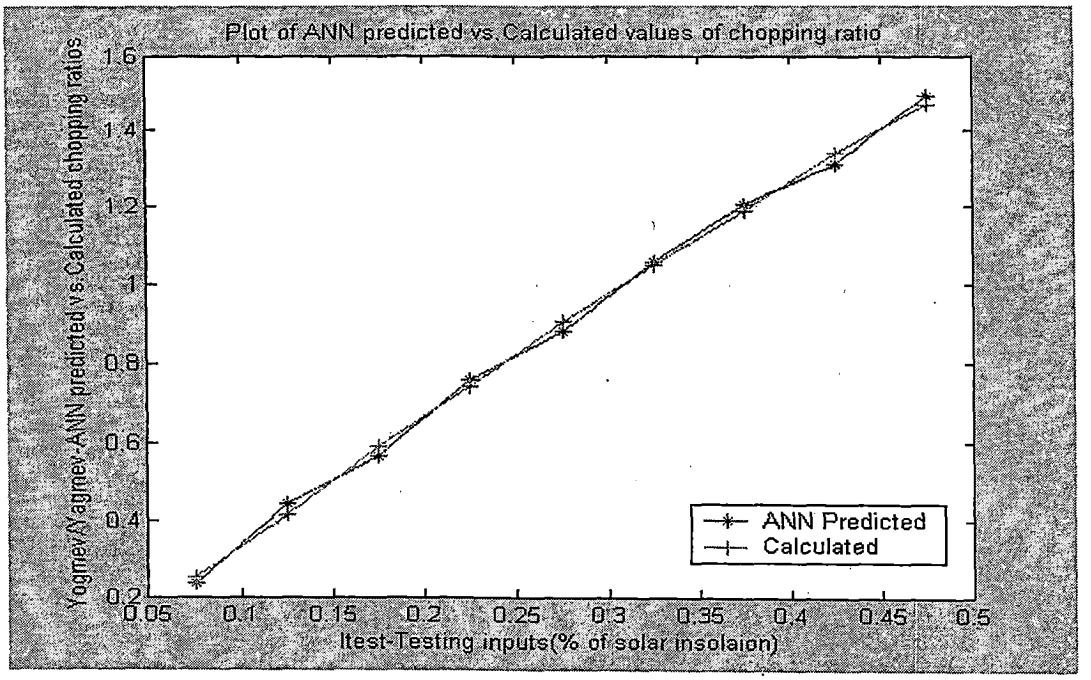

Fig. 54. Plot of calculated versus ANN predicted chopping ratio (tc3d).

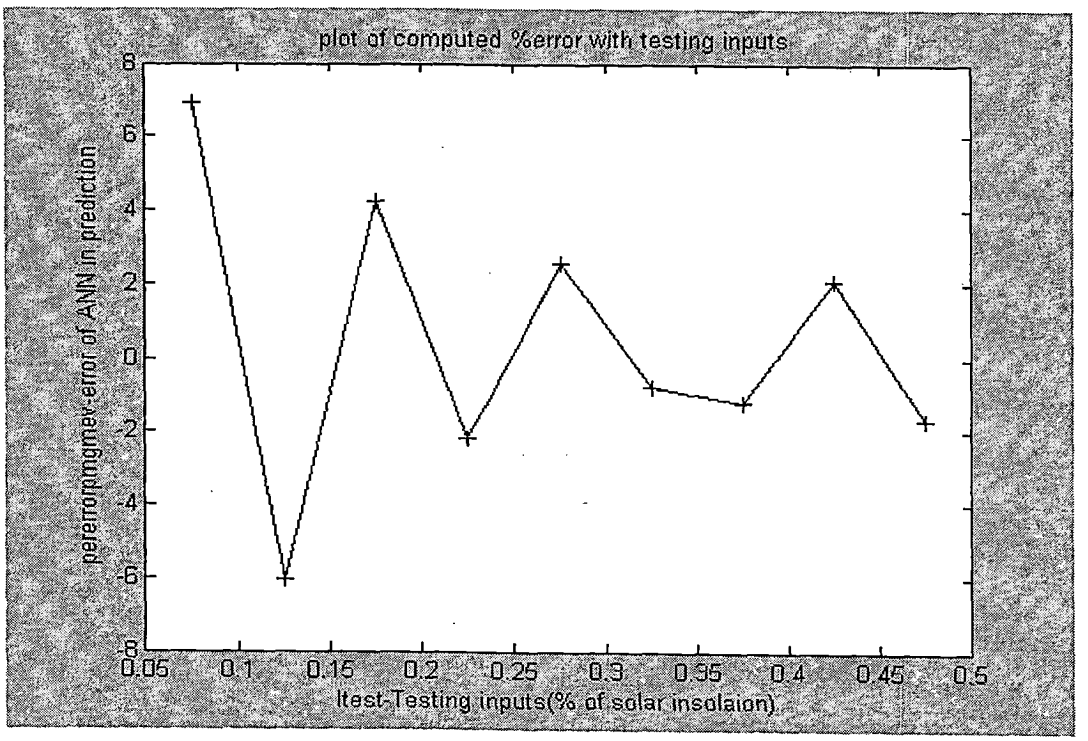

Fig. 55. Plot of percentage error versus testing inputs (tc3d).

The non-adaptive off-line controller using ANN is tested for different set of solar insolations and the results are close to the computed values for DC separately excited motor. The error in ANN prediction is less than (+-8%) for centrifugal and volumetric pump loads. It is observed from the results that the ANN even though trained for ten solar insolations the intermediate results obtained from the network are within the range. The results of MP and GME operations suggest that the ANN controller is accurate in identification or tracking optimal operating points even with stochastically varying solar insolations.

5.3 Series motor control by ANN

5.3.1 Training of Neural network for Maximum power of SCA operation

A 120V, 9.2A, 1500 rpm PV supplied series dc motor driving centrifugal pump load and was modeled using mathematical models of individual components and controlled by a neural network. The architecture of the network has been discussed in the previous section.

Training has been performed on various architectures using traingdm training function algorithm and back-propagation algorithm. The no. of input layer (neurons) and no. of output neurons are 1. This is constant for various cases of operation and for different training conditions. The no. of epochs/iterations, error criteria and performance functions are judiciously varied and prediction or estimation results are calculated.

5.3.1.1 Case 3a: Series motor driving centrifugal pump for MP operation

The training data for the network is shown below

Table 8. Training data for MP operation of series motor driving centrifugal pump.

PU Solar Insolation	Chopping ratio for MP operation for centrifugal pump (Ympc)
0.1	0.2812
0.20	0.4132
0.30	0.5406
0.40	0.6613
0.50	0.7704
0.60	0.8617
0.70	0.9703
0.80	1.0324
0.90	1.1215
1.0	1.2063

5.3.1.1.1 Results of case 3a

The results of training and testing for **case 3a** has been carried out for two conditions. They are given below.

1. Network with 1 hidden layer with 3 neurons in hidden layer with 10000 epochs
2. Network with 2 hidden layers with 3 neurons in each hidden layer with 10000 epochs

The error or performance criterion is set to 1e-7 with Mean square error as its performance function (MSE).The graph below shows plot of Training patterns (inputs) versus Target chopping ratio values.

5.3.1.1.1.1 Training condition 1

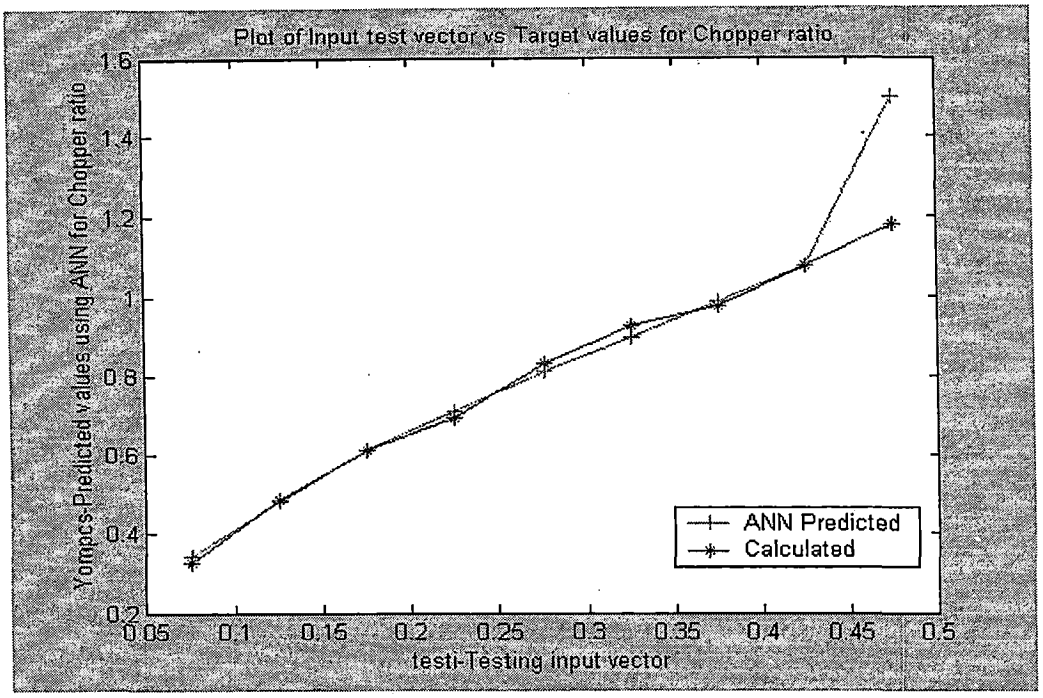

Fig. 56. Plot of calculated versus ANN predicted chopping ratio (tc1e)

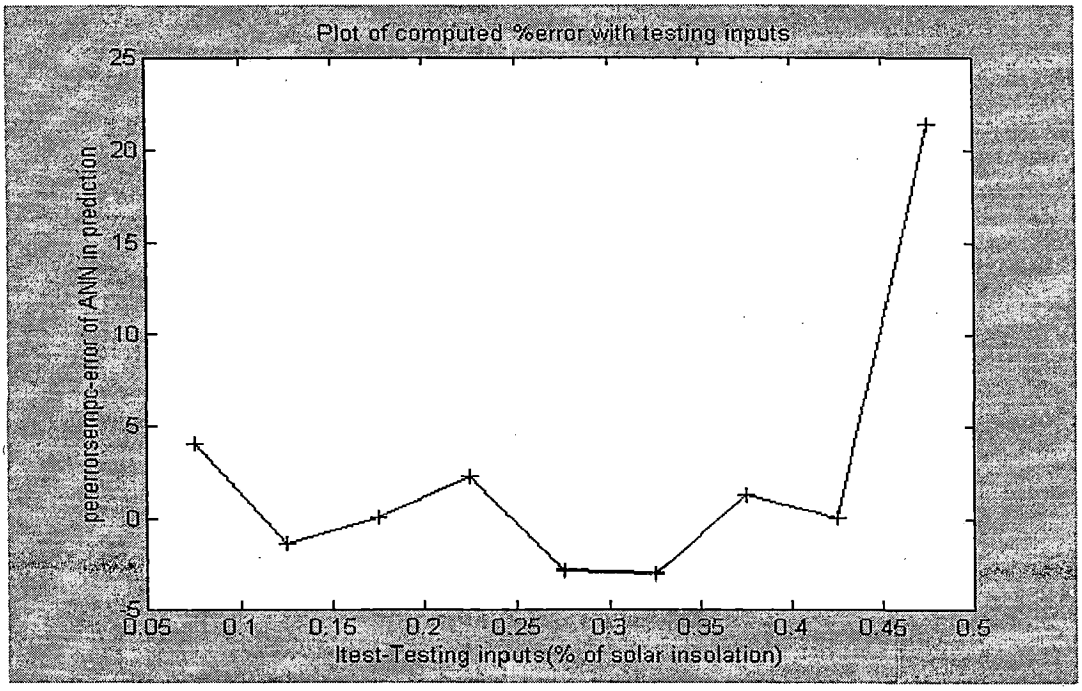

Fig. 57. Plot of percentage error versus testing inputs (tc1e)

5.3.1.1.1.2 Training condition 2

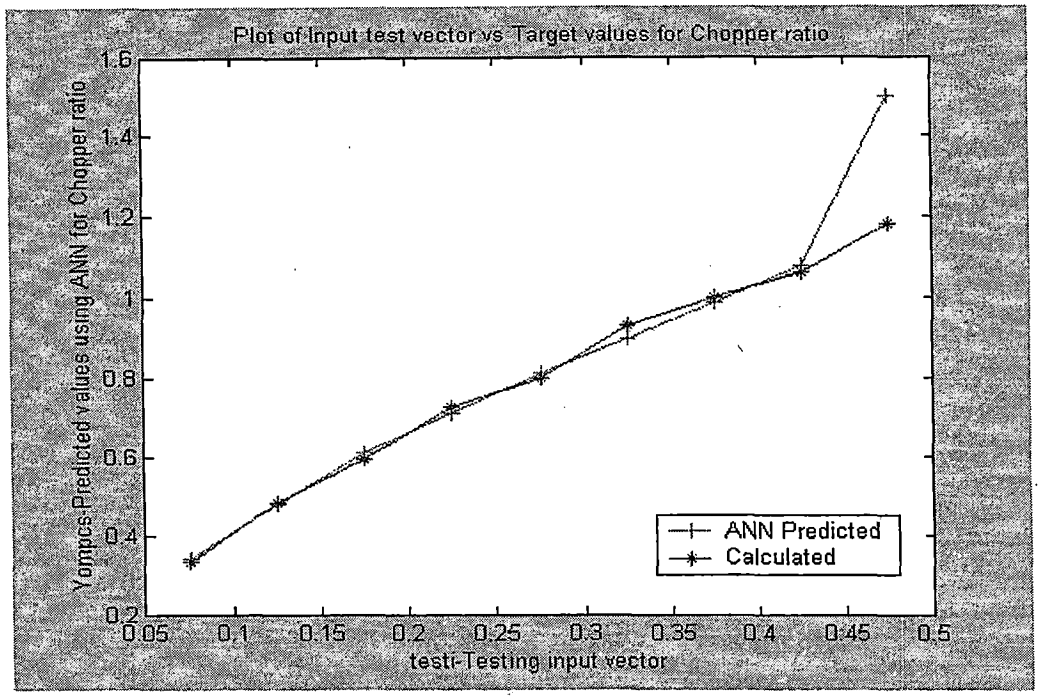

Fig. 58. Plot of calculated versus ANN predicted chopping ratio (tc2e).

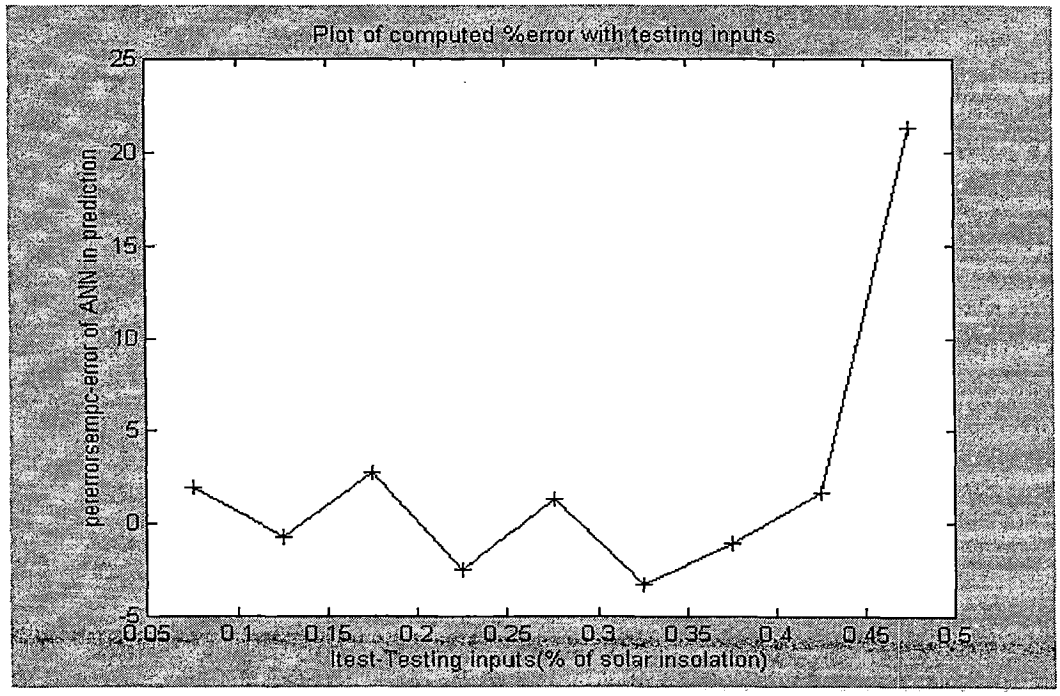

Fig. 59. Plot of percentage error versus testing inputs (tc2e).

5.3.2.1 Case 3b: series motor driving volumetric pump for GME operation

The training data for the network is shown below

Table 9. Training data for GME operation of series motor driving volumetric pump.

PU Solar Insolation	Chopping ratio GME
0.1	0.3403
0.20	0.5713
0.30	0.6923
0.40	0.8406
0.50	0.9234
0.60	1.1206
0.70	1.2238
0.80	1.3440
0.90	1.4263
1.0	1.5403

5.3.2.1.1 Results of case 3b

The results of training and testing for **case 3b** has been carried out for one condition.

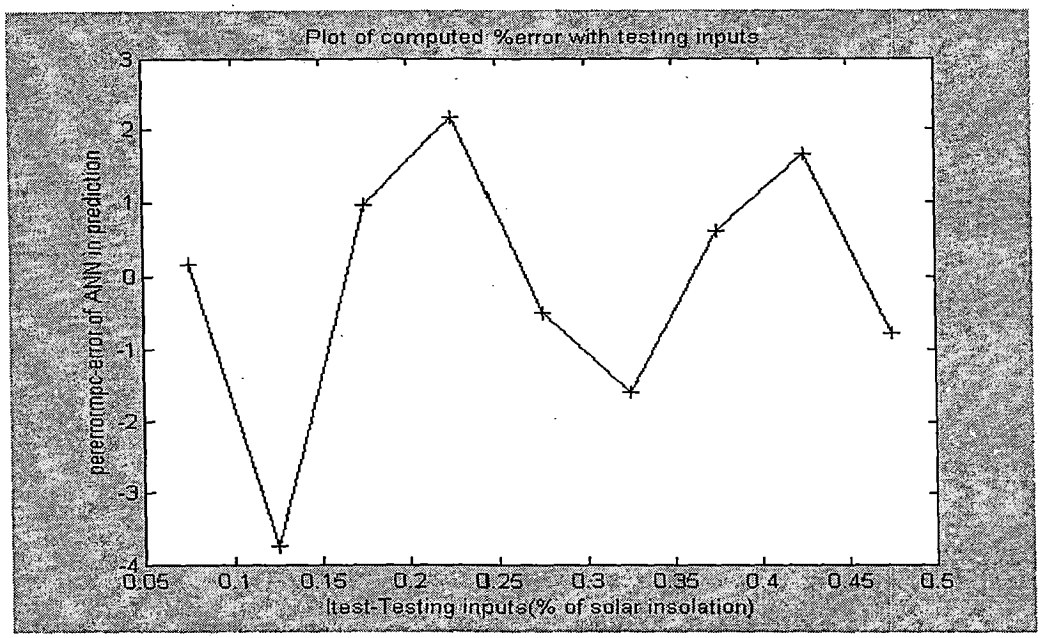

Fig. 60. Plot of percentage error versus testing inputs (tc3e)

Chapter 6

Neural Network model for Photovoltaic Pumping System

6.1 Statement of problem

It is impractical for a manufacturer to supply system output data for infinite combinations of the solar input (irradiance/insolation) and the pumping head. Moreover, the system output varies with the various combinations of the system components (photovoltaic module, linear current booster, pump, filter and the various pipes and fittings) that a system may be comprised. It is therefore necessary to develop a model for a particular system that can predict the output for any combination of head and irradiance. Estimation or prediction of flowrate for a photovoltaic pump is performed by using this ANN model.

6.2 Introduction

The flowrate is measured as a function of both irradiance and head. The pumping system is set up (installed at university of Curtin) such that it draws the water from a large pan (tank) and pumps it to a certain head where it discharges the water into a funnel. After the system starts up, its delivered flow rate is proportional to the radiation intensity. The relation between flow rate and radiation intensity is nonlinear in nature. At high levels of insulation, the rate of increase of pump discharge with increasing insolation is smaller than that at intermediate insolation levels. The nonlinear relationship between flow rate and insolation and the existence of the insolation threshold make the performance prediction of a PV pumping system difficult.

By applying the technique of Maximum Point Power Tracking (MPPT), the efficiency of the system rises whatever is the solar radiation value and the temperature of the environment. The technique of MPPT was applied by different ways and means. In this work, we execute this technique with the use of artificial neural network. A typical nonlinear relationship between pump flow rate and insolation for a PV pumping system is shown in Fig. 61.

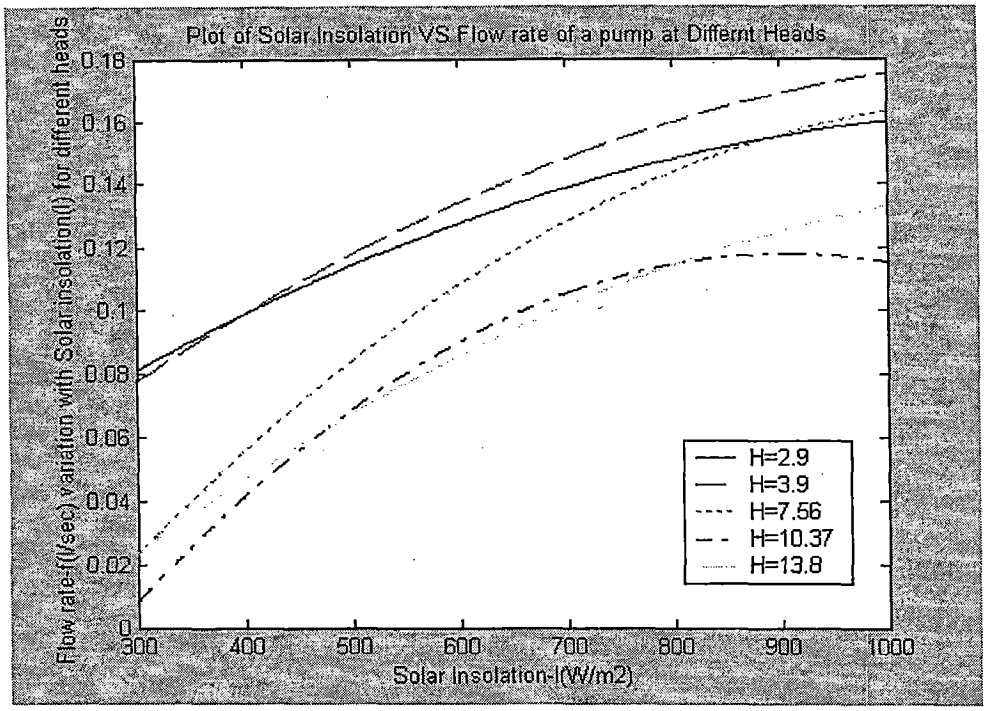

Fig. 61. Flowrate vs irradiance at various pumping heads.

6.3 Method of modeling the motor-pump combination

The pumping rate (flowrate, f) depends basically on two factors: the pumping head, H, and the irradiance, I. Fig. 61. show the dependence of the flowrate on both head and irradiance. Each line represents a different head. It is noted that the curves cross each other. This is attributed to the differences in the PV module efficiencies for different sets of data. The

effect may also be partially caused by the differences in the actual pump characteristics at different heads. The pump is less efficient at lower heads, because some energy is transferred to the pumped water in the form of kinetic energy. Ideally the pump should deliver water to a certain head with zero kinetic energy. In general, the flowrate increases with irradiance, but not linearly. A second order parabolic equation fits the data very well. Table10. shows the equations for the best fit curves and the correlation coefficients.

Table 10. Best fit equations and correlation coefficient (r^2) for curves in Fig. 61

Head(m)	Best fit equation	(r^2)
2.9	$f = 0.015+2.51*10^{-4}I - 1.06 * 10^{-7}I^2$	0.99
3.9	$f = -0.0017+3*10^{-4}I - 1.23 * 10^{-7}I^2$	0.99
7.56	$f = -0.099+4.69*10^{-4}I - 2.07 * 10^{-7}I^2$	0.98
10.37	$f = -0.127+5.40*10^{-4}I - 2.98 * 10^{-7}I^2$	0.99
13.8	$f = -0.06+3.16*10^{-4}I - 1.23 * 10^{-7}I^2$	0.99

The equations obtained in Table 10. are restricted to the heads shown in Fig. 61. We are particularly interested in determining the flowrate as a function of both irradiance and head from a single equation.

Flow rate, f = f (I, H) ..... (71)

In other words the model (equation) developed should be able to predict the flowrate for any combination of head and flowrate. It is noted that all the equations in Table 10. have one general form:

$$\text{Flow rate, } f = b_0 + b_1 I + b_2 I^2 \quad \ldots\ldots\ldots\ldots\ldots\ldots \quad (72)$$

The only difference is that the different heads have different co-efficients b_0, b_1 and b_2. These co-efficients are plotted against the head, as shown in Fig. 62. From Fig. 62. relationship between the co-efficients and head is shown. Again a second order parabolic regression is used to obtain the best fit equations. The results are shown in Table 11. The equations in Table 11. can now be combined with Eq. (72) to give a combined relationship for flowrate as a function of irradiance and head.

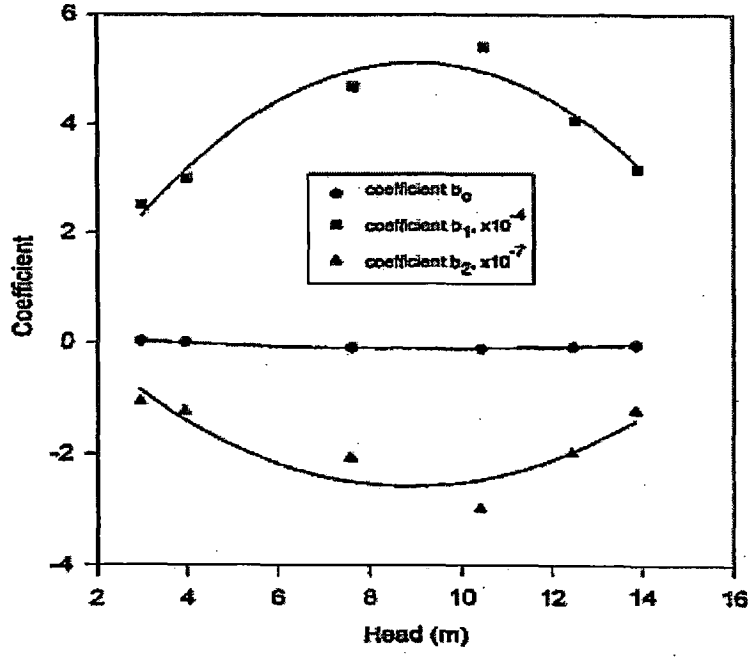

Fig. 62. Best fit co-efficients from Table 1 plotted against pumping heads

Table 11. Best fit equations and correlation coefficients (r^2) for coefficients of equations in fig. 61.

Co-efficient	Best fit equation	(r^2)
b_0	b_0= 0.175-0.06 H + 3.1* $10^{-3}H^2$	0.99
b_1	b_1=-1.06*10^{-4}+1.389*$10^{-4}H - 7.8 * 10^{-6}H^2$	0.94
b_2	$b_2 = 9.1 * 10^{-8} - 8.13 * 10^{-8}H + 4.7 * 10^{-9}H^2$	0.82

Thus $f = b_0 + b_1^* I + b_2^* I^2$ ..... (73)

Where f = flowrate in l/sec, I = irradiance in W m^{-2}, and b_0, b_1 and b_3 *are* given by equations in Table 11. This model can now be used to predict the flowrate for any combination of head and irradiance. Fig. 63. Shows the predicted flow rates plotted for a variety of heads (solid lines).Superimposed on these are the actual measured values.

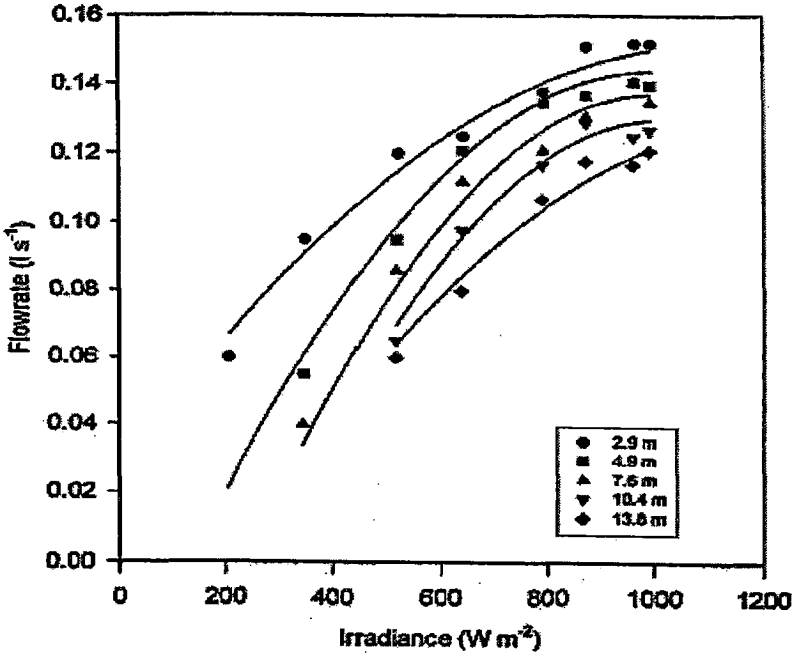

Fig. 63. Predicted flowrate vs irradiance at various heads.

The procedure is applied to the Solar Star 1000 pumping system to arrive at a model that predicts the volume flowrate, given the head and the irradiance. The parameters of the PV generator and motor are given in Appendix A.

Fig. 64. explains the increase of Q by the increase of E (insolation). At 25 C° the water flood from centrifugal pump is found to be optimal. Here, we chose to change the application of neural network by choosing Q and E as its output and input respectively, and tracking the error of algorithm back propagation in applying the learning program.

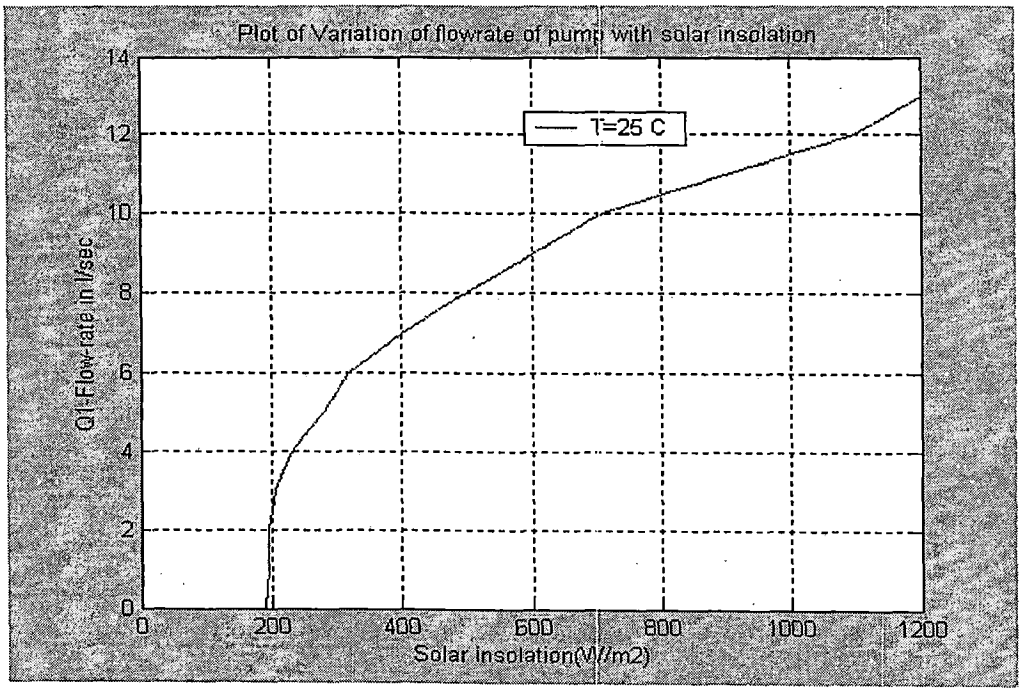

Fig. 64. Variation of flowrate of pump with solar insolation

The earth receives solar energy as electro-magnetic waves which we define as "solar parameters" as the average quantity of the radiation that is

incident on the earth level. The value of this parameter is between (0-1000) W/m^2.

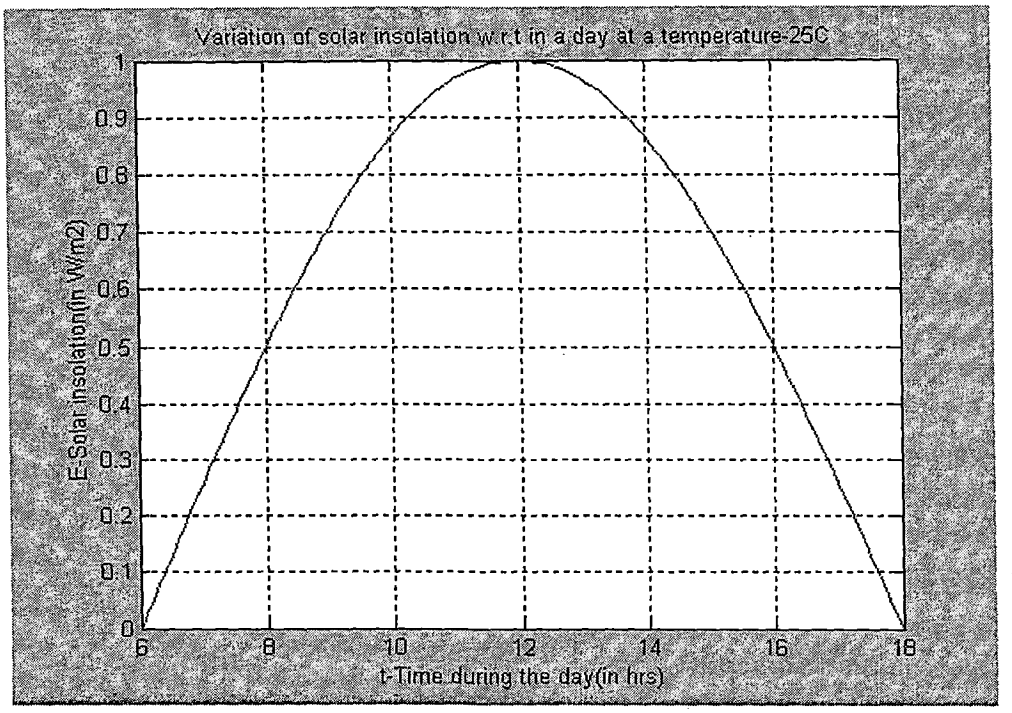

Fig. 65. Solar radiation variation w.r.t in a typical day at T=25 C.

The quantity of solar energy, which is incident, relies on many factors: The geographical situation, the time during the day and the season, the purity of the air, the determination of the variation in humidity and temperature, and the wind speed. All these factors were taken into account during the determination of solar radiation direction in the pumps flow rate-head chart. It is limited in 12 hours a day where it reaches the peak during the mid-day, like in fig. 65.

$$E(t) = E_m \sin(15(t-6)) \quad \text{..... (74)}$$

Where E_m = Maximum value of solar insolation = 1000 W/m^2.

t = Time of the day (in hours).

6.4 Neural network model

An artificial neural network model for predicting or estimating the flow rate of a photovoltaic water pump driven by a separately excited DC motor controlled by a MPPT (Maximum Power Point Tracker) is proposed and validated. The neural network architecture and the training algorithm, transfer functions used are explained in detail. This model predicts the output of the network which is flow rate of pump in (l/sec) with good accuracy. The application of the practical chosen neural network with cheap available electronic instruments rests an objective for generalizing and spreading the use of photovoltaic pumping system.

6.4.1 Neural network architecture

The neural network architecture developed has three layers. They are

1. Input layer
2. Hidden layer
3. Output layer

The single input to the network is the solar radiation and the single output is the required pumped water quantity.

6.4.2 Training the neural network

The training data for the proposed neural network is obtained either from the manufacturer's data charts and sheets for centrifugal pumps. As mentioned in the previous section, a model for small-scale photovoltaic pumping system was used to generate the training data. The data corresponds to different heads for which actual measurements were done. Training was performed with TRAINGDM-gradient descent function. The algorithm used was error back-propagation theorem. Training was

algorithm used was error back-propagation theorem. Training was performed for different conditions where the number of neurons in hidden layer was varied with training parameters kept constant. ANN prediction of output values (flowrate) and percentage error variation with insolation were graphically shown for each training condition.

6.4.2.1 Training conditions

Effect of network architecture on learning was analyzed from different training conditions as described below. They are

1. Training condition 1 with three hidden neurons in one hidden layer.
2. Training condition 2 with two hidden layers with 3 neurons in each layer

6.4.3 Head-2.9

6.4.3.1 Training condition 1: The training parameters are shown below.

Table 12. Training parameters for training condition 1

Training function	TRAINGDM
Performance function	Mean Square Error (MSE)
No. of Hidden layers	1
No. neurons in Hidden layer	3
Activation functions	tansig in hidden layer and purelin in output layer
Learning rate	0.7
Momentum constant	0.8

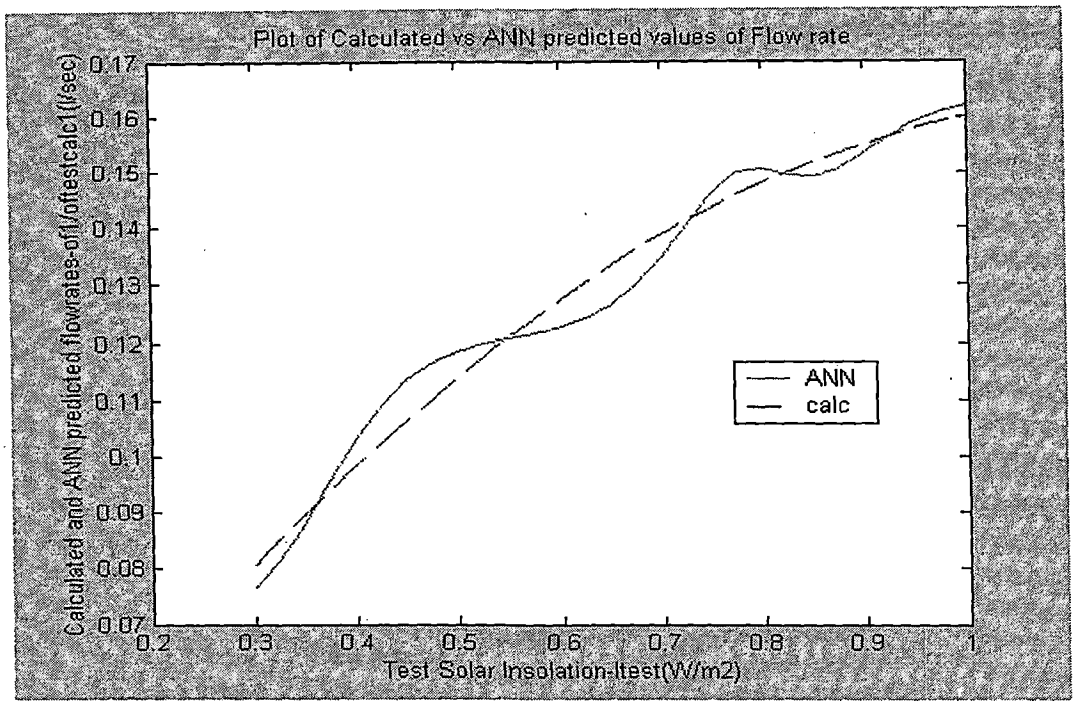

Fig. 66. Plot of calculated vs ANN predicted values of flow rate[tc1-H=2.9].

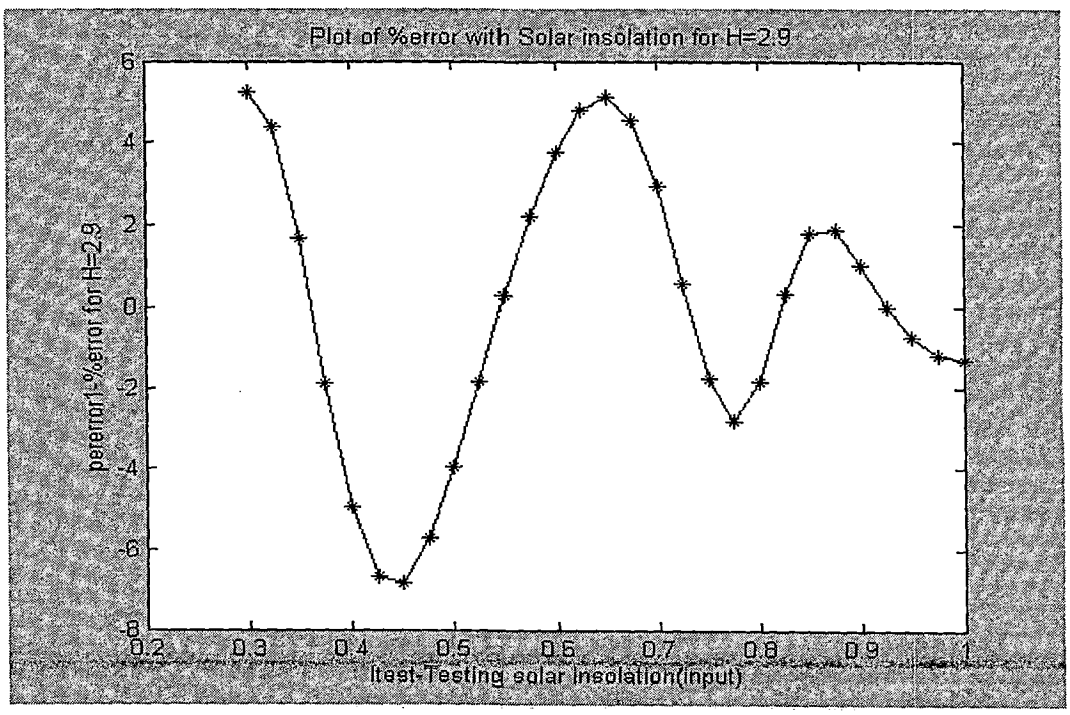

Fig. 67. Plot of %error with solar insolation for[tc1- H=2.9].

6.4.3.2 Training condition 2

The Training condition 2 is given by the following training Parameters.

Table 13. Training parameters for training condition 2

Training function	TRAINGDM
Performance function	Mean Square Error (MSE)
No. of Hidden layers	2
No. neurons in Hidden layer	3,5
Activation functions	tansig in hidden layer and purelin in output layer
Learning rate	0.6
Momentum constant	0.8

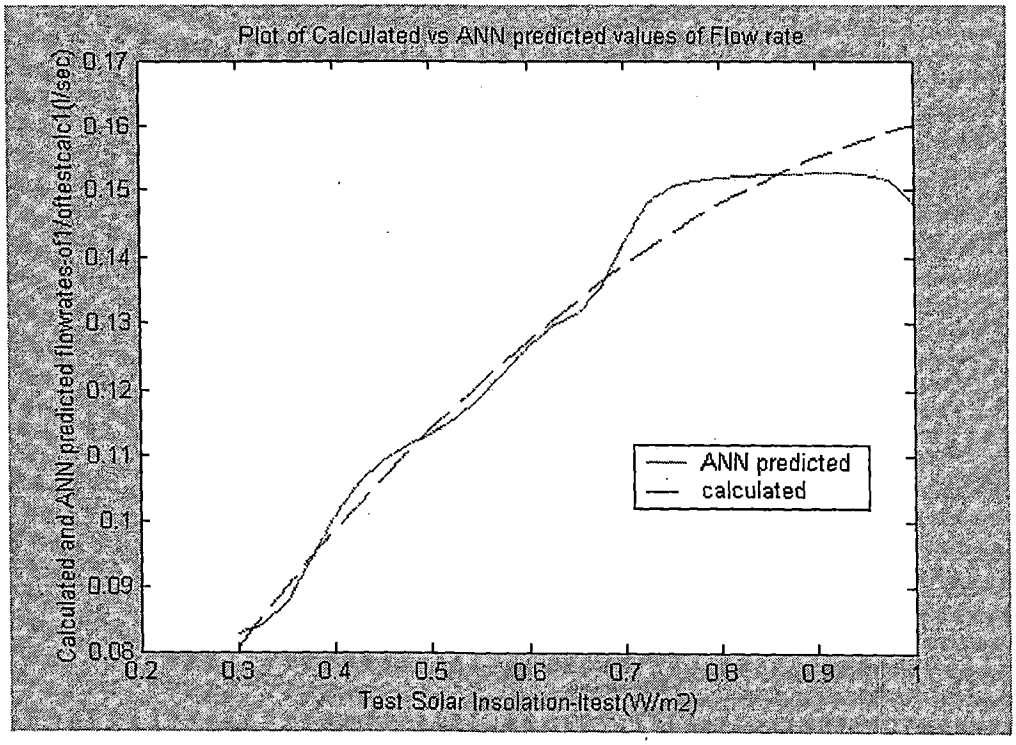

Fig. 68. Plot of calculated vs ANN predicted values of flow rate[tc2-H=2.9].

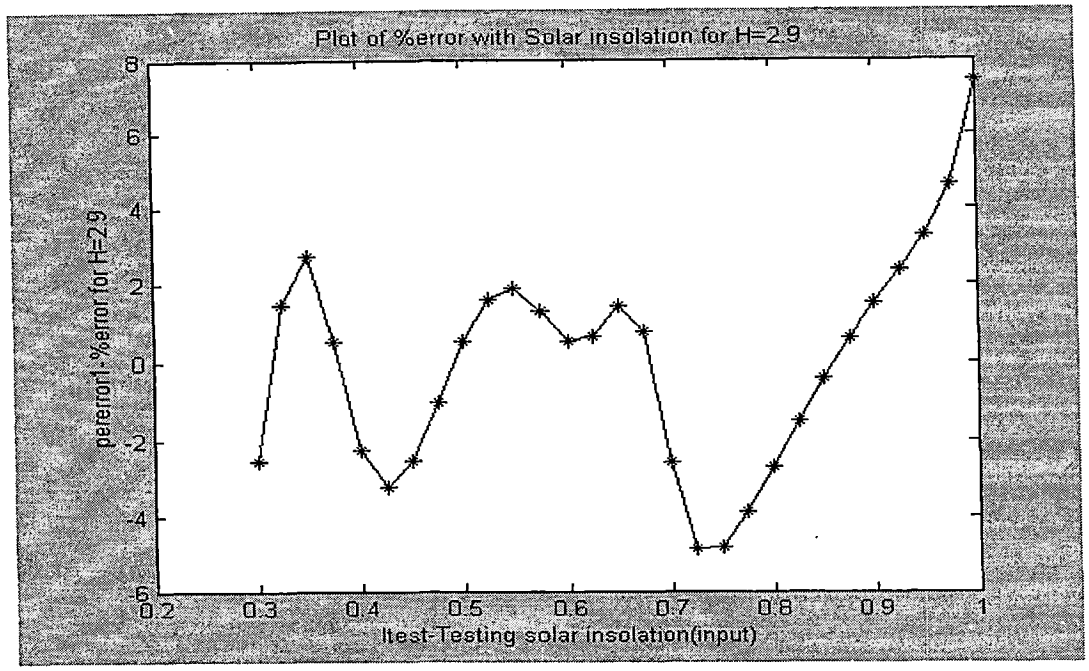

Fig. 69. Plot of %error with solar insolation for [tc2- H=2.9].

6.4.4 Head-3.9: output graphs for training condition 1 are shown below

6.4.4.1 Training condition 1

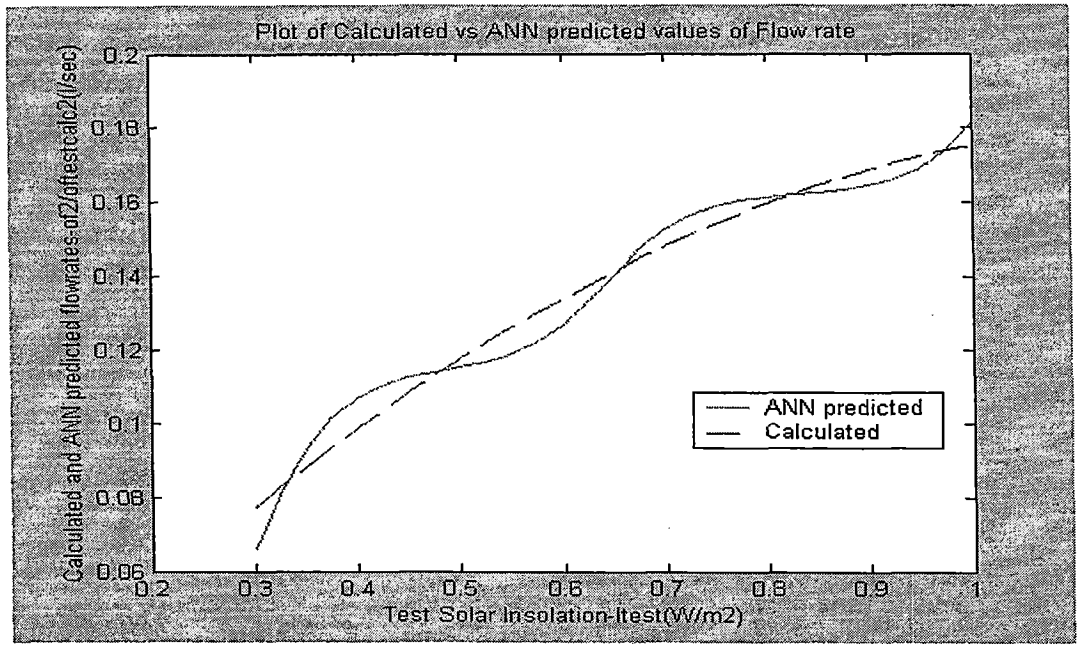

Fig. 70. Plot of calculated vs ANN predicted values of flow rate[tc1-H=3.9].

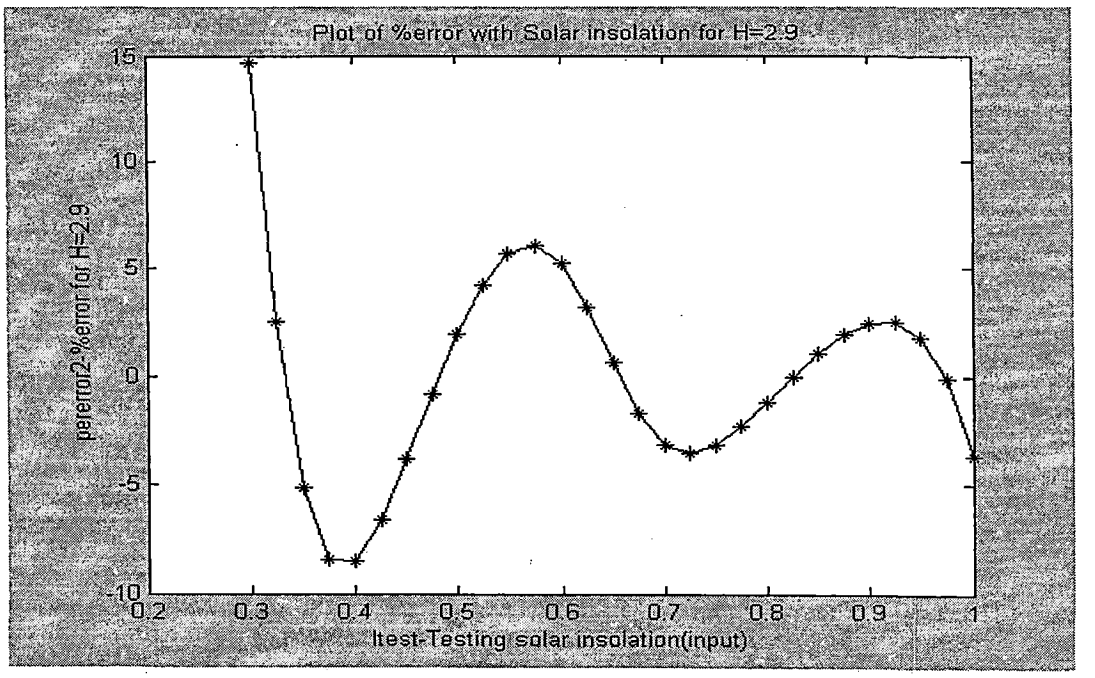

Fig. 71. Plot of %error with solar insolation for [tc1- H=3.9].

6.4.4.2 Training condition 2:

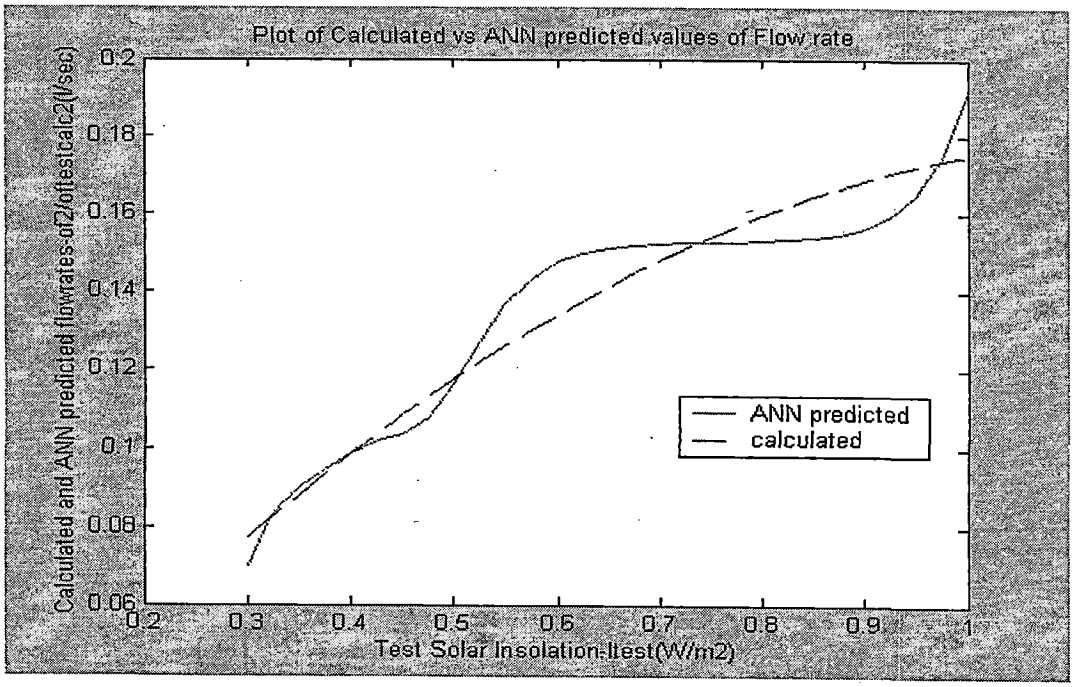

Fig. 72. Plot of calculated vs ANN predicted values of flow rate[tc2-H=3.9].

Fig. 73. Plot of %error with solar insolation for[tc2-H=3.9].

6.4.5 Head -7.56

6.4.5.1 Training condition 1

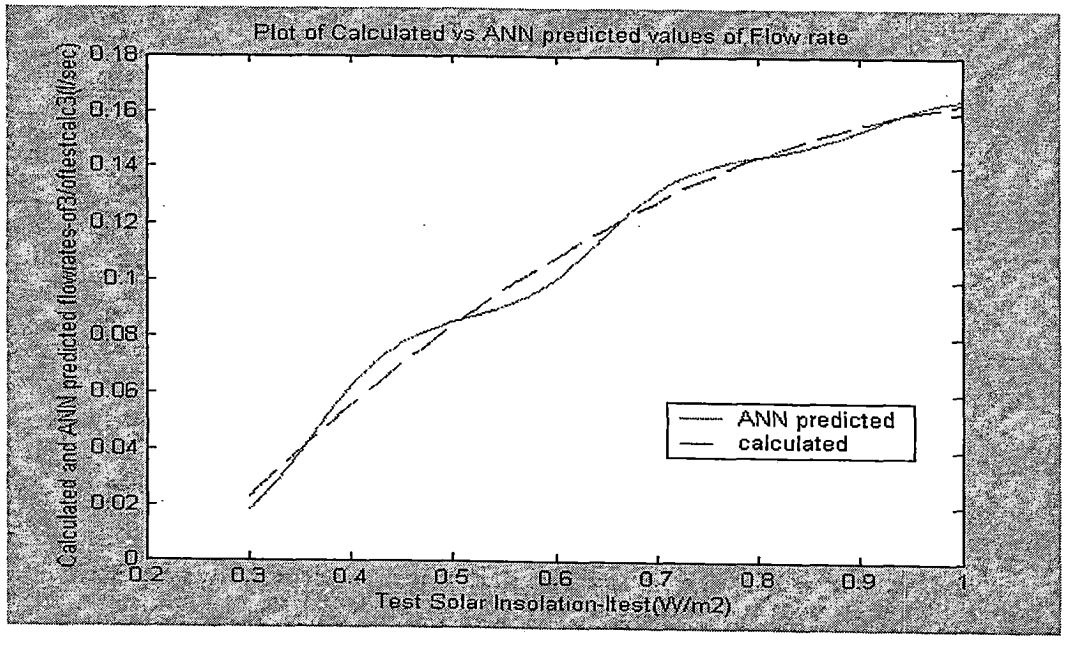

Fig. 74. Plot of calculated vs ANN predicted values of flow rate[tc1-H=7.56]

6.4.5.2 Training condition 2

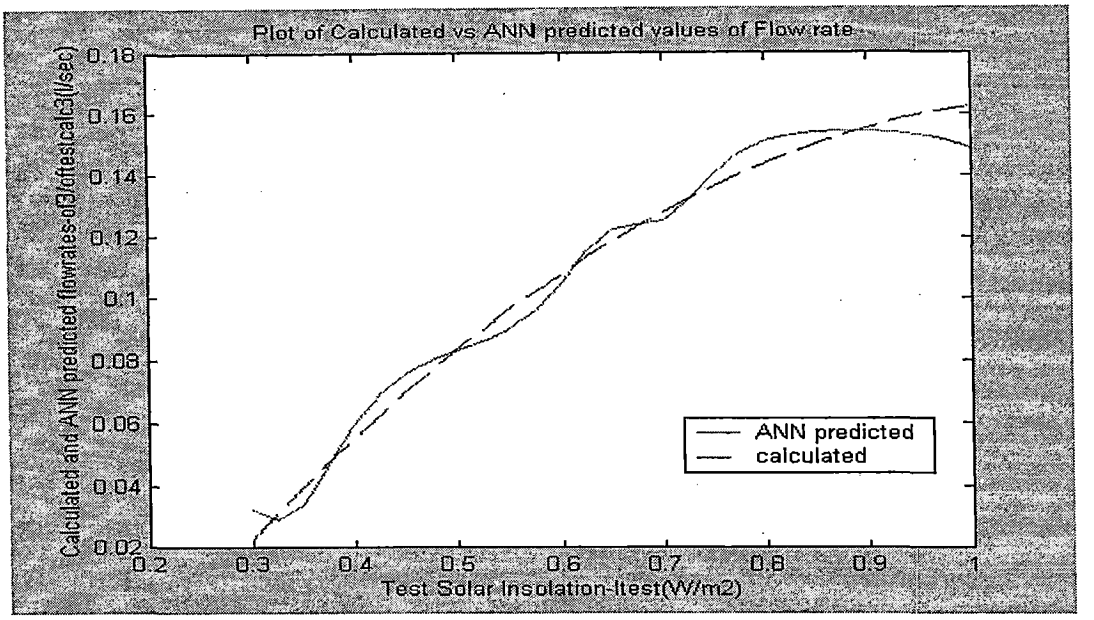

Fig. 75. Plot of calculated vs ANN predicted values of flow rate[tc2-H=7.56]

6.4.6 Head - 10.37

6.4.6.1 Training condition 1

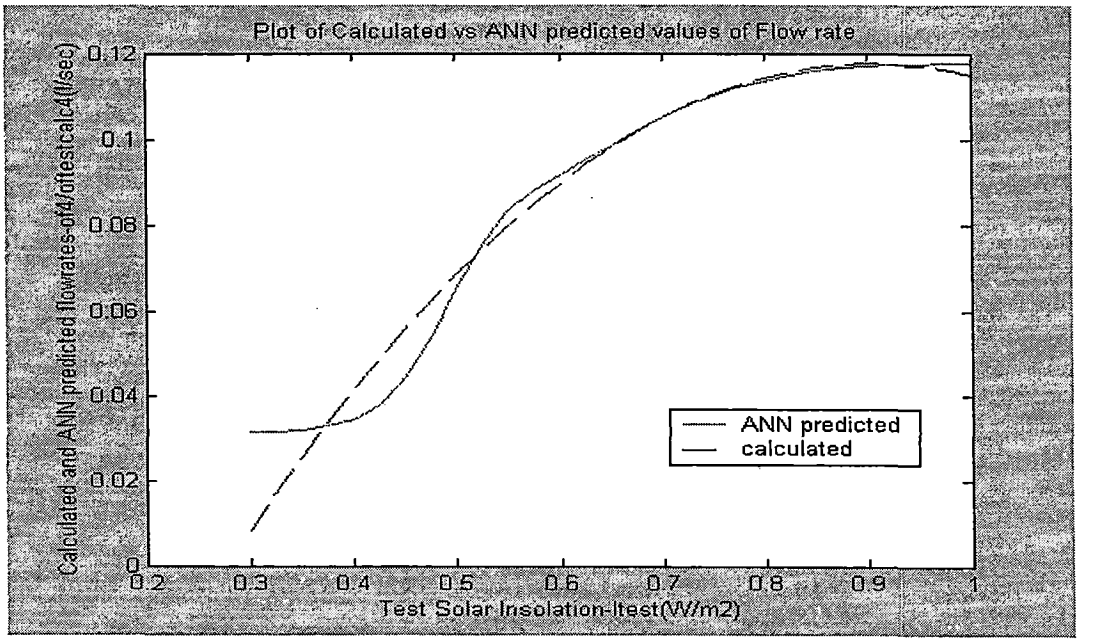

Fig. 76. Plot of calculated vs ANN predicted values of flow rate[tc1-H=10.37]

6.4.6.2 Training condition 2:

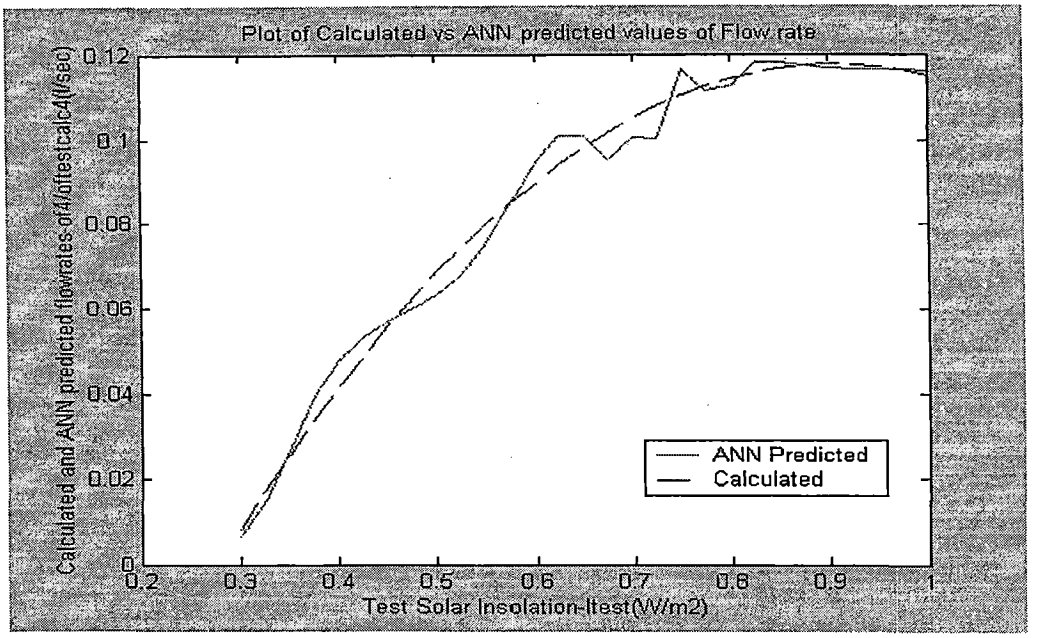

Fig. 77. Plot of calculated vs ANN predicted values of flow rate[tc2-H=10.37].

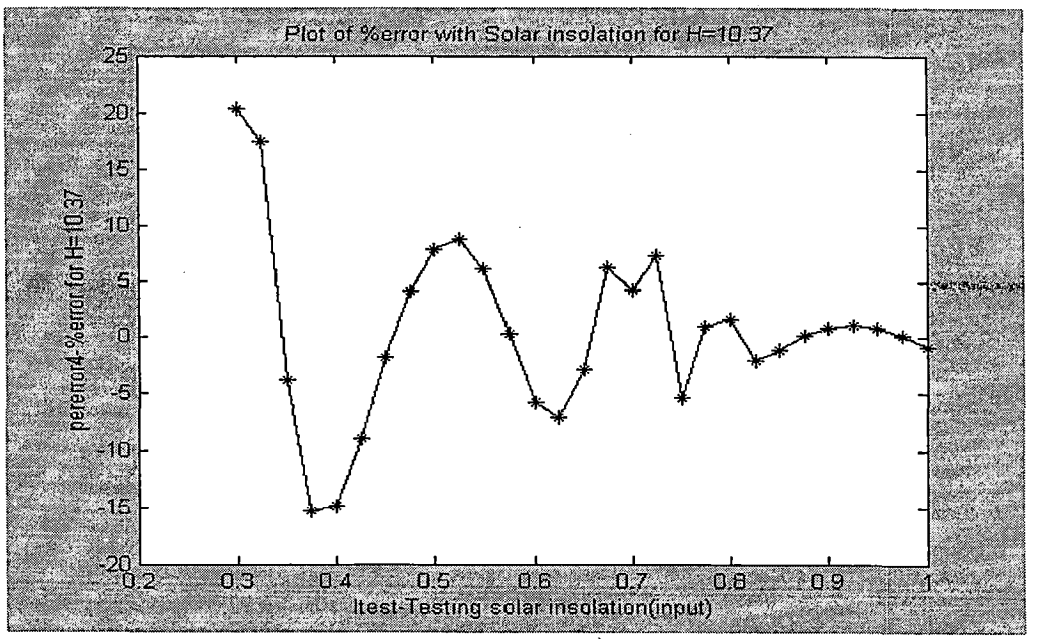

Fig. 78. Plot of %error with solar insolation for[tc2-H=10.37].

6.4.7 Head 13.8

6.4.7.1 Training condition 1

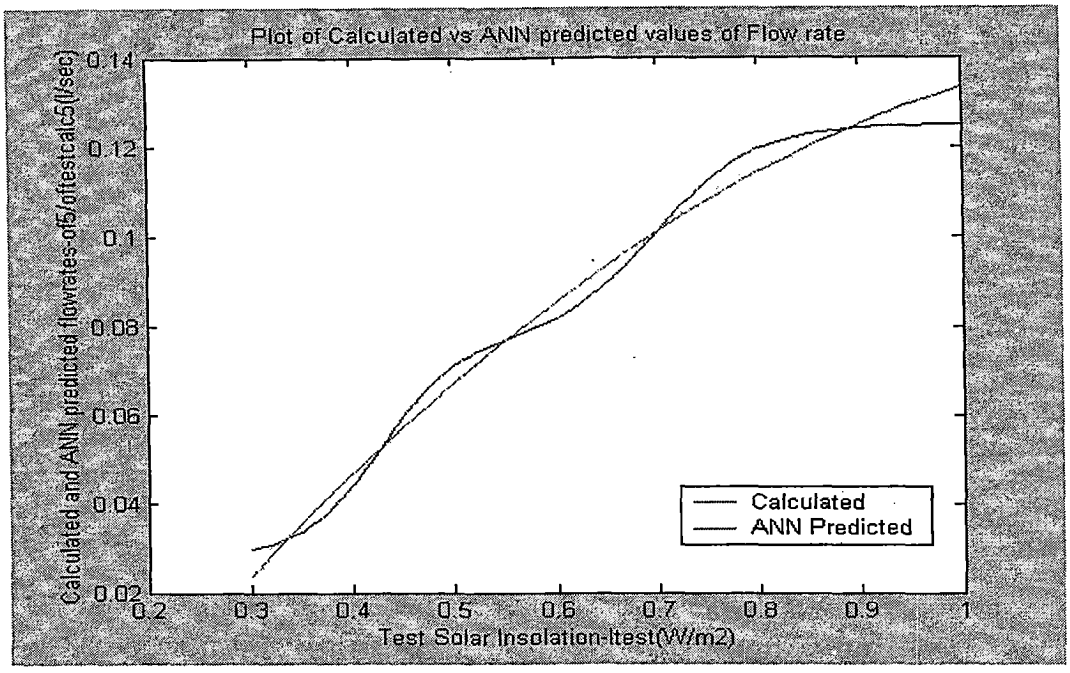

Fig. 79. Plot of calculated vs ANN predicted values of flow rate[tc1-H=13.8]

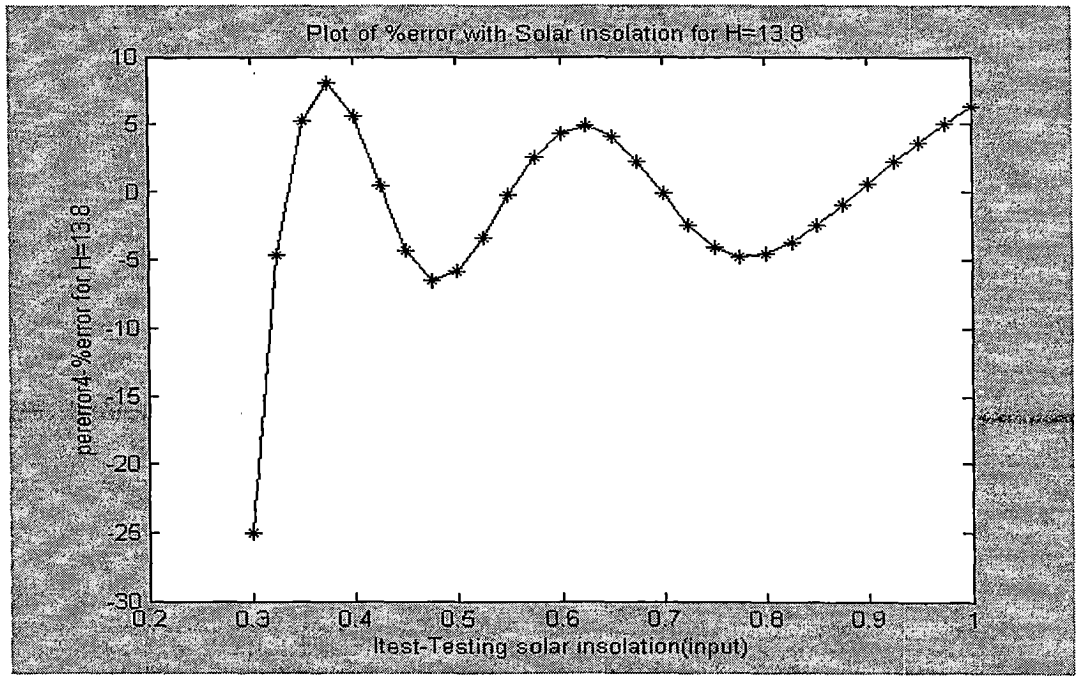

Fig. 80. Plot of %error with solar insolation for[tc1-H=13.8].

6.4.7.2 Training condition 2:

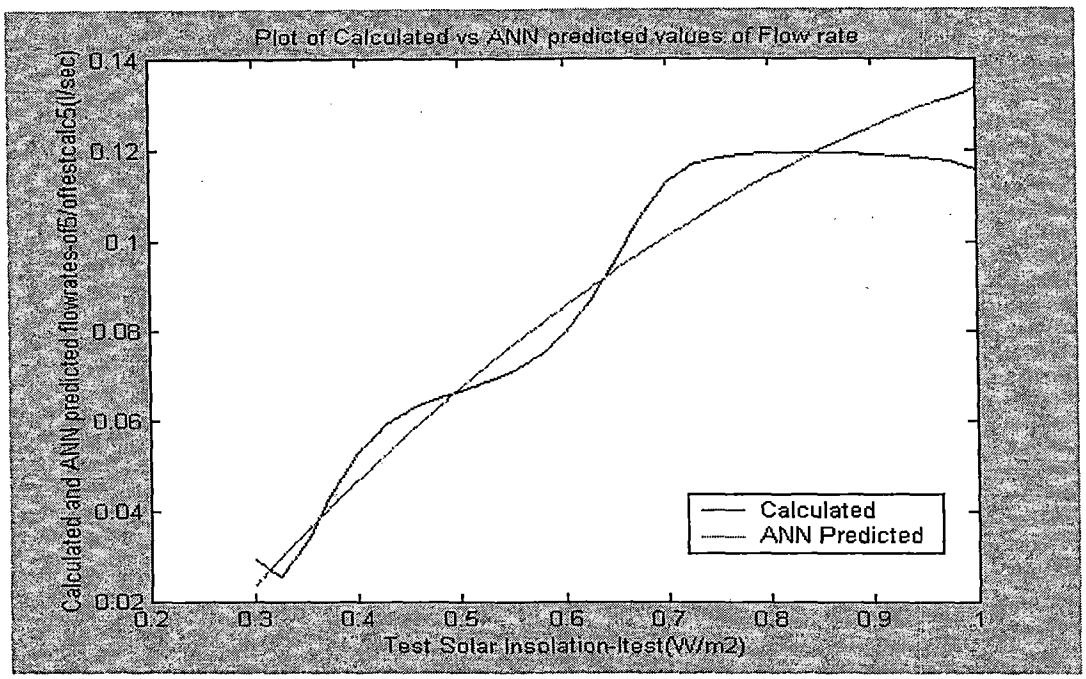

Fig. 81.Plot of calculated vs ANN predicted values of flow rate[tc2-H=13.8].

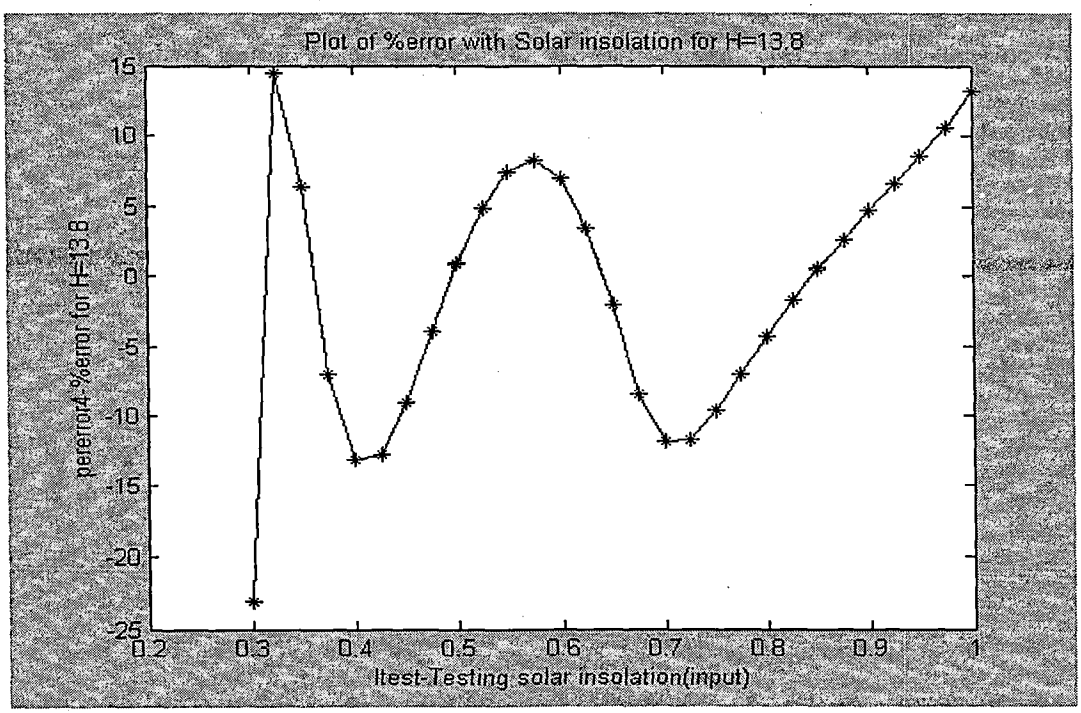

Fig. 82 plot of %error with solar insolation for[tc2-H=13.8].

Chapter 7

Conclusions and Future Scope of work

7.1 Conclusions

In this work steady-state performance of DC motors (PM and series) with a MPPT (intermediate converter) is analysed by mathematical modeling of individual components. From the simulation studies it has been observed that the use of the converter will influence the steady-state behavior of the pumping system. By suitable adjustment of power converter duty ratios, it is possible to operate at maximum power point of the SCA or gross mechanical energy output of the combined pumping system. It has been observed that the armature voltages for both the motors is higher for GME operation than the MP operation satisfying the relation $V_m^* > V_m$.

For both the machines, the GME operation results in efficiency improvement. The efficiency of the series motor is slightly less than the PM motor because of additional losses in the series field. These simulation studies forms the basis for training a neural network model for predicting chopping ratios of DC-DC converter. Comparative analysis is made between different architectures in chapter 4. The non-adaptive controller using ANN is tested for different set of solar insolations and the results are close to the computed values. From these studies it is found that the ANN provides a highly accurate identification/tracking of optimal operating points even with stochastically varying solar insolation. The percentage error in prediction for all cases of operation is found to be less than 10%.

A second ANN model is developed for modeling a photovoltaic water pumping system. ANN predicted values are compared with the flow rate values calculated from equations developed for a particular pumping system. The maximum percentage error is found to be around 20%. The deviation though small is attributed to fluctuations in the solar radiation and unsteady temperatures during the actual measurements.

The error in ANN prediction can be further reduced by judicially changing the neural network architecture. Training algorithm or function will also influence the performance during prediction. Training has been performed with TRAINGDM algorithm. Different training functions can be used for even optimal results.

7.2 Future Scope of work

The area of optimal operation of photovoltaic pumping systems is fast evolving in recent years. Different maximum power point tracking algorithms are successfully applied to photovoltaic pumping systems and their efficiency has been improved considerably. Artificial intelligence techniques such as artificial neural networks, fuzzy logic control and genetic algorithm mechanisms are used for optimal matching of PV generator to pump for maximizing utilizing efficiency. The following are few areas of the future scope of the present work

- **Genetic Algorithms:** Application of Genetic algorithms on a photovoltaic panel-pump motor matching to natural tracking of PV maximum power points. In this method, photovoltaic pumping systems controlled by different motors are optimized without any controller device like MPPT's (DC-DC converters). Investigations to

improve the performance of the system without adding any complex circuitry need to be done.

- **Robust control methods:** Robust control methods for identification and control of PV supplied DC motors coupled to constant and variable loads can further be investigated in good detail. Application of ULN's Universal Learning networks for detection of maximum power points and tracking the speed of the motor-pump unit need to be studied.

- **Fuzzy and ANN models:** Fuzzy and ANN models for global efficiency optimization and estimation or prediction of maximum power point of PV systems controlled by intermediate converters can be applied for performance evaluation.

- **Transient analysis:** In this work steady-state analysis of PV controlled dc motors were performed and later used for training an ANN controller in an off-line adaptive control mode. Transient analysis has not been dealt with. Transient performance of photovoltaic pumping systems can be done to decide the best combination of motor-pump unit for pumping applications.

[8] S.M.Alghuwainem: "Steady-state performance of dc motors supplied from photovoltaic generators with a step-up converter", IEEE Transactions on Energy Conversion, EC-7, pp. 267-272, 1995.

[9] S.M.Alghuwainem: "Application of a dc chopper to maximize utilization of solar cell generators" IEEE/PES Winter meeting, Paper 91, WM 145, EC-3, 1991.

[10] J.Appelbaum: "Starting and steady-state characteristics of dc motors powered by solar cell generators", IEEE Transactions on Energy Conversion", EC-1, pp. 17-25, 1997.

[11] M.M.Saied: "Matching of dc motors to photovoltaic generators for maximum daily gross mechanical energy", IEEE Transactions on Energy Conversion, EC-3, pp. 465-472, 1994.

[12] G.Kou and W.A.Beckman: "A method for estimating the long-term performance of directly coupled PV pumping systems", Energy Sources, Vol. 14, No. 3, pp. 143-154, 1993.

[13] A.Bennouna and Y.Ijdiyaou: "Water pumping using a photovoltaic dc solar pump without energy storage", Renewable energy, Vol. 4, No. 7, pp. 847-854, 1994.

[14] M.Moechtar, M.Juwono et al.: "Performance evaluation of ac and dc direct coupled photovoltaic water pumping system", Energy Conversion Management, Vol. 31, No. 6, pp. 521-527, 1991.

[15] A.Hadj Arab, F.Chenlis et al.: "Performance of PV water pumping systems", Renewable energy, Vol. 18, No.3, pp. 191-204, 1999.

[16] S.Weerasooriya and M.A.El-sharwaki: "Identification and control of dc motor using back-propagation neural networks", IEEE Transaction on Energy Conversion, Vol. EC-6, No. 4, pp. 663-669, December 1991.

[17] Chen, Zha et al.: "Implementation of a stand-alone photovoltaic pumping system with maximum point tracking", IEEE Transactions on Energy Conversion, Vol. 31, No. 4, pp. 215-218, 1999.

[18] Ahmed Hussein, Kotaro Hirasawa et al.: "A robust control method for a PV supplied dc motor using universal learning networks", Vol. 76, No. 4, pp. 771-780, 2004.

[19] M.Akbaba, I.Qamber et al.: "Matching of separately excited dc motors to photovoltaic generators for maximum power output", Solar Energy, Vol. 19, No. 6, pp. 375-385, 1998.

[20] M.Kolhe, J.C.Joshi et al.: "Performance analysis of a directly coupled photovoltaic water pumping system", IEEE Transactions on Energy Conversion, Vol. 19, No. 3, pp. 613-618, September 2004.

[21] B.Reshef, H.Suchrcke et al.: "Analysis of a photovoltaic water pumping system", Energy and Power systems Transactions, Vol. 45, No. 3, pp. 124-130, 1995.

[22] R.Anis and M.A.Nour: "Optimum design of a photovoltaic powered pumping system", Energy Conversion Management, Vol. 35, No. 12, pp. 1123-1130, 1994.

[23] O.C.Viela and N.Fraidenraich: "Analysis of solar fed electric drive for pumping applications", Energy Sources, Vol. 3, No.8, pp. 145-151, 1997.

[24] E.H.Amer, M.A.Younes et al.: "Estimating the monthly discharge of a photovoltaic water pumping system model: model verification", Energy Conversion Management, Vol. 47, No. 3, pp. 2092-2102, 2006.

[25] T.Senjyu, M.Veerachary et al.: "Steady-state analysis of a PV supplied separately excited dc motor fed from IDB converter", Solar Energy, Vol. 71, No. 5, pp. 493-510, 2002.

[26] A.Hadj Arab, F.Chenlo: "Loss of load-probability of photovoltaic water pumping systems", Vol. 76, No. 4, pp. 713-723, 2004.

[27] A.Hadj Arab. M.Benghanem, et al.: "Motor-pump system modelization", Renewable Energy, Article in Press, pp. 1-9, 2006.

[28] A.Saadi, A.Moussi: "Neural network use in the MPPT of photovoltaic pumping system", Reviews of Renewable Energy ICPWE, pp. 35-45, 2003.

[29] W.Lawrence, B.Wilchert: "Simulation and performance of a photovoltaic pumping system", IEEE Transaction on Energy Conversion, Vol. 2, No. 1, pp 513-518, 1995.

[30] Z.Abidin, Yesilata: "New approaches on the optimization of directly coupled PV pumping systems", Solar Energy, Vol. 77, No. 2, pp. 81-93, 2004.

[31] T.D.Short, R.Oldach: "Solar powered water pumps: The past, the present and the future", Solar Energy Engg., Vol. 125, pp. 76-82, 2003.

[32] A.A.Ghoneim: "Design optimization of photovoltaic powered water pumping systems", Energy Conversion Management, Vol. 47, No. 5, pp. 1449-1463, 2005.

[33] A.Kalogirou: "Artificial neural network in renewable energy systems applications: a review", Renewable and sustainable Energy reviews, Vol. 5, No. 3, pp. 373-401, 2001.

Appendix A

The machine data for both PMDC and series motor for steady-state analysis is given in the table below.

Table 14. Machine Data (PMDC and Series)

Machine data for the Analysis

Machine Data	Permanent Magnet DC motor	DC Series Motor
Ra -Armature Resistance	1.50 Ohm	1.50 Ohm
Rf-Field Resistance	--------	0.70 Ohm
La-Armature Inductance	0.02 H	0.02 H
Lf-Field Inductance	---------	0.13 H
Ce-Flux co-efficient	0.621/0.6626	--------
Maf-Mutual Inductance	----------	0.0675/0.12 H

Load data (centrifugal pump) is shown in the table below.

Table 15. Load data for Analysis

Load data (Centrifugal pump)

Load Data	PMDC Motor	Series Motor
J-Moment of Inertia	0.02367	0.02367
A1	0.00039	0.00031
B1	0.002387	0.002387
C1	0.5	0.46

Appendix B

Machine data of a PMDC motor coupled to photovoltaic water pump which is used for ANN modeling is given below

PV generator parameters at STC (Standard Temperature Conditions)

The PV generator parameters at STC are shown below.STC corresponds to following parameters:

(1) Temperature - 25°C
(2) Solar insolation or radiation – 1000 W/m^2
(3) Air mass(A.M-1.5)

Short-circuit current (A)	4.81
Open-circuit voltage (V)	224
Resistance Series (ohm)	2.25

Table 16. PV generator parameters

Motor parameters

Table 17.Motor Parameters

Nominal power (W)	690
Nominal speed (rpm)	3000
Supply voltage	200-220
Nominal current (A)	4.8

Tabular Data for MP and GME operations

The following section gives the tabular data from the analysis for both MP and GME operations and for both PMDC motor and series motor. The data shown here is used for training a neural network for prediction of chopping ratio of the Intermediate DC-DC converter. The tables are listed below.

Table 18. PV array Voltage Variation with Solar insolation for PMDC motor.

PV Voltage(V)-MP	PV Voltage(V)-GME	PU Solar Insolation
82	82	0.1
92	94	0.15
96	98	0.20
102	104	0.25
106	110	0.30
108	112	0.35
111	117	0.40
113	120	0.45
114	122	0.50
115	125	0.55
117	128	0.60
118	130	0.65
120	131	0.70
121	133	0.75
122	135	0.80
123	136	0.85
124	137	0.90
123	138	0.95
124	139	1.0

Table 19. Armature Voltage Variation with Solar insolation for PMDC motor.

Armature Voltage(V)-MP	Armature Voltage(V)-GME	PU Solar Insolation
42	45	0.1
53	56	0.15
62	65	0.20
69	76	0.25
78	82	0.30
82	87	0.35
88	95	0.40
96	101	0.45
100	106	0.50
105	116	0.55
109	118	0.60
116	122	0.65
119	125	0.70
121	130	0.75
124	133	0.80
129	136	0.85
133	138	0.90
136	141	0.95
138	146	1.0

Table 20. Armature Voltage Variation with Solar insolation for series motor.

Armature Voltage(V)-MP	Armature Voltage(V)-GME	PU Solar Insolation
22	26	0.1
33	40	0.15
40	54	0.20
48	66	0.25
58	76	0.30
65	82	0.35
74	95	0.40
79*	101	0.45
87	113	0.50
95	119	0.55
100	129	0.60
105	136	0.65
112	143	0.70
119	155	0.75
124	160	0.80
129	166	0.85
136	175	0.90
141	181	0.95
146	189	1.0

Table 21. Copper losses with solar insolation for PMDC motor.

Copper Losses MP	Copper Losses GME	PU Solar Insolation
8.10	8.07	0.1
17.12	17.06	0.15
20.12	20.06	0.20
23.24	22.93	0.25
30.35	30.17	0.30
33.45	32.85	0.35
45.51	44.21	0.40
54.32	53.65	0.45
62.41	60.64	0.50
70.61	68.82	0.55
80.82	78.33	0.60
82.34	80.43	0.65
94.63	90.32	0.70
105.42	101.87	0.75
112.32	110.67	0.80
116.77	113.34	0.85
137.54	135.52	0.90
146.67	142.53	0.95
155.2	152.48	1.0

Table 22. Copper losses with solar insolation for series motor.

Copper Losses MP	Copper Losses GME	PU Solar Insolation
35.12	20.21	0.1
50.23	30.43	0.15
55.67	40.43	0.20
70.23	45.62	0.25
86.42	50.13	0.30
94.14	57.25	0.35
102.33	64.26	0.40
112.23	70.35	0.45
122.35	75.24	0.50
130.45	80.41	0.55
135.66	85.13	0.60
145.23	90.45	0.65
154.33	92.34	0.70
161.12	98.49	0.75
170.88	101.52	0.80
180.37	104.52	0.85
185.10	110.55	0.90
195.27	115.47	0.95
200.10	120.60	1.0

Table 23. Efficiency with solar insolation for PMDC motor.

%Efficiency MP	% Efficiency GME	PU Solar Insolation
93.2	94.2	0.1
93.4	94.4	0.15
93.0	94.0	0.20
92.8	93.8	0.25
92.6	93.6	0.30
92.4	93.4	0.35
92.1	93.1	0.40
92.0	93.0	0.45
91.8	92.8	0.50
91.7	92.7	0.55
91.7	92.6	0.60
91.6	92.4	0.65
91.5	92.4	0.70
91.3	92.2	0.75
91.1	92.1	0.80
91.0	92.0	0.85
90.7	91.7	0.90
90.5	91.6	0.95
90.3	91.5	1.0

Table 24. Efficiency with solar insolation for series motor.

%Efficiency MP	% Efficiency GME	PU Solar Insolation
61.2	82.3	0.1
67.1	84.5	0.15
72.3	84.8	0.20
75.2	84.9	0.25
76.4	85.3	0.30
77.3	86.0	0.35
78.1	86.4	0.40
78.3	86.6	0.45
78.6	86.9	0.50
78.9	87.0	0.55
79.3	87.3	0.60
79.7	88.2	0.65
80.1	88.9	0.70
80.4	89.3	0.75
81.4	90.1	0.80
81.8	90.6	0.85
82.6	90.8	0.90
82.9	91.1	0.95
85.2	91.4	1.0

Table 25. Chopping ratio with solar insolation for PMDC motor.

Chopping ratio MP	Chopping ratio GME	PU Solar Insolation
0.5196	0.5515	0.1
0.5769	0.6122	0.15
0.6526	0.6922	0.20
0.6876	0.7291	0.25
0.7410	0.7853	0.30
0.7875	0.8341	0.35
0.8105	0.8582	0.40
0.8491	0.8987	0.45
0.8846	0.9359	0.50
0.9175	0.9704	0.55
0.9342	0.9876	0.60
0.9368	1.0185	0.65
0.9919	1.0476	0.70
1.0065	1.0627	0.75
1.0324	1.0889	0.80
1.0572	1.1152	0.85
1.0704	1.1287	0.90
1.0937	1.1527	0.95
1.1186	1.1784	1.0

Table 26. Chopping ratio with solar insolation for series motor.

Chopping ratio MP	Chopping ratio GME	PU Solar Insolation
0.2812	0.3402	0.1
0.3403	0.4625	0.15
0.4132	0.5713	0.20
0.4813	0.6113	0.25
0.5406	0.6923	0.30
0.6114	0.7843	0.35
0.6613	0.8406	0.40
0.7109	0.9215	0.45
0.7704	0.9834	0.50
0.8115	1.0793	0.55
0.8617	1.1206	0.60
0.9026	1.1718	0.65
0.9703	1.2238	0.70
0.9917	1.2836	0.75
1.0324	1.3440	0.80
1.0834	1.3814	0.85
1.1215	1.4263	0.90
1.1603	1.4605	0.95
1.2063	1.5403	1.0